

Statistical Genetics and Direct Coupling Analysis beyond Quasi-Linkage Equilibrium

Vito Dichio^{a,b,c}, Hong-Li Zeng^e and Erik Aurell^d

^a Inria, Aramis project-team, Paris, France

^b Institut du Cerveau et de la Moelle épinière, ICM, Paris, France

^c Sorbonne Université, Paris, France

^d Department of Computational Science and Technology, AlbaNova University Center, SE-106 91 Stockholm, Sweden;

^e School of Science, Nanjing University of Posts and Telecommunications, New Energy Technology Engineering Laboratory of Jiangsu Province, Nanjing, 210023, China

ARTICLE HISTORY

Compiled September 2, 2022

ABSTRACT

This work is about statistical genetics, an interdisciplinary topic between Statistical Physics and Population Biology. Our focus is on the phase of *Quasi-Linkage Equilibrium* (QLE) which has many similarities to equilibrium statistical mechanics, and how the stability of that phase is lost. The QLE phenomenon was discovered by Motoo Kimura in the mid-1960ies for a two-locus two-allele model, and was extended and generalized to the global genome scale by *Neher & Shraiman (2011)*. What we will refer to as the Kimura-Neher-Shraiman (KNS) theory describes a population evolving due to the mutations, recombination, genetic drift, natural selection (pairwise epistatic fitness). The main conclusion of KNS is that QLE phase exists at sufficiently high recombination rate (r) with respect to the variability in selection strength (fitness). Combining the results of the KNS theory with the techniques of the Direct Coupling Analysis (DCA), developed for applications in Statistical Physics and Computational Biology, we show that in QLE epistatic fitness can be inferred from the knowledge of the (dynamical) distribution of genotypes in a population. Extending upon our earlier work *Zeng & Aurell (2020)* here we present an extension to high mutation and recombination rate. We further consider evolution of a population at higher selection strength with respect to recombination and mutation parameters (r and μ). We identify a new bi-stable phase which we call the Non-Random Coexistence (NRC) phase where genomic mutations persist in the population without either fixating or disappearing. We also identify an intermediate region in the parameter space where a finite population jumps stochastically between QLE-like state and NRC-like behaviour. The existence of NRC-phase demonstrates that even if statistical genetics at high recombination closely mirrors equilibrium statistical physics, from a more general point of view a more apt analogy is non-equilibrium statistical physics with broken detailed balance, where self-sustained dynamical phenomena are ubiquitous.

KEYWORDS

statistical genetics; direct coupling analysis; quasi-linkage equilibrium; epistatic fitness; inference

Glossary

allele One of the possible alternative forms of a gene, often distinguished from other alleles by phenotypic effects. 6

archaea From the Greek word *archaios*, meaning “ancient” or “primitive”. Prokaryotic organisms (i.e. no nucleus) typically found inhabiting and thriving in extreme environmental conditions e.g. exceedingly salty or scorching. 4

bottleneck A drastic reduction in population size and consequent loss of genetic diversity, followed by an increase in population size. The rebuilt population has a gene pool with reduced diversity caused by genetic drift. 7

central dogma Originally stated by F. Crick, it says that the genetic information flow progresses from DNA to RNA (transcription) to proteins (translation). Exceptions are known. 4

chromosome In prokaryotes: DNA molecule containing the organism’s genome; in eukaryotes: DNA molecule complexed with RNA and proteins to form a thread-like structure containing genetic information arranged in a linear sequence. 6

crossing-over The exchange of genetic material during sexual reproduction between two homologous chromosomes. It happens during meiosis. 7

diploid ($2n$) A cell (by extension, an organism) that contains two copies of each chromosome. 6

DNA *Deoxyribonucleic Acid*. A macro-molecule usually consisting of nucleotide polymers comprising antiparallel chains in which the sugar residues are deoxyribose and which are held together by hydrogen bonds between base pairs. 4–6

eukaryote Organism having true nuclei and membranous organelles and whose cells divide by mitosis and meiosis. 4

evolution In biology, the change in inherited traits over successive generations in populations of organisms. 4

fitness Expected reproductive success of an organism. For modelling purposes, this is often equated to the average number of offspring in the subsequent generation (absolute fitness). 6

genetic drift Sampling fluctuations of genotypes or allele frequencies, most often observed in small populations. 7

genotype The allelic or genetic constitution of an organism; often, the allelic composition of one or a limited number of genes under investigation. 6

germ line cell In mammals, haploid cell able to unite with one from the opposite sex to form a new individual. 6

haploid (n) A cell (by extension, an organism) having one member of each pair of homologous chromosomes. 6

heredity (also *inheritance*). Transmission of traits from one generation to another. The study of heredity in biology is genetics. 4

hybridization A situation where two strains of one species that have been evolving in isolation for some time come in contact again. 7

meiosis The process of cell division in sexually-reproducing organisms during which the diploid number of chromosomes is reduced to the haploid number. 6

mutation Any process that produces an alteration in DNA or chromosome structure; in genes, the source of new alleles. Among the most common: insertion, duplication, deletion, translocation, inversion, point mutation. They are *silent* if they do not alter the polypeptide chain, *missense* if they cause a substitution of a different amino acid in the resulting protein, *nonsense* if they result in a premature stop codon. 6

natural selection Differential reproduction among members of a species owing to variable fitness conferred by genotypic differences. 6

nucleobases (also *nitrogenous bases*). Nitrogen-containing biological compounds, the most common being adenine (A), cytosine (C), guanine (G), thymine (T), and uracil (U). The bases A, T, C, G are found in the DNA, in the RNA T is replaced by U. 4

phenotype Ensemble of the observable characteristics or traits of an organism. 6

population A group of organisms of a species that interbreed and live in the same place at a same time. They are capable of interbreeding or reproduction. 6

population genetics Study of the genetic composition of populations, including distributions and changes in genotype and phenotype frequency in response to the processes of natural selection, genetic drift, mutation and gene flow. 6

prokaryote Organism lacking nuclear membranes and true chromosomes. Bacteria and blue-green algae are examples of prokaryotic organisms. 4

quantitative genetics Study of the genetic basis underlying phenotypic variation among individuals, with a focus primarily on traits that take a continuous range of values e.g. height, weight, longevity. 7

recombination The process that leads to the formation of new allele combinations on chromosomes. In eukaryotes, genetic recombination during *meiosis* can lead to a novel set of genetic information that can be passed on from the parents to the offspring. In bacteria recombination happens by *transformation* (ability to take up DNA from the surroundings), *transduction* (transfer of genetic material by the intermediary of viruses), and *conjugation* (direct transfer of DNA from a donor to a recipient). 6

RNA Similar to DNA but characterized by the pentose sugar ribose, the pyrimidine uracil, and the single-stranded nature of the polynucleotide chain. RNA molecules exist in different types in the cells: messenger RNA (mRNA), ribosomal RNA (rRNA), and transfer RNA (tRNA). 5

soma line cell In mammals, any cell of the body except germ cells. Somatic cells are diploid. Mutations in somatic cells can affect the individual and are not passed on to offspring. 6

transcription Transfer of genetic information from DNA by the synthesis of a complementary RNA molecule using a DNA template. 5

translation The derivation of the amino acid sequence of a polypeptide from the base sequence of an mRNA molecule in association with a ribosome and tRNAs.

1. Introduction

This work is about *statistical genetics*. In the broad area of theoretical biology, this is the field concerned with the development of statistical methods to describe the distribution of genotypes in a population. In this paper genotype means one genome out of all possible genomes of the same length. For a definition of biological terms used, see the Glossary. In this introductory section we will start with a description of Statistical Genetics in general in Section 1.1, followed by an introduction to the Kimura-Neher-Shraiman (KNS) theory in Section 1.2. In Section 1.3 we describe the phase of Quasi-Linkage Equilibrium (QLE) which can exist and can be stable in a naturally evolving population, in certain parameter ranges. In this section we also describe the Kimura-Neher-Shraiman theory in more detail, and what its predictions are for the limits to stability of QLE. Extensions to KNS are described in Appendices B and C.

1.1. *Subject Matter: Population Genetics in a Nutshell*

This section contains a brief introduction to the biology relevant to this paper. It is primarily aimed to physicists not conversant with these matters; biophysicists and biological physicists (and biologists) may skip to the next section. Technical terms are defined in the glossary in the beginning.

The central difference between living and non-living forms of matter is Darwin's great discovery of evolution, and the key element of evolution is heredity. If changes were not inherited life would start afresh in each generation, and no evolution would be possible. Since Life began information has flowed without interruption from generation to generation, in an ongoing process that has shaped the astonishing variety of complex organisms that inhabit this planet today. Several questions arise: how and where is information stored? how is information transmitted? what is the origin of the observed diversity of life?

Life on the planet falls under three domains: Eukaryotes, the cells of which have a defined nucleus and organelles; Prokaryotes, cells with no nucleus; Archaea, prokaryotic organisms that have distinct molecular characteristics that differentiate them from the previous two domains. It is believed that eukaryotes started as a symbiont between an archaea and a prokaryote that had acquired respiration, *i.e.* the ability to produce adenosine triphosphate (ATP) in the citric acid cycle. For this reason archaea genomes are in some respects closer to eukaryotes than to bacteria. Nevertheless, to this day almost all eukaryotic cells maintain a small part of the genes inherited from the original prokaryote in the mitochondria, the organelles where most of the energy that the cell needs is produced in a form that the cell can use. A similar event involving another type of bacterium led to the chloroplasts which can be found in almost all algae and plants, and where the energy of the Sun is transduced into chemical energy.

According to the central dogma of molecular biology, biological information is encoded in the DNA, a macro-molecule present in each cell that consists in two sugar-phosphate ribbon-like stands that coil around to form a double helix and whose horizontal rungs are pairs of complementary nucleobases: A-T, G-C, see Fig.1.

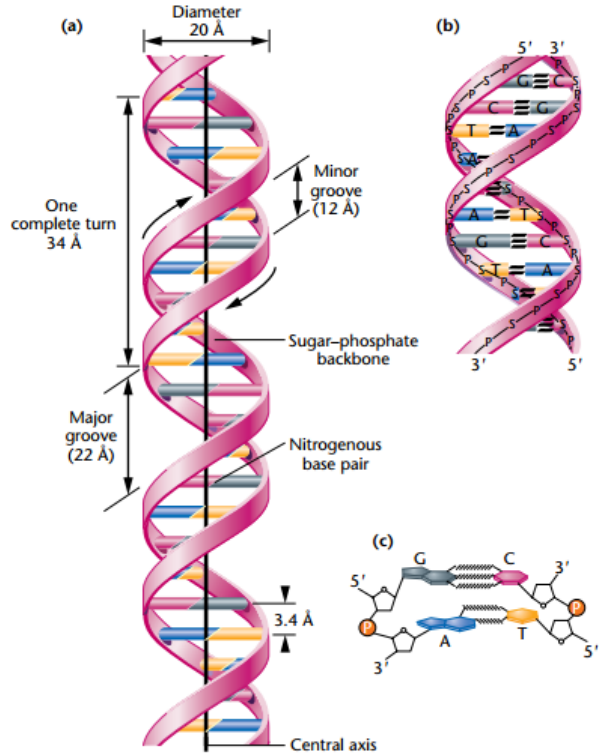


Figure 1.: The DNA double helix as proposed by J. Watson and F. Crick (a). The ribbon-like strands represent the sugar-phosphate backbones, and the horizontal rungs depict the nitrogenous base pairs (b-c). From [1].

The information lies in the exact *sequence* of nucleobases of each strand: by means of transcription DNA is converted into the closely related molecule RNA, and by means of translation, a stretch of RNA is translated into a polypeptide chain, which upon folding and other processes will eventually result in a protein. Such proteins in turn perform the many different functions needed to sustain life. Exceptions to the central dogma are well known. A gene refers to a stretch of DNA which is transcribed together, and a gene product typically means the protein produced from that RNA. In bacteria and viruses it is common that one gene leads to more than one protein by transcribing two or more translatable units after one another. In higher organisms it is also common that one gene leads to more than one protein by the genetic machinery optionally including or not including parts of the gene to be translated. In this way it is possible for *e.g.* humans to have about 20,000 genes but more than 100,000 proteins. Several classes of RNA exist that are functional in themselves, without being translated into proteins. Two of the most important are ribosomal RNA and transfer RNA, without which protein synthesis is not possible. Some types of heredity (epigenetics) exist that do not involve the sequence of nucleotides in DNA, the most well-known being chemical modifications of DNA (methylation and other) which is important in *e.g.* heritable gene silencing. Even if there are hence exceptions to the central dogma, it describes the overwhelming majority of biological information processing as pertaining to information stored as chemical molecules.

Complex regulatory mechanisms of the gene expression weave an intricate and

largely unknown network of interactions within genes. Some such gene expression patterns can be inherited over many generations and comprise another type epigenetics, even if often enhanced by methylation and similar processes in higher organisms. Many other gene expression patterns on the other hand change on fairly rapid time scale in response to changes in the environment. In bacteria this is in fact the main form of cellular information processing and it is vital in higher organisms as well, even if often overlayed by other and faster pathways. In eukaryotes the DNA is often condensed in the form of chromosomes: the set of chromosomes is the genetic heritage of an individual. A population in which each cell has one complete set of chromosomes is named haploid, if there are two such sets, diploid. In mammals the germ line cells (egg cell and sperm) are haploid and the soma line cells (the rest) are diploid. This form of life is hence diploid-dominated, and the organisms reproduce by going through an obligatory haploid phase where the germ line cells mix in sex. In other organisms very many different forms of reproduction and diploid/haploid division of labour are possible. Asexual reproduction has been found to occur naturally everywhere except among mammals (among birds in domesticated turkeys and chicken), but is generally less frequent the more complex the organism. Many bacteria reproduce mostly and maybe almost only asexually, and hence live like haploid genomes copying themselves to new haploid genomes. Certain yeasts have more than two mating types (gender, so to speak) that can only mate in specific combinations.

Let us now broaden the perspective and consider an entire population of individuals. In general, each gene is present in a population with different alleles, in different amounts. The goal of population genetics is to study the genetic composition and dynamics of biological populations. Several processes alter the genetic pool of a population. The most important of them are

- **Natural selection.** At the phenotype level, advantageous characteristics will enhance the probability for an individual to survive and reproduce (high fitness). This has consequences at the genotype level, even though the exact map between these two layers may be quite complex. Complexity here means it is not clear which characteristics of genotype elements lead to which phenotypic traits on which selection acts, especially when they act in combination.
- **Mutations.** They can arise by chance in a genomic sequence *e.g.* because of transcription errors. Mutations can have no consequences on the level of protein (*synonymous*) or cause alterations in the polypeptide chain they code for (*non-synonymous*). They represent a source of variability for the evolutionary process.
- **Recombination.** Several mechanisms of interaction between individuals of a population can lead to the exchange of genetic material. In a general sense they can all be called forms of sex, even if acting quite differently than sex in mammals. In prokaryotes, the main forms of recombination are *transduction*, *transformation*, *conjugation* where transduction means that genetic material is transferred from one bacterium to another one by a virus and transformation that one bacterium releases DNA into the environment where it is picked up by another one. Conjugation is similar to animal sex in that a donor cell injects genetic material into a recipient cell through a dedicated conduit (a pilus). In contrast to animal sex the transfer is only one way and does not give rise to a new organism; the effect is to transform the recipient cell. The amount of genetic material transferred during *e.g.* classic conjugation *Escherichia coli* is also only a small fraction of the whole genome. In eukaryotes, recombination happens during meiosis where the

mixing between two chromosomes from each of the parents is enhanced by the crossing-over mechanism. Just like mutations, recombination fuels variability in the population.

- **Chance.** Accidental events can alter the genetic pool of a population: bottlenecks, genetic drift, hybridization...

In the biological literature, a distinction is made between population genetics and quantitative genetics. This work is almost exclusively about the first. The second deals with the genetics of continuously varying characteristics, such as height and skin color in human. Historically this was referred to as *quantitative* (measured by a number), in opposition to characteristics that appear in only a few different types, as do *qualities* in classical philosophy. Inherited qualities are due to differences in genotypes on one or a few positions, of which one example in human is the type of ear wax, due to a single-nucleotide variation in the gene ABCC11 on chromosome 16 [2]. On the contrary most quantitative characteristics of higher organisms are due both inheritance ("nature") and environment ("nurture"); if one could isolate the genetic component it would be typically due to variations in many positions. For instance, height is partly genetically determined in human, and has recently been associated to variations at about 700 positions only among individuals of European ancestry [3].

In the pre-sequencing era population genetics was the realm of theory and explanations, while quantitative genetics was the realm of what could be measured and of direct interest to biology. In modern times this relationship is partly upended: whole genome sequences of many organisms can (and have been) obtained, and the predictions of population genetics can be compared to such data. This is the approach we have followed in this work. As an aside and an example of what can be done, in the ongoing COVID19 pandemic about half a million whole-genome sequences of the coronavirus SARS-CoV-2 have been found in different laboratories around the world, many of them likely determined to single/nucleotide accuracy [4]. Measuring quantitative traits remains however time-consuming and difficult, and the relationship between genotype and phenotype is one of the most complex and least known (though most studied) in all of science. In the spirit of Statistical Physics it is therefore natural to focus on the genotype scale (microstate), once that is measurable.

1.2. Model: Kimura-Neher-Shraiman Theory (KNS)

After outlining the subject matter we continue by setting up a *minimal* theoretical framework. The mathematical analysis of problems in population genetics started with Hardy and Weinberg in 1908 [5,6] who showed that in a population with diploid genomes evolving only due to recombination (sex) allele frequencies reach stationary values. This *Hardy-Weinberg equilibrium* is a special case of *Linkage Equilibrium* which we will introduce below. A result from 1930 is R. A. Fisher's celebrated *fundamental theorem of natural selection* [7] according to which *in the absence of mutations and in the limit of an infinite population the average fitness of the population cannot decrease in time, and becomes stationary only when all of the individuals in the population bear an optimal genome, corresponding to the maximum value of the fitness.*¹ This deterministic picture of evolution holds in some very specific cases and it is now regarded more as an exception than as the rule. A third early result was an effective model of the diffusion type for the change of allele frequencies over time, derived by Fisher and Kolmogorov and later by Wright, for reviews, see

¹ See [8] for a concise proof.

[8–10].

By *Statistical Genetics* (SG) we refer to the totality of this intersection between population genetics and probability theory and statistical mechanics. Our focus is on a situation at high enough recombination rate compared to the other processes in the population, which leads to a *Quasi-Linkage Equilibrium* (QLE) phase. This phase was discovered by Motoo Kimura in a model of two biallelic loci (two states per locus) [11], and later extended by Richard Neher and Boris Shraiman to the genome scale [12]. In what follows we will refer to the resulting theory of QLE as the Kimura-Neher-Shraiman (KNS) theory.

Before turning to the details of KNS one should question if methods or ideas akin to statistical mechanics should work at all in describing the evolution of a population of genomes. We will adopt a system approach to the evolutionary problem, according to which evolution is a collective phenomenon, stemming from interactions of many basic units, namely genes. An illuminating observation is that thermodynamics is conceptually very close to quantitative genetics. Following [12], let us try to draw some analogies between them:

- ★ **Thermodynamics** is a phenomenological description of observable physical properties of a large ensemble of particles. This is achieved by taking macroscopic averages over the random motion of individual particles at thermal equilibrium. Despite the complex and chaotic single-particle motion, deterministic laws of thermodynamic emerge thanks to the statistical properties of the ensemble of particles considered.
- ★ **Quantitative genetics** is a phenomenological description of observable phenotypic traits of a population of individuals (genomes). This is achieved by taking averages over the whole population, whose dynamics is governed by several drivers defined at the genotype level. Despite the largely unknown genotype-phenotype map and uncontrolled environmental effects, laws of quantitative genetics emerge due to the statistical properties of the ensemble of genomes.

The role of statistical mechanics is to provide a "bridge" between the physics at the microscopic scale and the thermodynamic quantities, the latter expressed as ensemble averaged functions of the coordinates and momenta of the constituent particles. We seek likewise a coarse-grained phenomenological theory bridging the gap between the genotype dynamics and the population averaged observables of quantitative genetics, hence the name *statistical genetics*.

1.2.1. KNS Hypotheses

We here set the stage of the KNS theory, in the form of a list of hypotheses. Details and limits of validity on the hypotheses, and extensions of them, of either a easy/feasible or difficult/impractical nature, are discussed later.

- (1) **Genomic structure.** We consider a haploid genome $g = (s_1, \dots, s_L)$ of L loci s_i where $i = 1, \dots, L$. The number L of loci is fixed and equal for all the individual genomes. A population is a collection $\{g^\alpha\}_{\alpha \in A}$, where A is a set of indices. Each genome g appears in the population with probability $P(g)$.

- (2) **Ising genes**². We suppose bi-allelic loci *i.e.* $s_i = \pm 1 \forall i$; the genotype space is then represented by the 2^L vertices of the hypercube $\{-1, 1\}^L$.
- (3) **Constant population.** The total number of individuals is fixed $|A| = \text{const.}$ With this hypothesis we model *e.g.* the struggle for survival in an environment with limited resources. Mostly we will make the further assumption of an infinite population $|A| = \infty$, as that allows us to neglect stochastic effects in a first approximation.
- (4) **Evolution.** The genome distribution $P(g, t)$ evolves in time. The dynamics is driven by the three operators representing natural selection Sec.(1.2.2), mutations Sec.(1.2.3) and recombination Sec.(1.2.4). Their action is encoded in a master equation *i.e.* a phenomenological first-order differential equation

$$\frac{d}{dt}P(g, t) = \frac{d}{dt}\Big|_{fit} P(g, t) + \frac{d}{dt}\Big|_{mut} P(g, t) + \frac{d}{dt}\Big|_{rec} P(g, t) . \quad (1)$$

In order to provide an explicit expression for eq.(1), we now turn to analyse the terms in the RHS one by one.

1.2.2. Fitness

The approach we follow for a mathematical description of natural selection is based on the definition of the *fitness function* $F(g)$, which is proportional to the average number of offspring of an individual whose genotype is g . In other words, $F(g)$ expresses the propensity of a genotype to transfer its genomic material to the next generations. The explicit form of $F(g)$ is said to define the *fitness landscape* of the population. Even if broad, this definition only partially represents what (Darwinian) fitness in Biology stands for. Let us stress the limitations by emphasizing what the definition does *not* cover:

- * It assumes that fitness *only* depends on the genotype (with a proviso, to be discussed below). This is not true in general as the reproductive rate of a given genome (or genomic trait) may depend on its frequency in the population *e.g.* because of some feedback regulation system. Effects of cooperation and strategic behaviour (games) are not included in this model.
- * It also sets aside issues related to a possible fluctuating environment (*fitness seascapes*) and the related time-dependence of selection.

If however we accept this limited view of fitness, the first term in eq.(1) can be written as

$$\frac{d}{dt}\Big|_{fit} P(g, t) = [F(g) - \langle F \rangle]P(g, t) ; \quad (2)$$

$\langle F \rangle(t) = \sum_g F(g)P(g, t)$ is the average fitness that ensures the normalisation of $P(g, t)$. Fit individuals (high fitness) will grow in proportion, and the unfit ones will decrease. Furthermore, whether an individual is fit or not depends on the other individuals that are present in the population. However, it does so in the simple way that a priori fitness distribution and the actual population together set a threshold ($\langle F \rangle$) on who is (or is not) a fit individual.

² The identification of genes as spins in a lattice, heralded by this name, will become clearer as we build up the theory. At this stage, it is only a formal similarity.

We need to provide an explicit expression for $F(g)$; previous researchers have explored different possibilities³. We consider only the type of fitness functions with linear and pairwise interactions:

$$F(g) = \bar{F} + \sum_i f_i s_i + \sum_{i < j} f_{ij} s_i s_j . \quad (3)$$

\bar{F} is a constant, irrelevant for eq.(2). The first order contribution f_i represent the *additive fitness* at locus i , which influences fitness independently of all other loci in the genome. Higher terms such as f_{ij} (and f_{ijk}, f_{ijkl}, \dots if they were present) represent genetic interactions between loci, also called *epistasis*. We characterize total fitness as a functional of the *a priori* fitness function as

$$\sigma(f) = \sqrt{\sum_i f_i^2 + \sum_{i < j} f_{ij}^2} , \quad (4)$$

Analogously we define epistatic fitness by σ_e , with the same definition as eq.(4) except that only the epistatic contribution appears and the additive fitness by σ_a analogously. As it is clear from eq.(2), $F(g)$ has dimension $[t^{-1}]$, by consequence the same is true for all the coefficients f_i, f_{ij}, \dots and for $\sigma, \sigma_e, \sigma_a$.

It is worth noting that fitness in statistical genetics plays a similar role as energy (modulo a minus sign) in statistical mechanics. The terminology of *fitness landscape* underlines the analogy with an energy landscape: $F(g)$ would be an Hamiltonian $-\mathcal{H}$ in statistical physics. We can further exploit this analogy to depict the evolutionary process of a population as an erratic motion of a point *on* the fitness landscape: contrary to what happens in an energy landscape, where the systems slides toward the valleys (min. energy), we will see here our point particle climbing the fitness hill as much as possible (to where the expected number of offspring is highest).

1.2.3. Mutations

The definition of mutation includes a multitude of different biological mechanism whose effect is to modify the genome sequence. Our model includes only single-locus swap $s_i \rightarrow -s_i$.

In mathematical terms one introduces an operator M_i the action of which on a genomic sequence is to swap the i -th bi-allelic gene *i.e.*

$$M_i(s_1, \dots, s_i, \dots, s_L) = (s_1, \dots, -s_i, \dots, s_L) .$$

Let also μ be the tunable *mutation parameter* we need to weight the mutation mechanism in our model. We assume it to be constant in time and the same for all loci; analogously to σ it has dimensions $[t^{-1}]$, it is a rate. The mutation term in the master equation will simply take the form

$$\frac{d}{dt} \Big|_{mut} P(g, t) = \mu \sum_{i=1}^L [P(M_i g, t) - P(g, t)] . \quad (5)$$

³ See for example [8] for a detailed discussion of the cases $F(g) = \sum_i s_i$ (Fujiyama landscape) or $F(g) = \epsilon \delta_{gg_0}$ (sharp-peak landscape).

1.2.4. Recombination

Through mating and recombination, two parents $g^{(1)}, g^{(2)}$ mix their genomic sequences giving birth to two new individuals g, g' . The mechanism we here have in mind is the *crossing over of homologous gametes during meiosis where haploid individuals produce an haploid offspring*. Albeit relatively simple, this is sufficient to describe some forms of bacterial recombination (transformation, transduction where material goes in both ways) as well as recombination in several RNA viruses including HIV and coronaviruses. In contrast, it cannot model some other biological mechanisms of genes-mixing, for instance bacterial conjugation.⁴

Following [12] it is convenient to introduce a set of random variables $\{\xi_i\}$ to describe recombination by defining a crossover pattern. Consider the gene at locus i of the new individual g , if it has been inherited from $g^{(1)}$ then $\xi_i = 1$ while if it comes from $g^{(2)}$ then $\xi_i = 0$. The sequence g' is simply complementary to g . In symbols g, g' can be written as

$$\begin{aligned} \mathbf{g} : s_i &= \xi_i s_i^{(1)} + (1 - \xi_i) s_i^{(2)} , \\ \mathbf{g}' : s'_i &= (1 - \xi_i) s_i^{(1)} + \xi_i s_i^{(2)} . \end{aligned} \quad (6)$$

Each different crossover pattern $\{\xi_i\}$ comes with a probability $C(\xi)$. Similarly to the mutation case, let r be the tunable *overall recombination parameter* (dimensions $[t^{-1}]$) which in this case can be accompanied by a relative parents-dependent rate $Q(g^{(1)}, g^{(2)})$ (dimensionless). Collecting everything we have so far, it is possible to express the time variation of the genomic sequence due to recombination as

$$\frac{d}{dt} \Big|_{rec} P(g, t) = r \sum_{\xi, g'} C(\xi) \left[Q(g^{(1)}, g^{(2)}) P_2(g^{(1)}, g^{(2)}, t) - Q(g, g') P_2(g, g', t) \right] , \quad (7)$$

where the sum runs over all possible recombination patterns and all possible sequences g' and P_2 is the two-genome distribution (read two-particle distribution). Two more steps:

- ★ Until further notice, we set $Q(g_\alpha, g_\beta) = 1 \forall g_\alpha, g_\beta$ which means that any genome pair has the same recombination rate r : this means assuming of a *panmictic* population, where any individual is equally likely to interact with anyone else.
- ★ It is hard to handle eq.(7) without a *closure*, so we will also assume that

$$P_2(g_\alpha, g_\beta) = P(g_\alpha)P(g_\beta) , \quad (8)$$

which is valid if genomic sequences undergoing recombination are uncorrelated. This assumption is crucial and we will come back to it. The recombination process is therefore akin to a collision process in the kinetic theory of gases where

⁴In [12], Neher and Shraiman model recombination of a slightly different kind: two parents each produce a mating body (copy of genome) and these two merge and give birth to a new individual while the remaining half of genetic material is discarded. This models the sexual recombination in some fungi, and lead to slightly simpler arguments. However, on the level of analysis used here, the resulting evolution are the same.

eq.(8) is Boltzmann's *molecular chaos hypothesis* (or *Stoßzahlansatz*): the velocities of colliding particles are uncorrelated, and independent of position. As in Physics so in Biology (8) is *never* exactly true. In a realistic biological environment, several phenomena introduce correlations between different individuals *e.g.* competition for limited resources, geographical separation, existence of classes of individuals, or *phylogenetic* effects. We will assume that such correlations are weak enough for eq.(8) to hold approximately.

Inserting these assumptions in eq.(7) we have

$$\frac{d}{dt} \Big|_{rec} P(g, t) = r \sum_{\xi, g'} C(\xi) \left[P(g^{(1)}, t) P(g^{(2)}, t) - P(g, t) P(g', t) \right]. \quad (9)$$

1.2.5. Dynamics of Genotype Distribution

The aim in this section is to parameterize the distribution $P(g, t) \forall g$ by its cumulants⁵. The cumulants of first and second order are $\chi_i = \langle s_i \rangle$ and $\chi_{ij} = \langle s_i s_j \rangle - \langle s_i \rangle \langle s_j \rangle$. According to this definition the one-locus second-order cumulant is $\chi_{ii} = 1 - \chi_i^2$. It is hence not an independent quantity, but allows to state some formulae more compactly. we also define the frequency $\nu_i(\alpha)$ of the allele α at locus i and the element of the covariance matrix $M_{ij}(\alpha, \beta)$ relative to the alleles α, β at loci i, j as

$$\begin{aligned} \nu_i(\alpha) &= \langle \delta_{\alpha, s_i} \rangle, \\ M_{ij}(\alpha, \beta) &= \langle \delta_{\alpha, s_i} \delta_{\beta, s_j} \rangle - \langle \delta_{\alpha, s_i} \rangle \langle \delta_{\beta, s_j} \rangle, \end{aligned} \quad (10)$$

it is easy to find relations with the $\{\chi_i, \chi_{ij}\}$: $\nu_i(1) = \frac{1}{2}(1 + \chi_i)$, $\nu_i(-1) = \frac{1}{2}(1 - \chi_i)$ and $M_{ij}(1, 1) = -M_{ij}(1, -1) = -M_{ij}(-1, 1) = M_{ij}(-1, -1) = \frac{1}{4}\chi_{ij}$.

The starting point is now the full master equation for the evolution of $P(g)$ obtained by plugging in (2), (5) and (9) into eq.(1):

$$\begin{aligned} \frac{d}{dt} P(g, t) &= [F(g) - \langle F \rangle] P(g, t) + \mu \sum_{i=1}^L [P(M_i g, t) - P(g, t)] + \\ &+ r \sum_{\xi, g'} C(\xi) \left[P(g^{(1)}, t) P(g^{(2)}, t) - P(g, t) P(g', t) \right], \end{aligned} \quad (11)$$

valid in the limit $N \rightarrow \infty$. Now that the time dependencies are clear, we also drop the t in order to lighten the notation as much as possible. It is straightforward to obtain dynamical equations for χ_i and χ_{ij} , as shown below.

$\dot{\chi}_i$. We observe that the recombination term has no effect on the dynamics of χ_i as can be verified explicitly; this is understood in light of the fact that recombination does not create nor destroy alleles, it simply reshuffles them. Neglecting the last

⁵For an introduction and discussion on cumulants, see App.(A).

term in eq.(11) one has

$$\begin{aligned}
\dot{\chi}_i &= \frac{d}{dt} \left(\sum_g s_i P(g) \right) \\
&= \sum_g s_i \frac{d}{dt} P(g) \\
&= \sum_g \left(s_i [F(g) - \langle F \rangle] P(g) + \mu s_i \sum_{j=1}^L [P(M_j g) - P(g)] \right) \\
&= \langle s_i [F(g) - \langle F \rangle] \rangle - 2\mu \langle s_i \rangle , \tag{12}
\end{aligned}$$

where the last line follows from $\sum_g s_i P(M_j g) = (-1)^{\delta_{ij}} \langle s_i \rangle$.

$\dot{\chi}_{ij}$. The dynamics of the second order cumulant (and in general all higher order cumulants) involves the recombination term. As a preliminary result, let us evaluate the time derivative of $\langle s_i s_j \rangle$ under the recombination term alone⁶:

$$\begin{aligned}
\frac{d}{dt} \Big|_{rec} \langle s_i s_j \rangle &= \sum_{\xi, g, g'} C(\xi) s_i s_j \left[P(g^{(1)}) P(g^{(2)}) - P(g) P(g') \right] \\
&\stackrel{(a)}{=} \sum_{\xi, g^{(1)}, g^{(2)}} \left[C(\xi) (\xi_i s_i^{(1)} + (1 - \xi_i) s_i^{(2)}) \times \right. \\
&\quad \times \left. (\xi_j s_j^{(1)} + (1 - \xi_j) s_j^{(2)}) P(g^{(1)}) P(g^{(2)}) \right] + \\
&\quad - \sum_{\xi, g, g'} C(\xi) s_i s_j P(g) P(g') \\
&= \sum_{\xi} C(\xi) \left[\xi_i \xi_j \langle s_i s_j \rangle + \xi_i (1 - \xi_j) \langle s_i \rangle \langle s_j \rangle + \right. \\
&\quad \left. + (1 - \xi_i) \xi_j \langle s_i \rangle \langle s_j \rangle + (1 - \xi_i) (1 - \xi_j) \langle s_i s_j \rangle - \langle s_i s_j \rangle \right] \\
&= \langle s_i s_j \rangle \sum_{\xi} C(\xi) (1 - \xi_i - \xi_j + \xi_i \xi_j - 1) + \\
&\quad + \langle s_i \rangle \langle s_j \rangle \sum_{\xi} C(\xi) (\xi_i (1 - \xi_j) - (1 - \xi_i) \xi_j) \\
&\stackrel{(b)}{=} - c_{ij} \chi_{ij} . \tag{13}
\end{aligned}$$

In (a) we have used eq.(6) and changed the first sum over g, g' in a sum over $g^{(1)}, g^{(2)}$; in (b) we have exploited the definition of χ_{ij} and introduced a new characteristic quantity

$$c_{ij} = \sum_{\xi} C(\xi) (\xi_i (1 - \xi_j) + (1 - \xi_i) \xi_j) . \tag{14}$$

⁶ The reader will easily notice how, following the same steps of this derivation but in the easier case of a single $\langle s_i \rangle$, one gets $\frac{d}{dt} \Big|_{rec} \langle s_i \rangle = 0$.

We now have all that is needed to evaluate, for $i \neq j$,

$$\begin{aligned}
\dot{\chi}_{ij} &= \frac{d}{dt}(\langle s_i s_j \rangle - \chi_i \chi_j) \\
&= \frac{d}{dt} \langle s_i s_j \rangle - \dot{\chi}_i \chi_j - \chi_i \dot{\chi}_j \\
&\stackrel{(a)}{=} \langle s_i s_j \left[[F(g) - \langle F \rangle] \right\rangle + \mu \sum_g s_i s_j \sum_{k=1}^L [P(M_k g) - P(g)] \right\rangle + r \frac{d}{dt} \Big|_{rec} \langle s_i s_j \rangle \\
&\quad + 4\mu \chi_i \chi_j - \langle s_i [F(g) - \langle F \rangle] \rangle \chi_j - \chi_i \langle s_j [F(g) - \langle F \rangle] \rangle \\
&\stackrel{(b)}{=} \langle (s_i - \chi_i)(s_j - \chi_j) [F(g) - \langle F \rangle] \rangle - 4\mu \langle s_i s_j \rangle + r \frac{d}{dt} \Big|_{rec} \langle s_i s_j \rangle + 4\mu \chi_i \chi_j \\
&\stackrel{(c)}{=} \langle (s_i - \chi_i)(s_j - \chi_j) [F(g) - \langle F \rangle] \rangle - 4\mu \chi_{ij} - r c_{ij} \chi_{ij} . \tag{15}
\end{aligned}$$

In (a) we have used eq.(11-12); in (b) we exploited $\sum_g s_i s_j P(M_k g) = (-1)^{\delta_{ik} + \delta_{jk}} \langle s_i s_j \rangle$ and added $\chi_i \chi_j \langle F(g) - \langle F \rangle \rangle = 0$; (c) comes again from the definition of χ_{ij} and from eq.(13).

The eq.(12) and (15) are at the core of the KNS theory of statistical genetics. It is important to underline that so far we have not made any specific choice for $P(g)$. However, before we go any further, let us add a few comments on the results we got so far.

* c_{ij} . Given the definition eq.(14), c_{ij} can be easily interpreted as the probability that, in the offspring, the alleles at the two loci i, j come from different parents. When recombinations are completely random, we clearly expect $c_{ij} = 1/2 \forall i, j$. Let us discuss how it is possible to guess the value of c_{ij} .

o **Crossover rate.** One easy way to get c_{ij} is to assume that, if there is recombination between two genomes, then each locus undergoes a crossover with probability ω , which we call *crossover rate*. We will show now that this completely determines c_{ij} .

Consider for simplicity a population of only two individuals $g^{(A)} = \{s_i^{(A)}\}_{i=1}^L$ and $g^{(B)} = \{s_i^{(B)}\}_{i=1}^L$. A crossover event in the k -th site means $s_k^{(A)} \leftrightarrow s_k^{(B)}$ (exchanged). Note that the crossover rate ω for each site i does not depend on the present value of the spin $s_i^{(A)} = \pm 1$ but it only refers to the labels A, B ; explicitly, if there is a recombination, then $P(A \rightarrow B \wedge B \rightarrow A) = \omega$ and $P(A \rightarrow A \wedge B \rightarrow B) = 1 - \omega$. In order to emphasise this, we temporarily clean the notation in the following way $g^{(A)} = \{A_i\}_{i=1}^L$ and $g^{(B)} = \{B_i\}_{i=1}^L$. Let us now focus on the loci i, j and suppose that there is a recombination event, one possible result is for instance:

$$\begin{aligned}
g^{(A)}; g^{(B)} &: (\dots A_i \dots A_j \dots); (\dots B_i \dots B_j \dots) \\
g^{(D_1)}; g^{(D_2)} &: (\dots A_i \dots B_j \dots); (\dots B_i \dots A_j \dots)
\end{aligned}$$

where $g^{(D_1)}$ is the genome of the descendant D_1 and analogously for $g^{(D_2)}$. We do not lose information if we focus on just one of them, say $g^{(D_1)}$.

With respect to the alleles in the loci i, j of $g^{(D_1)}$, it is possible to define two states: $T = (A_i A_j) \cup (B_i B_j)$ if it is true that those allele come from the

same parent and $F = (A_i B_j) \cup (B_i A_j)$ otherwise. As can be easily found, starting from a T state before a recombination event, the probability that after the recombination the state is found to be F is $c_{ij} = 2\omega(1 - \omega)$. In this first model the coefficient c_{ij} ignores any spatial effect, it is the same for all pairs i, j , regardless of their position in the genome (could they be neighbours or very far apart). This is certainly not biologically realistic in many (most) settings, wherefore we turn to

- o **Neighbouring variability.** (an approach also adopted in [13]). If two loci are very far apart then we expect them to be mostly uncorrelated, hence we need to introduce a penalization for genomic distance. Assume a fixed probability ρ that a recombination causes a crossover such that ξ_i is flipped with respect to ξ_{i+1} . In other words, the assumption is here that the rate of recombination happening is the same between each pair of neighboring loci. The simplification with respect to Biology is on the one hand that loci of variability can be spaced unevenly along a genome, and that recombination may happen at a higher rate at certain genomic positions ("recombination hot-spots").

Keeping a similar notation as in the previous case, before recombination one has

$$g^{(A)} = (\dots - A_i - A_{i+1} - A_{i+2} - \dots - A_{j-2} - A_{j+1} - A_j - \dots)$$

$$g^{(B)} = (\dots - B_i - B_{i+1} - B_{i+2} - \dots - B_{j-2} - B_{j+1} - B_j - \dots)$$

After the recombination event, focusing again on just one of the new chains, one possible result is:

$$g^{(D_1)} = (\dots - A_i \stackrel{T}{-} A_{i+1} \stackrel{F}{-} B_{i+2} \stackrel{T}{-} \dots \stackrel{T}{-} A_{j-2} \stackrel{F}{-} B_{j-1} \stackrel{T}{-} B_j - \dots)$$

Where the T, F indicate whether it is true/false that the two neighbouring loci come from the same parent, there are $n = |i - j|$ of them. According to our hypothesis, the outcome F has probability $P(F) = \rho$ and $P(T) = 1 - \rho$. As a first approximation, the number of F can be assumed to be binomial distributed⁷: the probability that we find a number k of F is $P(k; n, \rho) = \binom{n}{k} \rho^k (1 - \rho)^{n-k}$.

To get the total probability that alleles at i, j are different after a recombi-

⁷How is it possible? One has a binomial distribution if the T, F are independent "draws from an urn", which is apparently in sharp contrast with their definition. In practice, the loci that here appear as neighbours are not physically so: when dealing with a real genomic chain, typically we will analyze only a small subset of all the loci (for instance, those that show substantial variability), that we here "tie together" in our ideal model. Since in general these loci are physically separated by a number of bases, it is possible to assume that T/F at the two sides of the same locus (as above) are independent.

nation, it is sufficient to sum $P(k; n, \rho)$ over all odd k :

$$\begin{aligned}
c_{ij} &= \sum_{k \text{ odd}}^n \binom{n}{k} \rho^k (1-\rho)^{n-k} \\
&= \frac{1}{2} \left[\sum_{k=0}^n \binom{n}{k} \rho^k (1-\rho)^{n-k} - \sum_{k=0}^n \binom{n}{k} (-\rho)^k (1-\rho)^{n-k} \right] \\
&= \frac{1}{2} [(\rho + (1-\rho))^n - (-\rho + (1-\rho))^n] \\
&= \frac{1}{2} [1 - (1-2\rho)^n] \\
&\simeq \frac{1}{2} [1 - e^{-2\rho|i-j|}] , \tag{16}
\end{aligned}$$

where the last line holds if $\rho|i-j| \sim 1$ and $|i-j| \gg 1$. In the limit $|i-j| \rightarrow \infty$ we find (consistently) $c_{ij} \sim 1/2$.

* **Linkage (dis)equilibrium.** The words *linkage disequilibrium* (LD) stand for a non-random association of alleles at two or more loci [14]. Contrary to what the name may suggest, LD does not ensure either linkage or a lack of equilibrium. Focusing on LD for a pair of loci, several definitions have been proposed, for instance as $M_{ij}(\alpha, \beta)$ defined in eq.(10), but all of them are obviously related to the quantity $\chi_{ij} = \langle s_i s_j \rangle - \chi_i \chi_j$. The absence of correlation $\chi_{ij} = 0 \forall i \neq j$ is naturally termed *linkage equilibrium* (LE) and implies no correlations between loci. If the population only evolved under mutation and recombination then χ_{ij} tends to zero. The KNS model provides us with a law for the evolution of this last quantity, namely eq.(15), from which we see how selection drives χ_{ij} away from zero, while mutations and recombination act in the opposite way. The tendency of natural selection is indeed to fix the most fit alleles in a population. If this process is run to completion all individuals are identical and variability is lost. In that limit of extreme LD the population may be said to be in a (trivial) state of linkage equilibrium, as all quantities χ_{ij} vanish.

Between LE and LD there is an intermediate phase of weak and steady correlations between loci called *quasi-linkage equilibrium* (QLE): this is the topic for the next section.

1.3. Quasi-Linkage Equilibrium: KNS Theory

The last ingredient we need to master eq.(11) is a specific mathematical form for the distribution $P(g)$. The fundamental insight came from the pioneering work of Motoo Kimura in 1965 [11], where he showed that in a population genetics model which includes recombination, if selection is weak on the time scale of recombination $\sigma \ll r$ then the allele frequencies change slowly and the selection-induced correlations are weak, steady and can be treated as a perturbation. Such a state for a population Kimura termed *quasi-linkage equilibrium* (QLE). In the following presentation we follow [12] where the problem is considered on the genome scale and not only for one pair of loci. The authors of [12] introduced the following *ansatz* for the parameterization

of the one-genome probability distribution:

$$P(g, t) = \frac{1}{\mathcal{Z}(t)} \exp \left(\sum_i h_i(t) s_i + \sum_{i < j} J_{ij}(t) s_i s_j \right) \quad (17)$$

Obviously (17) is the Gibbs-Boltzmann distribution of an Ising model with time dependent parameters. The factor $\mathcal{Z}(t) = \sum_g \exp \left(\sum_i h_i(t) s_i + \sum_{i < j} J_{ij}(t) s_i s_j \right)$ is a normalization (partition function) while $h_i(t)$ and $J_{ij}(t)$ are time dependent single-site and pairwise coefficients (external magnetic fields and interactions), respectively; we will drop again the t from now on.

We here implement the QLE hypothesis: the second order terms $\{J_{ij}\}$ capture to the leading order the correlations induced by selection, hence they are assumed to be small. The exponential distribution in eq.(17) satisfies (like all equilibrium distributions in statistical physics) a *maximum entropy principle* [15]: it is the one that maximizes information (Shannon entropy) under the constraints of having $\{\chi_i\}$ and $\{\chi_{ij}\}$ as first and second order cumulants, see Sec.(2) and App.(E). The following relations hold:

$$\chi_i = \frac{\partial \log \mathcal{Z}}{\partial h_i}, \quad \chi_{ij} = \frac{\partial^2 \log \mathcal{Z}}{\partial h_i \partial h_j}, \quad (18)$$

as can be easily verified. Let us evaluate these quantities in the QLE regime: we first evaluate perturbatively the partition function,

$$\begin{aligned} \mathcal{Z} &= \sum_g e^{\sum_i h_i s_i + \sum_{i < j} J_{ij} s_i s_j} \\ &\stackrel{(a)}{=} \sum_g e^{\sum_i h_i s_i} \left(1 + \sum_{k < j} J_{kj} s_k s_j \right) \\ &= \sum_g e^{\sum_i h_i s_i} + \sum_{k < j} J_{kj} \sum_g e^{\sum_i h_i s_i} s_k s_j \\ &= \prod_i 2 \cosh h_i + \sum_{k < j} J_{kj} \left(\prod_{i \neq j \neq k} 2 \cosh h_i \right) (2 \sinh h_k) (2 \sinh h_j) \\ &= 2^L \left(1 + \sum_{k < j} J_{kj} \tanh h_k \tanh h_j \right) \prod_i \cosh h_i, \end{aligned} \quad (19)$$

where in (a) we have used $J_{ij} \sim 0 \ \forall i \neq j$ and expanded to the first order in $|J_{ij}|$. Using eq.(18) we get

$$\begin{aligned}
\chi_i &\sim \frac{1}{\mathcal{Z}} \frac{\partial}{\partial h_i} \left[2^L \left(1 + \sum_{k < j} J_{kj} \tanh h_k \tanh h_j \right) \prod_i \cosh h_i \right] \\
&= \frac{2^L}{\mathcal{Z}} \left[\left(1 + \sum_{k < j} J_{kj} \tanh h_k \tanh h_j \right) \prod_{l \neq i} \cosh h_l \sinh h_i + \right. \\
&\quad \left. + \left(1 + \sum_{i \neq j} J_{ij} \frac{\tanh h_j}{\cosh^2 h_i} \right) \prod_i \cosh h_i \right] \\
&\sim \tanh h_i + \frac{1}{1 + \sum_{k \neq j} J_{kj} \tanh^2 h_k \tanh h_j} \sum_{i \neq j} J_{ij} (1 - \tanh^2 h_i) \tanh h_j \\
&\sim \tanh h_i + \sum_{i \neq j} J_{ij} (1 - \tanh^2 h_i) \tanh h_j
\end{aligned} \tag{20}$$

$$\chi_{ii} \stackrel{(a)}{\sim} 1 - \tanh^2 h_i \stackrel{(b)}{\sim} 1 - \chi_i^2 \tag{21}$$

$$\chi_{ij} \stackrel{(a)}{\sim} J_{ij} (1 - \tanh^2 h_i) (1 - \tanh^2 h_j) \stackrel{(b)}{\sim} J_{ij} (1 - \chi_i^2) (1 - \chi_j^2) \tag{22}$$

where in (a) we have derived eq.(20) w.r.t. h_i or h_j , while in (b) we have used again eq.(20), upon moving the sum to the LHS. All of the eq.(20 - 22) are correct to the first order in $|J_{ij}|$. One final remark to stress that QLE is very reminiscent of the high-temperature expansion.

1.3.1. The Central Result of KNS theory

The goal now is to understand the dynamics of the parameters in the genotype distribution as a function of the KNS-theory parameters $\mu, r, \{f_i\}, \{f_{ij}\}$ and the observable first and second order cumulants. Before delving into calculations, let us recap the assumptions we have already made:

- (1) In eq.(8) a closure: the two-genome distribution factorizes.
- (2) In eq.(17) a one-particle distribution function of the generalized Ising form.
- (3) Couplings $\{J_{ij}\}$ small and treated as perturbations in the QLE regime of small correlations.

In addition, as done in [12] we introduce for simplicity one last assumption:

- iv. The mutational contribution can be omitted, the mutation rate is sufficiently small for the approximation $\mu \sim 0$ to be valid.

Note that it cannot be $\mu = 0$ otherwise QLE in an infinite population would only be a long-lived transient as the population drifts towards fixation, see eq.(12). Non-zero mutations are necessary to maintain any variability, yet we are assuming that their rate is *small enough* to forget their contribution in what comes next.

If we now rewrite eq.(11) as an equation for $\log P(g)$ and substitute eq.(17) we get:

$$-\frac{\dot{\mathcal{Z}}}{\mathcal{Z}} + \sum_i \dot{h}_i s_i + \sum_{i < j} \dot{J}_{ij} s_i s_j = F(g) - \langle F \rangle + r \sum_{\xi, g'} C(\xi) P(g') \left[\frac{P(g^{(1)}) P(g^{(2)})}{P(g) P(g')} - 1 \right] \quad (23)$$

Let us analyze separately the last term of the RHS. For simplicity, we set $\bar{\xi}_i = 1 - \xi_i$:

$$\begin{aligned} & \sum_{\xi, g'} C(\xi) P(g') \left[\frac{P(g^{(1)}) P(g^{(2)})}{P(g) P(g')} - 1 \right] = \\ & \stackrel{(a)}{=} \sum_{\xi, g'} C(\xi) P(g') \left(e^{\sum_{i < j} J_{ij} [(\xi_i s_i + \bar{\xi}_i s'_i)(\xi_j s_j + \bar{\xi}_j s'_j) + (\bar{\xi}_i s_i + \xi_i s'_i)(\bar{\xi}_j s_j + \xi_j s'_j) - s_i s_j - s'_i s'_j]} - 1 \right) \\ & = \sum_{\xi, g'} C(\xi) P(g') \left(e^{\sum_{i < j} J_{ij} [(\xi_i \xi_j + \bar{\xi}_i \bar{\xi}_j - 1)(s_i s_j + s'_i s'_j) + (\xi_i \bar{\xi}_j + \bar{\xi}_i \xi_j - 1)(s_i s'_j + s'_i s_j)]} - 1 \right) \\ & \stackrel{(b)}{\approx} \sum_{\xi, g'} C(\xi) P(g') \sum_{i < j} J_{ij} [(\xi_i \xi_j + \bar{\xi}_i \bar{\xi}_j - 1)(s_i s_j + s'_i s'_j) + (\xi_i \bar{\xi}_j + \bar{\xi}_i \xi_j)(s_i s'_j + s'_i s_j)] \\ & \stackrel{(c)}{=} \sum_{\xi} C(\xi) \sum_{i < j} J_{ij} [(\xi_i \xi_j + \bar{\xi}_i \bar{\xi}_j - 1)(s_i s_j + \langle s_i s_j \rangle) + (\xi_i \bar{\xi}_j + \bar{\xi}_i \xi_j)(s_i \langle s_j \rangle + \langle s_i \rangle s_j)] \\ & \stackrel{(d)}{=} \sum_{i < j} c_{ij} J_{ij} [(s_i \langle s_j \rangle + \langle s_i \rangle s_j) - (s_i s_j + \langle s_i s_j \rangle)] \end{aligned} \quad (24)$$

In (a) we have used eq.(17), inverted the relations eq.(6) to express $s_i^{(1)} = \xi_i s_i + \bar{\xi}_i s'_i$, $s_i^{(2)} = \bar{\xi}_i s_i + \xi_i s'_i$, clearly $s_i^{(2)} + s_i^{(1)} - s_i + s'_i = 0$ cancel for each field h_i ; in (b) we have expanded to the first order in $|J_{ij}|$; in (c) we have averaged over $P(g')$; in (d), finally, we have used $c_{ij} = \sum_{\xi} C(\xi) (\xi_i \bar{\xi}_j + \bar{\xi}_i \xi_j) = \sum_{\xi} C(\xi) (1 - \xi_i \xi_j - \bar{\xi}_i \bar{\xi}_j)$.

Substituting eq.(24) into eq.(23) and using eq.(3) we get:

$$\begin{aligned} & -\frac{\dot{\mathcal{Z}}}{\mathcal{Z}} + \sum_i \dot{h}_i s_i + \sum_{i < j} \dot{J}_{ij} s_i s_j = \\ & = \bar{F} - \langle F \rangle + \sum_i f_i s_i + \sum_{i < j} f_{ij} s_i s_j + r \sum_{i < j} c_{ij} J_{ij} [(s_i \langle s_j \rangle + \langle s_i \rangle s_j) - (s_i s_j + \langle s_i s_j \rangle)] \end{aligned} \quad (25)$$

Dynamical equations for $\{h_i, J_{ij}\}$ emerge when collecting together terms with the same monomials in s_i :

$$\dot{h}_i = f_i + r \sum_{j \neq i} c_{ij} J_{ij} \chi_j \quad (26)$$

$$\dot{J}_{ij} = f_{ij} - r c_{ij} J_{ij} \quad (27)$$

In the case where the recombination rate is very high $\sigma/r \ll 1$, the $\{J_{ij}\}$ rapidly reach the steady state, which deserves to be emphasized:

$$f_{ij} = J_{ij} \cdot rc_{ij} \quad (28)$$

This is a crucial result for the KNS theory because it paves the way for the inference of the epistatic fitness landscape encoded in the $\{f_{ij}\}$ from the couplings $\{J_{ij}\}$ that, even if not observable, can be inferred from data. We will extensively discuss and exploit this observation in Sec.(2). Finally, substituting the steady-state eq.(28) in eq.(26), we find

$$\dot{h}_i = f_i + \sum_{j \neq i} f_{ij} \chi_j = \hat{f}_i , \quad (29)$$

where \hat{f}_i is the effective strength of selection on locus i and it collects the contribution of every χ_i by means of the epistatic interaction. From eq.(21 - 22) we note that while the χ_{ii} depends exclusively on the frequency χ_i , the off-diagonal correlations are determined by the trade-off between epistasis and recombination *i.e.* σ_e/r .

In conclusion of our discussion on the QLE phase, let us look at its consequences for the dynamics of the first and second order cumulants.

In view of eq.(28) and considering eq.(15) with $\mu \sim 0$, the correlations will rapidly approach the expression:

$$\bar{\chi}_{ij} = \frac{f_{ij}}{rc_{ij}} (1 - \chi_i^2)(1 - \chi_j^2) , \quad i \neq j . \quad (30)$$

Neglecting all terms but the one due to recombination in eq.(15), we can write the dynamics of the second order cumulants χ_{ij} as an exponential decay to the asymptotic value $\bar{\chi}_{ij}$ *i.e.*

$$\chi_{ij} = \bar{\chi}_{ij} (1 - e^{-rc_{ij}t}) , \quad (31)$$

whose dynamic is indeed driven by the ordinary differential equation

$$\dot{\chi}_{ij} = rc_{ij} \bar{\chi}_{ij} e^{-rc_{ij}t} \stackrel{(a)}{=} rc_{ij} (\bar{\chi}_{ij} - \chi_{ij}) \stackrel{(b)}{=} f_{ij} (1 - \chi_i^2)(1 - \chi_j^2) - rc_{ij} \chi_{ij} , \quad (32)$$

where in (a) we have used eq.(31) and in (b) eq.(30).

The first order cumulants instead evolve according to the following dynamical equations:

$$\dot{\chi}_i \stackrel{(a)}{=} \langle s_i F \rangle - \chi_i \langle F \rangle = \partial_{h_i} \langle F \rangle \stackrel{(b)}{\sim} \sum_j \partial_{\phi_i} \chi_j \partial_{\chi_j} \langle F \rangle \stackrel{(c)}{=} \sum_j \chi_{ij} \partial_{\chi_j} \langle F \rangle , \quad (33)$$

where in (a) we have used eq.(12) with $\mu = 0$; in (b) the chain rule of differentiation; in (c) the fact that $\chi_{ij} = \partial \chi_i / \partial h_j$, see eq.(18). We see from the RHS of eq.(33) that the allele means evolve so to maximize $\langle F \rangle$, there are L such equations and they are all coupled by the correlations $\{\chi_{ij}\}$.

This is nevertheless an enormous simplification with respect to the 2^L ordinary differential equations for each possible g that we would have in general: in the QLE regime

where $\sigma/r \ll 1$ and the correlations rapidly approach their steady state, the L eq.(33) are the only relevant dynamical equations and they define the L -dimensional *QLE manifold*. As long as the QLE holds, the genotype distribution (hence the population average of any trait) is confined on such manifold *i.e.* it can be parameterized by the set of time-dependent first cumulants $\{\chi_i(t)\}$.

For variations of the theory presented here to finite-size populations or to genomes with multi-allelic loci, we refer to App. B and App. C, respectively.

2. Inverse Statistical Physics: Direct Coupling Analysis (DCA)

In Section 1, under Quasi-Linkage Equilibrium conditions, we paved the way for the inference from data of the epistatic fitness landscape by means of eq.(28). Yet this last equation does not directly relate the $\{f_{ij}\}$ to statistics of the data, instead we there see in the RHS the couplings $\{J_{ij}\}$ of the Ising-like eq.(17) that, by assumption, describes the one-genome distribution.

From the point of view of statistics the task of DCA is to find the parameters in a family of generating functions, the exponential family of the Gibbs-Boltzmann distributions of equilibrium statistical mechanics [16,17]. While maximum likelihood and analogous Bayesian point estimate methods are feasible for small enough instances, for larger instance these become computationally demanding. A number of alternative inference methods have therefore been invented, of which the most widely used are mean-field or variational methods [16,18], and pseudo-likelihood maximization [19,20], to which one can add its more recent extensions [21–23].

From the view of computational biology DCA was proposed as a general data analysis tool motivated by maximum-entropy arguments *e.g.* in [24]. A major breakthrough was made in relating the parameters in a model inferred from protein sequences in the same family to physical proximity of residues in the common protein structure [25–38]; recently DCA-based method have however been overtaken by AI/deep learning methods in this application [39,40]. For other biological inference tasks with less abundant number of training examples and/or where the goal is uncover new biology DCA remain an important tool *cf.* [41–47]. The applications of DCA and DCA-like techniques to biology has been reviewed multiple times *e.g.* [10,48–50].

Our perspective here is one of statistical genetics. In contrast to pure data-driven models we assume that distributions over genotypes in a population are actually of the Gibbs-Boltzmann type, and leverage the relations obtained in Section 1 to infer parameters describing an evolutionary process. While we follow the previous literature *e.g.* [17] as to methodology, the perspective and ultimate goal is somewhat different.

2.1. An Inverse Paradigm

2.1.1. Inverse Ising Problem

As a first step, we set the framework. Let us consider an Ising model with L binary spin variables⁸ $s_i = \pm 1$, with $i = 1, \dots, L$. The Hamiltonian for an Ising system reads

$$\mathcal{H}_{\mathbf{J}, \mathbf{h}}(\mathbf{s}) = - \sum_i h_i s_i - \sum_{i < j} J_{ij} s_i s_j, \quad (34)$$

where the \mathbf{J} are the pairwise couplings between the spin variables ($J_{ii} = 0 \ \forall i$) and the \mathbf{h} are the local magnetic fields; they are collectively referred as the *parameters* of the Ising problem. Under equilibrium conditions, the probability of a configuration \mathbf{s} is the Boltzmann distribution

$$p(\mathbf{s}) = \frac{1}{\mathcal{Z}} e^{-\mathcal{H}_{\mathbf{J}, \mathbf{h}}(\mathbf{s})}. \quad (35)$$

The inverse temperature β has been set to 1, this implies no loss of generality since in eq.(35) only the products βh_i and βJ_{ij} appear. The normalization \mathcal{Z} is the standard partition function

$$\mathcal{Z}(\mathbf{J}, \mathbf{h}) = \sum_{\mathbf{s}} e^{-\mathcal{H}_{\mathbf{J}, \mathbf{h}}(\mathbf{s})}. \quad (36)$$

The general expression for the expected value of a function $Q(\boldsymbol{\sigma})$ of the spin variables is

$$\langle Q(\boldsymbol{\sigma}) \rangle = \sum_{\mathbf{s}} p(\mathbf{s}) Q(\mathbf{s}); \quad (37)$$

In Sec. 1.2.5 we have already assigned the notations $\chi_i = \langle \sigma_i \rangle$ for the first order cumulant and $\chi_{ij} = \langle \sigma_i \sigma_j \rangle - \chi_i \chi_j$ for the second order cumulant. In this chapter it will be more convenient to use the moments instead, the first ones being the same χ_i as the first cumulants, the second ones defined as $\phi_{ij} = \langle \sigma_i \sigma_j \rangle = \chi_{ij} + \chi_i \chi_j$, see App.(A). In the present context, $\{\chi_i\}$ are the equilibrium *magnetizations* while $\{\phi_{ij}\}$ are the *pair correlations*. In the *Forward Ising Problem* the parameters \mathbf{J}, \mathbf{h} of the Boltzmann distribution eq.(35) are known and the job is to compute statistical *observables* e.g. χ_i, ϕ_{ij} . In an *Inverse Ising Problem* (IIP) the paradigm is reversed, let us emphasize it.

Statement of the Inverse Ising Problem (IIP)

Let $D = \{\mathbf{s}^m\}$, $m = 1, \dots, M$ be a set of independent samples of spin configurations of an Ising system the parameters of which are unknown. The goal of the IIP is to infer the parameters from D .

We note that IIP defined this way is also referred to as equilibrium Inverse Ising Problem. The problem of inferring the parameters of a kinetic Ising model, which may or may not satisfy detailed balance, is then analogously referred to a

⁸We use the notation s_i for a realization of the spin variable and σ_i indicates the spin random variable. When it is not confusing, the bold notation will indicate the whole set of spin variables $\mathbf{s} = \{s_i\}$. Analogously meaning for the bold notation for other quantities, e.g. \mathbf{J}, \mathbf{h} .

non-equilibrium Inverse Ising Problem. Depending on the kind of data available (a time series or not a time series) the non-equilibrium problem can be substantially easier or much harder than the equilibrium version, for more details, see [10,17]. In this work we will only deal with the *equilibrium reconstruction*, therefore from now on this specification will be implied.

2.1.2. Thermodynamics of the Inverse Ising Problem

The purpose of this subsection is to make the connection to the terminology of statistical mechanics. As noted above, temperature is not a pertinent concept for the inverse problem, as it cannot be separated from an overall scale of the model parameters. The starting point is thus *Helmholtz free energy* at a temperature which can conventionally be taken to be one:

$$\mathcal{F}(\mathbf{J}, \mathbf{h}) = -\log \mathcal{Z}(\mathbf{J}, \mathbf{h}) , \quad (38)$$

The right hand side of above is minus the logarithm of the partition function. In the forward problem, the first and second order moments can be evaluated by means of simple derivatives of eq.(38):

$$\chi_i = -\frac{\partial \mathcal{F}}{\partial h_i}(\mathbf{J}, \mathbf{h}) ; \quad \phi_{ij} = -\frac{\partial \mathcal{F}}{\partial J_{ij}}(\mathbf{J}, \mathbf{h}) = \frac{\partial \mathcal{F}}{\partial h_i}(\mathbf{J}, \mathbf{h}) \frac{\partial \mathcal{F}}{\partial h_j}(\mathbf{J}, \mathbf{h}) - \frac{\partial^2 \mathcal{F}}{\partial h_i \partial h_j}(\mathbf{J}, \mathbf{h}) \quad (39)$$

In the thermodynamical version of IIP the roles of the parameters \mathbf{J}, \mathbf{h} and the observables ϕ, χ are reversed: the latter are now fixed, the former to be determined. We seek accordingly a thermodynamic potential which is function of the observables and from which we can compute the parameters by means of simple derivatives, similarly to what is done in eq.(39) for the forward problem. As first noted in [51], we get such potential by operating a Legendre transform of the Helmholtz free energy with respect to both couplings and fields:

$$\mathcal{S}(\phi, \chi) = \min_{\mathbf{J}, \mathbf{h}} \left[-\sum_i h_i \chi_i - \sum_{i < j} J_{ij} \phi_{ij} - \mathcal{F}(\mathbf{J}, \mathbf{h}) \right] , \quad (40)$$

which can be seen to be the Shannon entropy function for the distribution eq.(35), see App.(E). To see how the parameters of the Ising model follow from the latter, we perform the inverse transformation (*i.e.* again a Legendre transform, which is its own inverse) to write

$$\mathcal{F}(\mathbf{J}, \mathbf{h}) = \min_{\phi, \chi} \left[-\sum_i h_i \chi_i - \sum_{i < j} J_{ij} \phi_{ij} - \mathcal{S}(\phi, \chi) \right] ; \quad (41)$$

setting the derivatives of the term in the square brackets to zero one gets

$$J_{ij} = -\frac{\partial \mathcal{S}}{\partial \phi_{ij}}(\phi, \chi) , \quad h_i = -\frac{\partial \mathcal{S}}{\partial \chi_i}(\phi, \chi) . \quad (42)$$

However, from eq.(39) we see that the derivatives of the Helmholtz free energy with respect to \mathbf{J} can be expressed in terms of those with respect to \mathbf{h} , therefore for our

purposes it is sufficient to operate a Legendre transform of the latter set. We define accordingly the *Gibbs free energy* as

$$\mathcal{G}(\mathbf{J}, \boldsymbol{\chi}) = \max_{\mathbf{h}} \left[\sum_i h_i \chi_i + \mathcal{F}(\mathbf{J}, \mathbf{h}) \right] \quad (43)$$

i.e. $\mathcal{G}(\mathbf{J}, \boldsymbol{\chi})$ is defined to be minus the Legendre transform of $\mathcal{F}(\mathbf{J}, \mathbf{h})$ with respect to \mathbf{h} , in view of the relation $\min f = -\max(-f)$. The magnetic fields can readily be computed with

$$h_i = \frac{\partial \mathcal{G}}{\partial \chi_i}(\mathbf{J}, \boldsymbol{\chi}) . \quad (44)$$

A great interest is in the second derivative of G with respect to the magnetizations

$$\frac{\partial^2 \mathcal{G}}{\partial \chi_i \partial \chi_j}(\mathbf{J}, \boldsymbol{\chi}) = \frac{\partial h_i}{\partial \chi_j}(\mathbf{J}, \boldsymbol{\chi}) \stackrel{(a)}{=} (\chi^{-1})_{ij} , \quad (45)$$

where in (a) we have used the inverse function theorem $[\partial \mathbf{h} / \partial \boldsymbol{\chi}]_{ij} = [(\partial \boldsymbol{\chi} / \partial \mathbf{h})^{-1}]_{ij}$ and the linear response theory to relate the second order cumulant $(\chi)_{ij} = \chi_{ij} = \partial \chi_j / \partial h_i(\mathbf{J}, \mathbf{h})$ to the susceptibility of the magnetization to a variation in the magnetic field [18]. Eq.(45) is the basis of *naive mean-field inference*: the RHS can be computed from data and, if \mathcal{G} is known, the corresponding system of equations can be solved yielding the couplings \mathbf{J} . We will discuss this straightforward and very useful method in Sec.(2.3).

Many of these methods are based on a *variational principle*; for the case of the Gibbs free energy it reads

$$\mathcal{G}(\mathbf{J}, \boldsymbol{\chi}) = \max_{\mathbf{h}} \left\{ \sum_i h_i \chi_i + \min_q \{U[q] - \mathcal{S}[q]\} \right\} , \quad (46)$$

which comes from eq.(43) and from the variational principle for the Helmholtz free energy

$$\mathcal{F}(\mathbf{J}, \mathbf{h}) = \min_q \{U[q] - \mathcal{S}[q]\} = \min_q \mathcal{F}[q] : \quad (47)$$

here q is a probability distribution for the spin configurations, $U[q] = \langle \mathcal{H} \rangle_q$ and $\mathcal{S}[q] = -\langle \log q \rangle_q$. Eq.(47) in turn stems from asking the *Kullback-Leibler distance* $D_{KL}(q||p)$ between the trial distribution q and the Boltzmann distribution p to be minimal, App.(E). The usefulness of this approach is lies in the fact that we may want to put constraints on q *i.e.* to focus on a particular family of trial distributions q , hence obtaining an upper bound for $\mathcal{F}(\mathbf{J}, \mathbf{h})$.

As a final remark, we observe that when q is taken from the set \mathcal{G} of distributions for which $\langle \sigma_i \rangle_q = \chi_i$, the double extremum problem eq.(46) is equivalent to the single conditional minimization

$$\mathcal{G}(\mathbf{J}, \boldsymbol{\chi}) = \min_{q \in \mathcal{G}} \left\{ - \sum_{i < j} J_{ij} \langle \sigma_i \sigma_j \rangle_q - \mathcal{S}[q] \right\} . \quad (48)$$

2.2. Maximum Likelihood for the Inverse Ising Problem

We here describe the benchmark statistical inference method maximum likelihood for IIP. According to this criterion the best estimate θ^{ML} based on the available data is given by

$$\theta^{ML} = \arg \max_{\theta} p(x_1, \dots, x_M | \theta) . \quad (49)$$

In a Bayesian context (49) is a point estimate (one predicted parameter value) assuming a flat (information-free) *prior* information $p(\theta)$ on the parameter. To avoid dealing with small numbers, it is common practice to maximize the logarithm of the likelihood, which has no consequences on the result: since the logarithm is a strictly monotonic function, the arg max is preserved. The log-likelihood per sample

$$\mathcal{L}_D(\mathbf{J}, \mathbf{h}) = \frac{1}{M} \log p(D | \mathbf{J}, \mathbf{h}) \quad (50)$$

is for the Ising parameters \mathbf{J}, \mathbf{h} upon measurement of M independent samples $D = \{\mathbf{s}^m\}$ of the Boltzmann distribution eq.(35):

$$\begin{aligned} \mathcal{L}_D(\mathbf{J}, \mathbf{h}) &= \sum_i h_i \frac{1}{M} \sum_m s_i^m + \sum_{i < j} J_{ij} \frac{1}{M} \sum_m s_i^m s_j^m - \log \mathcal{Z}(\mathbf{J}, \mathbf{h}) \\ &= \sum_i h_i \langle \sigma_i \rangle^D + \sum_{i < j} J_{ij} \langle \sigma_i \sigma_j \rangle^D - \log \mathcal{Z}(\mathbf{J}, \mathbf{h}) , \end{aligned} \quad (51)$$

where $\langle Q \rangle^D = \frac{1}{M} \sum_m Q(\mathbf{s}^m)$ is the *sample average* of the function $Q(\mathbf{s}^m)$ of the spin variables \mathbf{s}^m . It is well known that nothing but the sample averages $\langle \sigma_i \rangle^D, \langle \sigma_i \sigma_j \rangle^D$ is needed from data to determine eq.(51) *i.e.* they are *sufficient statistics* for this problem. Maximum likelihood solution of the inverse Ising Problem can schematically be written

$$\{\mathbf{J}^{ML}, \mathbf{h}^{ML}\} = \arg \max_{\mathbf{J}, \mathbf{h}} \mathcal{L}_D(\mathbf{J}, \mathbf{h}) . \quad (52)$$

where the superscript indicates the criterion/method. (*Boltzmann machine learning*) is a gradient-descent algorithm with an adjustable learning rate η so that at equilibrium (converged values) one has

$$0 = \frac{\partial \mathcal{L}_D}{\partial h_i}(\mathbf{J}^n, \mathbf{h}^n) = \langle \sigma_i \rangle^D - \langle \sigma_i \rangle , \quad (53)$$

$$0 = \frac{\partial \mathcal{L}_D}{\partial J_{ij}}(\mathbf{J}^n, \mathbf{h}^n) = \langle \sigma_i \sigma_j \rangle^D - \langle \sigma_i \sigma_j \rangle . \quad (54)$$

The disadvantage of Boltzmann machine learning is that one has to estimate ensemble averages which is computationally costly, and that convergence may be slow.

2.3. Mean Field inference for the Inverse Ising Problem

Mean-field inference is based on an assumption that the distribution is in the simpler class of factorizable distributions. The first step is thus to assume a trial distribution of the form

$$p^{MF}(\mathbf{s}) = \prod_i \frac{1 + \tilde{\chi}_i s_i}{2} , \quad (55)$$

where different spins are independent variables and the *effective* magnetization $\tilde{\chi}_i$ results from both the local field h_i and from the couplings J_{ij} with all other spins. We recall that the set \mathcal{G} of distributions q over which the minimization is operated is that for which $\langle \sigma_i \rangle_q = \chi_i$ which in the MF case reads $\tilde{\chi}_i = \chi_i$. The minimization is trivial, since there is only one mean-field distribution eq.(55) in \mathcal{G} , therefore we write:

$$\mathcal{G}^{MF}(\mathbf{J}, \mathbf{\chi}) = - \sum_{i < j} J_{ij} \chi_i \chi_j + \sum_i \left[\frac{1 + \chi_i}{2} \log \frac{1 + \chi_i}{2} + \frac{1 - \chi_i}{2} \log \frac{1 - \chi_i}{2} \right] . \quad (56)$$

By the variational equation eq.(44) we have for the fields h_i

$$h_i^{MF} = - \sum_{j \neq i} J_{ij} \chi_j + \frac{1 + \chi_i}{2} \frac{1 - \chi_i}{1 + \chi_i} = - \sum_{j \neq i} J_{ij} \chi_j + \text{arctanh} \chi_i . \quad (57)$$

Since p^{MF} does not depend on interactions between spins, something more is needed to infer the couplings J_{ij} and the above is not yet defined. This is done by using correlation-response which for the Ising model is

$$(\chi)_{ij} = \frac{\partial \chi_i}{\partial h_j} \quad (58)$$

Combining the exact result (58) and the approximation (57) one finds for $i \neq j$,

$$J_{ij}^{MF} = -(\chi^{-1})_{ij} ; \quad (59)$$

One can then insert backwards this inferred value J_{ij}^{MF} into (57) to get h_i^{MF} . This mean field inference scheme can be improved in two different directions. On the one hand one can modify the thermodynamic potential, either by adding a Onsager reaction term as in *Thouless-Anderson-Palmer* [52] or by a systematic expansion (Plevka expansion) in interaction strength [53]. On the other hand one can start from a more detailed model that (55) and then apply correlation-response from that starting point [54]. For a unified treatment, see [17].

2.4. Pseudolikelihood Maximization for the Inverse Ising Problem

The second method that we discuss is the *Pseudo-Likelihood Maximization* (PLM). The starting point this time is not a thermodynamic potential, instead one directly exploits the structure of the Ising Hamiltonian \mathcal{H} eq.(34) as follows. Consider a particular spin variable σ_i and distinguish the part \mathcal{H}_i of the Hamiltonian that depends on σ_i from

the rest, that we collectively indicate with $\mathcal{H}_{\setminus i}$:

$$\begin{aligned}\mathcal{H}(\mathbf{s}) &= \mathcal{H}_i + \mathcal{H}_{\setminus i} \\ &= -h_i s_i - \sum_{j \neq i} J_{ij} s_i s_j + \mathcal{H}_{\setminus i}(\mathbf{s}_{\setminus i}) .\end{aligned}\quad (60)$$

We can sum explicitly the terms related to σ_i in the partition function eq.(36)

$$\mathcal{Z}(\mathbf{J}, \mathbf{h}) = \sum_{\mathbf{s}_{\setminus i}} 2 \cosh \left(h_i + \sum_j J_{ij} s_j \right) e^{-\mathcal{H}_{\setminus i}(\mathbf{s}_{\setminus i})} , \quad (61)$$

and from eq.(39) we get the first and second moments (one and two spin expectations) involving σ_i , by simple derivatives with respect to the parameters:

$$\langle \sigma_i \rangle = \left\langle \tanh \left(h_i + \sum_{j \neq i} J_{ij} \sigma_j \right) \right\rangle , \quad (62)$$

$$\langle \sigma_i \sigma_j \rangle = \left\langle \sigma_j \tanh \left(h_i + \sum_{k \neq i} J_{ik} \sigma_k \right) \right\rangle . \quad (63)$$

The average in the RHS of the last equations is over the entire Boltzmann distribution eq.(35) and these are still *exact* equations. The approximation is implemented in the next step: we substitute the (computationally) prohibitive averages in eq.(62 - 63) with sample averages, labelled with the superscript D .

$$\langle \sigma_i \rangle^D = \left\langle \tanh \left(h_i^{PL} + \sum_{j \neq i} J_{ij}^{PL} \sigma_j \right) \right\rangle^D , \quad (64)$$

$$\langle \sigma_i \sigma_j \rangle^D = \left\langle \sigma_j \tanh \left(h_i^{PL} + \sum_{k \neq i} J_{ik}^{PL} \sigma_k \right) \right\rangle^D . \quad (65)$$

The simplification is self-evident: eq.(64 - 65) are a system of non-linear equations in the L variables $h_i^{PL}, \{J_{ij}^{PL}\}_{j \neq i}$ that can be solved with standard methods. The net effect of our assumption hence is to split the problem of estimating L^2 parameters (fields and couplings) in L separate problems, each of them involving only L parameters.

A different but equivalent interpretation of this approximation scheme is the following: let σ_i be a spin variable, we consider the conditional probability of s_i under the observation of the other variables $\mathbf{s}_{\setminus i}$

$$p(s_i | \mathbf{s}_{\setminus i}) = \frac{1}{1 + e^{-2s_i(h_i + \sum_{j \neq i} J_{ij} s_j)}} = \frac{1}{2} \left[1 + s_i \tanh \left(h_i + \sum_{j \neq i} J_{ij} s_j \right) \right] \quad (66)$$

and depends only on the field h_i and on the couplings $\{J_{ij}\}_{j \neq i}$. The last quantities also appear in the log-likelihood per sample \mathcal{L}_D^i for the last distribution of probability, which reads

$$\mathcal{L}_D^i(J_{i*}, h_i) = \frac{1}{M} \sum_m \log \frac{1}{2} \left[1 + s_i^m \tanh \left(h_i + \sum_{j \neq i} J_{ij} s_j^m \right) \right] , \quad (67)$$

cf eq.(50), we used the notation $J_{i*} = \{J_{ij}\}_{j \neq i}$. eq.(64 - 65) simply follow from setting the derivatives of \mathcal{L}_D^i with respect to h_i and $\{J_{ij}\}_{j \neq i}$ to zero, hence they are found to maximize the log-likelihood. Altogether, one might define the so-called *pseudolikelihood* as

$$\mathcal{L}^{PL}(\mathbf{J}, \mathbf{h}) = \sum_i \mathcal{L}_D^i(J_{i*}, h_i) \quad (68)$$

whose maximization yields the whole set of Ising parameters. Note that in general for the inferred couplings $J_{ij} \neq J_{ji}$, even if the underlying model has symmetric couplings, due to sampling noise; in the latter case, a practical solution is to use the average $\frac{1}{2}(J_{ij} + J_{ji})$.

2.5. MF vs PLM

We have not yet discussed the accuracy of the methods discussed in the previous sections. A standard procedure to test an approximate solution of the IIP (especially for uncontrolled ones) is to simulate data from an Ising model with known fields and couplings, then compare the results of the inference with the input values of the parameters. As mentioned above, the reconstruction errors depend on many factors (network topology of the couplings, ergodicity of the system...), we here focus on the dependence on the size M of the dataset D and on the coupling strength, by re-establishing and tuning the inverse temperature β in eq.(35). The high temperature limit $\beta \rightarrow 0$ hence corresponds to that of low couplings/fields and vice versa. In Fig.2 the performance of several inverse techniques are shown. The underlying data are generated from a Sherrington-Kirkpatrick model where $J_{ij} \sim \mathcal{N}(0, \beta/\sqrt{L})$ and a fully connected graph of interactions is assumed. For each couple (β, M) , 10^4L Monte Carlo steps with Metropolis transition rule are used to reach an equilibrium state and collect the samples. Let J_{ij}^0 be the input parameters of the simulation, the reconstruction error γ_J can be quantified as follows:

$$\gamma_J = \sqrt{\frac{\sum_{i < j} (J_{ij} - J_{ij}^0)^2}{\sum_{i < j} (J_{ij}^0)^2}}. \quad (69)$$

Overall, we see that the PLM approximation yields a more accurate reconstruction of the model parameters with respect to the MF theory; the latter is indeed known to overestimate large couplings. In the top panel, we see that all methods equally fail for $\beta \rightarrow 0$, since for too low coupling strengths the reconstruction is democratically hampered by sampling noise. On the other hand, for sufficiently high β the approximations on which our methods are based break down and the errors blow up, a possible cause being the ergodicity breaking for strong coupling. As for the dependence on M , differently from the MF, in a PLM algorithm the reconstruction error can always be compensated by a larger dataset, which leads to the polynomial behaviour shown in the lower panel for all the tested values of β . What if the true couplings are not known? This is usually the case with real data. One possibility might be to try different methods and compare the likelihood of the resulting parameters, the better techniques resulting in higher likelihoods. Alternatively one can compare the statistics resulting from data generated from reconstructed parameters with those observed.

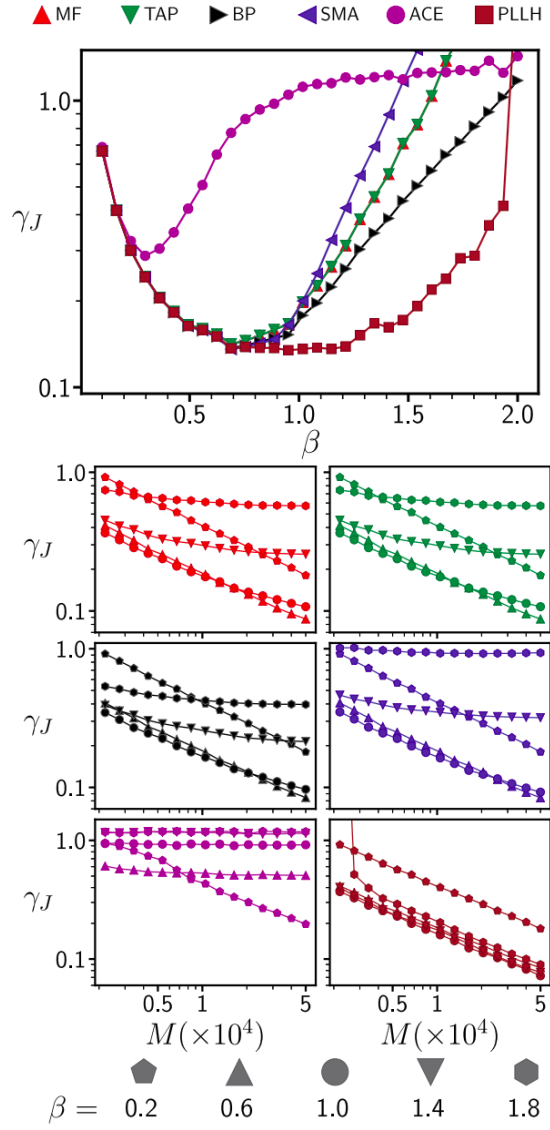


Figure 2.: Reconstruction of a fully connected Ising model. Both panels show the reconstruction error as in eq.(69), in the upper one $\gamma_J(\beta)$ for $M = 15000$, in the lower one $\gamma_J(M)$ for different values of β . $L = 64$. Results are shown for the following approximations: **Mean Field** (MF), TAP reconstruction (TAP), Bethe-Peierls method (BP), Sessak-Monasson method (SMA), Adaptive Cluster Expansion (ACE), **Pseudo-likelihood Maximization** (PLLH). Figure taken from [17], reproduced here with permission from J. Berg and Taylor & Francis Ltd (www.tandfonline.com).

2.6. Inference in the KNS theory

We are now in the position to test eq.(28), since the missing link between raw data and the couplings \mathbf{J} has been provided by the methods above. This is exactly what has been done in [13], the content of which we now illustrate.

The testing strategy is very similar to the one employed in Sec.(2.5) and it is based on the following three steps: simulating evolutionary data by means of **FFPopSim**, inferring couplings by means of **MF/PLM**, finally comparing the epistatic parameters as they result from eq.(28) with the input ones. Let us expand on these points.

- (1) **Simulating data.** We exploit the our simulation tool **FFPopSim** to generate evolutionary data, as discussed in App.(D). Since we are interested here in testing the QLE regime, we set the initial parameters accordingly. A crucial choice is that of the fitness landscape, we here consider a Sherrington-Kirkpatrick fitness function, so we set $f_i = 0 \forall i$ and $f_{ij} \sim \mathcal{N}(0, \sigma_e)$. We will mainly focus on the dependence of our results on the parameters r, μ, σ_e , a comprehensive summary of the initial parameters for the simulations is shown in Tab.(1), we will refer to this set as the Neher-Shraiman Test (**NST**).

	FFPopSim	NST	Description
Drivers Structure	N	200	carrying capacity
	L	25	n. of loci
	T	2.500	n. of generations
	ω	0.5	crossover rate
	r	[0.0, 1.0]	outcrossing rate
	μ	[0.005, 0.1]	mutation rate
	σ_e	[0.001, 0.02]	$f_{ij} \sim \mathcal{N}(0, \sigma_e)$

Table 1.: Parameters on the **NST**. In light gray the parameters that are varied, the range indicated in the square brackets. SK fitness function. Random initial conditions.

- (2) **Inferring couplings.** Raw data from the previous point are a sequence of states of the population at each time t . From such data, we can compute empirical population averages to feed one or more of the inverse techniques discussed in this section, in particular **MF** (sometimes also referred as *naive* mean field **nMF**) and **PLM**. Due to random drift, the empirical quantities (averages over the population) fluctuate in time, in order to smooth fluctuations out we compute the averages not only on the final state of the population but on the whole time series: if a single state is a matrix $N \times L$, the whole time series is a matrix $(N \cdot T) \times L$; as an example, $\langle \sigma_i \rangle = \frac{1}{NT} \sum_{j=1}^{NT} s_i(j)$, where j is the row index. The **MF** and **PLM** inference on data obtained from the whole time series are referred as *alltime*-**MF** and *alltime*-**PLM**, this specification will be always implied hereinafter.
- (3) **Testing epistasis.** The couplings resulting from the inverse methods enable us to reconstruct the epistasis by means of eq.(28): r is the known (input) recombination rate, c_{ij} in [13] is computed as in eq.(16) with $\rho = \omega = 0.5$. Let f_{ij}^* be the inferred value of the epistatic fitness component between the loci i, j , similarly

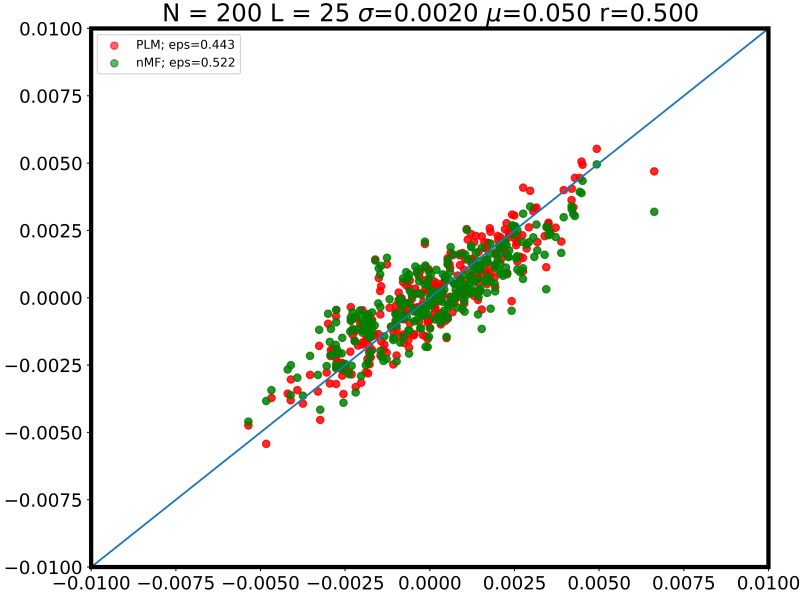


Figure 3.: Example of a scatter plot for the *reconstructed* epistatic fitness components f_{ij}^* (y-axis) versus the *true* parameters f_{ij} (x-axis). Simulation NST, Tab.(1). Here $r = 0.5$, $\mu = 0.05$, $\sigma_e = 0.002$. The RMSE (Root Mean Square Error) is the reconstruction error as in eq.(70). Both MF (green) and PLM (red) are used for the inference procedure, their performances are similar in this regime.

to eq.(69), we quantify the reconstruction error ε by

$$\varepsilon = \sqrt{\frac{\sum_{i < j} (f_{ij}^* - f_{ij})^2}{\sum_{i < j} f_{ij}^2}}. \quad (70)$$

Obviously, we want ε to be as small as possible, a wrong functional dependence of f_{ij}^* on the model parameters will yield $\varepsilon \gg 0$.

In Fig.3 we see a typical outcome of the algorithm described just now, for the case when the inference procedure is reasonably accurate. The input and reconstructed epistatic fitness components are compared by means of a scatter plot; in the optimal case we would see the points along the diagonal line indicated, this is usually the case for the ML reconstruction, in the few cases when it is feasible. We also observe no relevant difference between MF and PLM in the final result of the inference procedure. We can repeat the same steps for different values of the parameters and see if/how the performance of the NS inference of epistasis changes. This is done in Fig.4, where the parameter space is explored in the directions $r - \mu$, $r - \sigma_e$. Here follows a list of conclusions that we can draw from these charts:

- * μ . The NS fitness reconstruction fails for low mutation rates. In fact, when mutation is insufficient, the structure of the population is essentially frozen and even if a defined fitness structure is present, for finite N, T it is not reflected in data. On the other hand, we do not expect eq.(28) to work for high μ , too, since in deriving it we assumed $\mu \sim 0$. We will discuss this case in Sec.(3).
- * $High \sigma_e/r$. The reconstruction error ε blows up for sufficiently low values of r ,

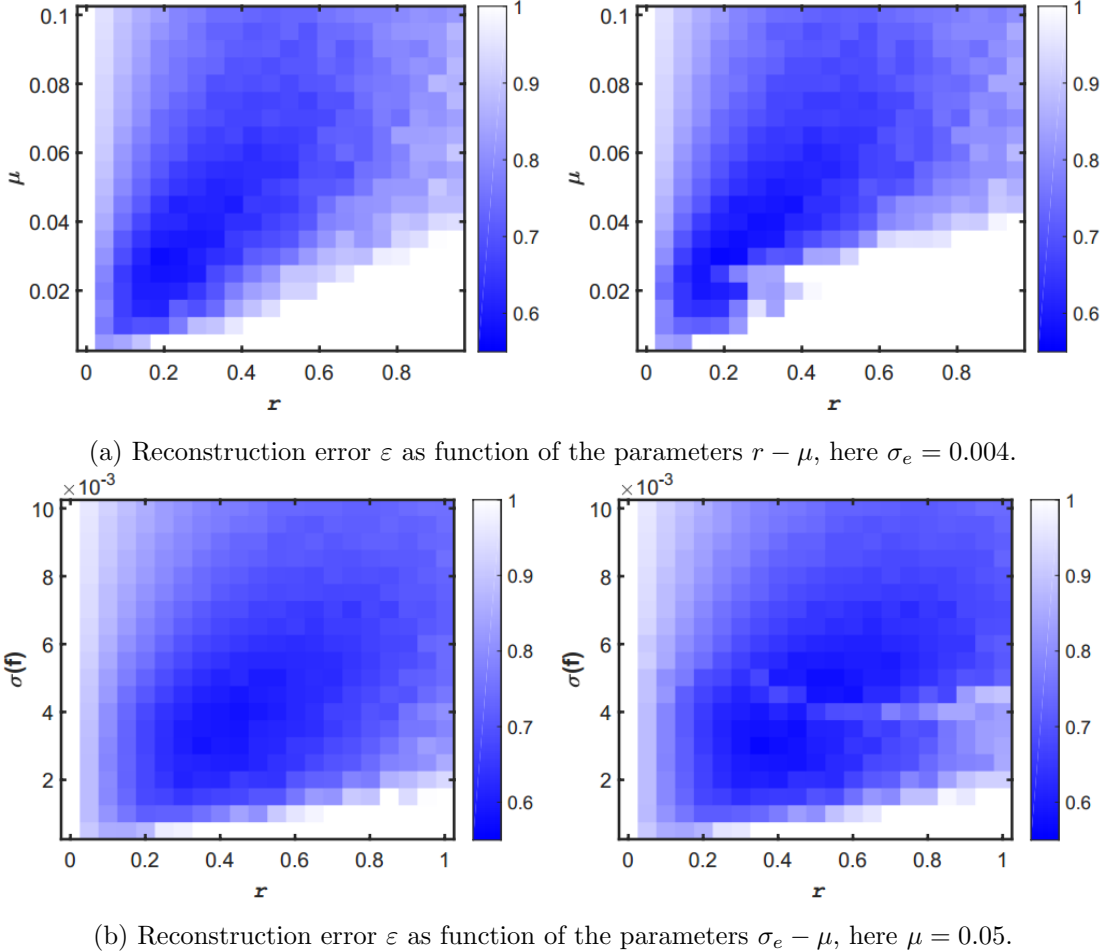


Figure 4.: Phase diagrams for the reconstruction of the epistatic fitness components, from eq.(28). NST simulations, as in Tab.(1). In the left column, *alltime-MF* is used to infer the couplings J_{ij} from data, in the right column *alltime-PLM*. The magnitude of the reconstruction error eq.(70) is encoded in the colours of the heat-map. From [13]

which can be easily understood in view of eq.(28) *i.e.* $f_{ij}^* = J_{ij}^* \cdot r c_{ij} \sim 0$ which implies $\varepsilon \sim 1$ regardless of the inference method employed. The case of too high values of σ_e will be discussed in Sec.(4).

- ★ *Low σ_e/r .* Results also are worse for sufficiently high recombination rates r : this is due to the fact that the higher the reshuffling the smaller the couplings J_{ij} inferred from data, which become subject more and more to small-sample noise. For the same reason, we see worse results for sufficiently small σ_e .

Further plots and discussions can be found in [13], the ones presented above will be the starting point for our next section.

3. QLE at high mutation rate (but low fitness variation)

Let us go back to the NS theory as encoded in eq.(12, 15): we already know that these equations are not sufficient to draw quantitative predictions, a specific expression for

$P(g)$ has to be provided. Once $P(g)$ is known, the solutions of the two equations above are in principle determined but hardly accessible from an analytical point of view; for instance, it is true that one can parameterized $P(g)$ (and its dynamics) in terms of its cumulants $\chi_{ij\dots k}$, but there are $2^L - 1$ of them, and in general they all appear in the RHS of eq.(12, 15). The last ingredient that we need in order to tame these equations and make them accessible for a formal analysis is typically an additional assumption. In Sec.(1.3) this was done in the QLE framework $\sigma \ll r$ and an inference formula eq.(28) was derived in the case where mutations are negligible $\mu \sim 0$. The additional hypothesis was in this case the perturbation expansion in the $|J_{ij}|$.

Our goal now is to relax the hypothesis of $\mu \sim 0$ and generalizing eq.(28) to the case where the mutation rate is arbitrarily high with respect to the fitness variation. In doing so, we introduce a new approach alternative to the one proposed in [12] and recently introduced by *Mauri et al.* [55], based on a Gaussian closure of the dynamical equations for the first and second order cumulants. The new inference formula for $\mu \gg 1$ has first appeared in [56] where it is derived both as a generalization of the method of Neher and Shraiman [12], as described in Sec.(1.3), and from the Gaussian closure approach by means of a perturbation expansion, that we describe below. We further show here how in the latter framework it is possible to push the expansion to arbitrary orders in a systematic and straightforward fashion. In order to assess the performance of the new formula, we design a numerical test akin to the one employed in Sec. (2.6).

3.1. A Gaussian Ansatz

3.1.1. The Logic Of The Gaussian Ansatz

In order to understand where exactly the Gaussian Ansatz comes into play, let us move one step further and substitute in the dynamical equations for first and second order cumulants eq.(12, 15) the explicit form of the fitness landscape eq.(3), up to pairwise terms:

$$F(g) = \sum_i f_i s_i + \sum_{i < j} f_{ij} s_i s_j , \quad (71)$$

where we set $f_{ii} = 0 \forall i$ and $f_{ij} = f_{ji} \forall i, j$. The resulting expressions are

$$\begin{aligned} \dot{\chi}_i &= \langle s_i [F(g) - \langle F \rangle] \rangle - 2\mu\chi_i \\ &= \sum_j f_j \langle s_i s_j \rangle + \sum_{j < k} f_{jk} \langle s_i s_j s_k \rangle - \sum_j f_j \chi_i \chi_j - \sum_{j < k} f_{jk} \chi_i \langle s_j s_k \rangle - 2\mu\chi_i \end{aligned} \quad (72)$$

$$\begin{aligned} \dot{\chi}_{ij} &= \langle (s_i - \chi_i)(s_j - \chi_j) [F(g) - \langle F \rangle] \rangle - (4\mu + r c_{ij}) \chi_{ij} ; \\ &= \langle s_i s_j [F(g) - \langle F \rangle] \rangle - \chi_i (\dot{\chi}_j + 2\chi_j \mu) - \chi_j (\dot{\chi}_i + 2\chi_i \mu) - (4\mu + r c_{ij}) \chi_{ij} \\ &= \sum_k f_k \langle s_i s_j s_k \rangle + \sum_{k < l} f_{kl} \langle s_i s_j s_k s_l \rangle - \sum_k f_k \chi_k \langle s_i s_j \rangle - \sum_{k < l} f_{kl} \langle s_i s_j \rangle \langle s_k s_l \rangle + \\ &\quad - \chi_i (\dot{\chi}_j + 2\chi_j \mu) - \chi_j (\dot{\chi}_i + 2\chi_i \mu) - (4\mu + r c_{ij}) \chi_{ij} ; \end{aligned} \quad (73)$$

for the latter we have used eq.(12) and left implicit $\dot{\chi}_i$.

Our goal is to express the expectations in the RHS of eq.(72, 73), in terms of the cumulants of the distribution $P(g)$ (of all orders, in principle). We already know

how to relate the 2–points expectation $\langle s_i s_j \rangle$ to the cumulants *i.e.* by definition of $\chi_{ij} = \langle s_i s_j \rangle - \langle s_i \rangle \langle s_j \rangle$. Evidently, the crucial issue is how to evaluate $\langle s_i s_j s_k \rangle$ and $\langle s_i s_j s_k s_l \rangle$ which are respectively the 3, 4–points expectation. We can slightly reduce the burden of this task by observing that, since for our Ising-alleles $s_i^2 = 1$, we only need to know $\langle s_i s_j s_k \rangle_{i \neq j \neq k}$, $\langle s_i s_j s_k s_l \rangle_{i \neq j \neq k \neq l}$, no two same indices. We are now forced to choose a specific form of $P(g)$, here comes the Gaussian Ansatz.

Let us consider *a population where the mutation rate is high enough with respect to the fitness strength that no two individuals are present with the same genotype (clones). In such a system, where $\mu \gg \sigma$, we expect correlations of order > 2 to be negligible, therefore, for the purpose of estimating 3, 4–points expectations, we model the distribution of probability as:*

$$P(g, t) = \frac{1}{Z} \exp \left[-\frac{1}{2} \sum_{i,j} (s_i - \chi_i)(\chi^{-1})_{ij}(s_j - \chi_j) \right], \quad (74)$$

where Z is a normalization and χ is the covariance matrix *i.e.* $\chi_{ij} = \langle s_i s_j \rangle - \langle s_i \rangle \langle s_j \rangle$. In words, we model $P(g)$ as a *multivariate Gaussian distribution*, whose cumulants (connected correlation functions) of order > 2 are *exactly* zero, see App.(A). Let us stress that for eq.(74) to be valid, we are forced to allow $s_i \in \mathbb{R}$.

Metaphorically, we are describing a population as a cloud of similar sequences distributed around the value $\{\chi_1, \dots, \chi_L\}$, where L as usual is the number of loci [55]. A first crystal-clear advantage of the Gaussian ansatz is that it will allow us to write only $L(L + 1)/2$ dynamical equations for $\{\chi_i\}_i$ and $\{\chi_{ij}\}_{i \neq j}$ instead of 2^L for each possible g .

Using eq.(74) and with some effort, one is able to express the 3, 4–points correlations in terms of the first and second order cumulants, a proof is provided in App.(A).

$$\langle s_i s_j s_k \rangle_{i \neq j \neq k} = \chi_i \chi_j \chi_k + \chi_i \chi_{jk} + \chi_j \chi_{ik} + \chi_k \chi_{ij} \quad (75)$$

$$\begin{aligned} \langle s_i s_j s_k s_l \rangle_{i \neq j \neq k \neq l} = & \chi_i \chi_j \chi_k \chi_l + \chi_i \chi_j \chi_{kl} + \chi_i \chi_k \chi_{jl} + \chi_i \chi_l \chi_{jk} + \chi_j \chi_k \chi_{il} + \\ & + \chi_j \chi_l \chi_{ik} + \chi_k \chi_l \chi_{ij} + \chi_{ij} \chi_{kl} + \chi_{ik} \chi_{jl} + \chi_{il} \chi_{jk} \end{aligned} \quad (76)$$

Let us notice that in the RHS of eq.(72, 73), apart from parameters of the model, only $\{\chi_i\}$, $\{\chi_{ij}\}$ will be found; this is the reason why the Gaussian assumption above is termed *closure* (GC).

The key contribution of the Gaussian Ansatz is exactly and nothing more of the content of eq.(75, 76), and now we can exploit it to carry out the calculation of the dynamical equations.

3.1.2. Closed Equations for Cumulants Dynamics

$\dot{\chi}_i$ Dynamics of the first cumulants, from eq.(72). $\forall i \in 1, \dots, L$

$$\begin{aligned}
\dot{\chi}_i &= \sum_j f_j \langle s_i s_j \rangle + \sum_{j < k} f_{jk} \langle s_i s_j s_k \rangle - \sum_j f_j \chi_i \chi_j - \sum_{j < k} f_{jk} \chi_i \langle s_j s_k \rangle - 2\mu \chi_i \\
&\stackrel{(a)}{=} \sum_j f_j \chi_{ij} + \sum_{j \neq i} f_{ij} \chi_j + \sum_{\substack{j < k \\ j, k \neq i}} f_{jk} (\chi_i (\chi_j \chi_k + \chi_{jk}) + \chi_j \chi_{ik} + \chi_k \chi_{ij}) + \\
&\quad - \sum_{j < k} f_{jk} \chi_i (\chi_{jk} + \chi_j \chi_k) - 2\mu \chi_i \\
&= \sum_j f_j \chi_{ij} + \sum_{j \neq i} f_{ij} \chi_j - \sum_{j \neq i} f_{ij} \chi_i (\chi_{ij} + \chi_i \chi_j) + \sum_{\substack{j < k \\ j, k \neq i}} f_{jk} (\chi_j \chi_{ik} + \chi_k \chi_{ij}) - 2\mu \chi_i \\
&= \sum_j f_j \chi_{ij} - \sum_{j \neq i} f_{ij} \chi_i \chi_{ij} + \sum_{j \neq i} f_{ij} \chi_j (1 - \chi_i^2) + \sum_{\substack{j \neq k \\ j, k \neq i}} f_{jk} \chi_j \chi_{ik} - 2\mu \chi_i \\
&\stackrel{(b)}{=} \sum_j f_j \chi_{ij} - \sum_{j \neq i} f_{ij} \chi_i \chi_{ij} + \sum_{j \neq i} f_{ij} \chi_j \chi_{ii} + \sum_{j \neq i} \sum_{\substack{k \neq i \\ k \neq j}} f_{jk} \chi_j \chi_{ik} - 2\mu \chi_i \\
&\stackrel{(c)}{=} \sum_j f_j \chi_{ij} - \sum_{j \neq i} f_{ij} \chi_i \chi_{ij} + \sum_{j \neq i} \sum_{k \neq j} f_{jk} \chi_j \chi_{ik} \pm \sum_{k \neq i} f_{ik} \chi_i \chi_{ik} - 2\mu \chi_i \\
&= \sum_j f_j \chi_{ij} - 2 \sum_{j \neq i} f_{ij} \chi_i \chi_{ij} + \sum_j \sum_{k \neq j} f_{jk} \chi_k \chi_{ij} - 2\mu \chi_i \\
&\stackrel{(d)}{=} \sum_j \chi_{ij} \left(f_j + \sum_k f_{jk} \chi_k - 2 f_{ij} \chi_i \right) - 2\mu \chi_i
\end{aligned} \tag{77}$$

In (a) we expanded $\langle s_j s_k \rangle$ and, after distinguishing the case where $i \neq j \neq k$, we exploited eq.(75); in (b) we used $\chi_{ii} = \langle s_i^2 \rangle - \langle s_i \rangle^2 = 1 - \chi_i^2$; in (c) we added and subtracted a sum; in (d) we used $f_{ii} = 0 \forall i$. This first result deserves to be emphasized, $\forall i$

$$\dot{\chi}_i = \sum_j \chi_{ij} \left(f_j + \sum_k f_{jk} \chi_k - 2 f_{ij} \chi_i \right) - 2\mu \chi_i .$$

$$\boxed{\dot{\chi}_i = \sum_j \chi_{ij} \left(f_j + \sum_k f_{jk} \chi_k - 2 f_{ij} \chi_i \right) - 2\mu \chi_i .} \tag{78}$$

$\dot{\chi}_{ij}$ Dynamics of the second cumulants, from eq.(73). $\forall i, j \in 1, \dots, L \wedge i \neq j$

$$\begin{aligned}
\dot{\chi}_{ij} &= \sum_k f_k \langle s_i s_j s_k \rangle + \sum_{k < l} f_{kl} \langle s_i s_j s_k s_l \rangle - \langle s_i s_j \rangle \left(\sum_k f_k \chi_k + \sum_{k < l} f_{kl} \langle s_k s_l \rangle \right) + \\
&\quad - \cancel{\chi_i} \sum_{\textcolor{blue}{k}} \cancel{\chi_{jk}} (\hat{f}_k - 2 f_{jk} \chi_j) - \chi_j \sum_k \chi_{ik} (\hat{f}_k - 2 f_{ik} \chi_i) - (4\mu + r c_{ij}) \chi_{ij}
\end{aligned} \tag{79}$$

where we have substituted the result eq.(78) and the definition $\hat{f}_k = f_k + \sum_j f_{jk} \chi_j$. For the sake of clarity, let us analyze separately the terms highlighted in blue (B), red (R) and violet (V) and cyan (C). In order to substitute eq.(75,

76) we again have to deconstruct the sums distinguishing cases where some of the indices are equal.

$$\begin{aligned}
\textcolor{violet}{V} &= (\chi_{ij} + \chi_i \chi_j) \left(\sum_k f_k \chi_k + \sum_{k < l} f_{kl} (\chi_{kl} - \chi_k \chi_l) \right) \\
&= (\chi_{ij} + \chi_i \chi_j) \left(\sum_{k \neq i, j} f_k \chi_k + f_i \chi_i + f_j \chi_j + \sum_{\substack{k < l \\ k, l \neq i, j}} f_{kl} (\chi_{kl} + \chi_k \chi_l) + \right. \\
&\quad \left. + \sum_{k \neq i, j} [f_{ik} (\chi_{ik} + \chi_i \chi_k) + f_{jk} (\chi_{jk} + \chi_j \chi_k)] + f_{ij} (\chi_{ij} + \chi_i \chi_j) \right) \\
\textcolor{blue}{B} &= \sum_{k \neq i, j} f_k \langle s_i s_j s_k \rangle + f_i \chi_j + f_j \chi_i \\
&= \sum_{k \neq i, j} f_k (\chi_i \chi_j \chi_k + \chi_i \chi_{jk} + \chi_j \chi_{ik} + \chi_k \chi_{ij}) + f_i \chi_j + f_j \chi_i \\
\textcolor{red}{R} &= \sum_{\substack{k < l \\ k, l \neq i, j}} f_{kl} \langle s_i s_j s_k s_l \rangle + \sum_{k \neq i, j} [f_{ik} \langle s_j s_k \rangle + f_{jk} \langle s_i s_k \rangle] + f_{ij} \\
&= \sum_{\substack{k < l \\ k, l \neq i, j}} f_{kl} (\chi_i \chi_j \chi_k \chi_l + \chi_i \chi_j \chi_{kl} + \chi_i \chi_k \chi_{jl} + \chi_i \chi_l \chi_{jk} + \chi_j \chi_k \chi_{il} + \chi_j \chi_l \chi_{ik} + \\
&\quad + \chi_k \chi_l \chi_{ij} + \chi_{ij} \chi_{kl} + \chi_{ik} \chi_{jl} + \chi_{il} \chi_{jk}) + \sum_{k \neq i, j} [f_{ik} (\chi_{jk} + \chi_j \chi_k) + \\
&\quad + f_{jk} (\chi_{ik} - \chi_i \chi_k)] + f_{ij} \\
\textcolor{cyan}{C} &= \chi_i \sum_k \chi_{jk} (f_k + \sum_l f_{kl} \chi_l - 2 f_{jk} \chi_j) \\
&= \chi_i \sum_{k \neq i, j} \chi_{jk} (f_k + \sum_l f_{kl} \chi_l - 2 f_{jk} \chi_j) + \chi_i \chi_{ij} (f_i + \sum_l \chi_{il} \chi_l - 2 f_{ij} \chi_j) + \\
&\quad + \chi_i (1 - \chi_j^2) (f_j + \sum_l f_{jl} \chi_l)
\end{aligned}$$

In the last line we have used $\chi_{ii} = 1 - \chi_i^2$, $f_{ii} = 0 \forall i$ and the definition of \hat{f}_i . Moreover, let us note that there is a term in eq.(79) which is nothing but (C) after exchanging $i \leftrightarrow j$.

Summing the all the terms in eq.(79) and simplifying everything possible we get :

$$\begin{aligned}
\dot{\chi}_{ij} = & - (4\mu + rc_{ij}) - 2f_i\chi_i\chi_{ij} - 2f_j\chi_j\chi_{ij} + f_{ij}(1 - \chi_{ij}^2 - \chi_i^2\chi_j^2 + 2\chi_i\chi_j\chi_{ij}) + \\
& + \sum_{k \neq i,j} f_{ik}(\chi_{jk} + \chi_j\chi_k - \chi_{ij}\chi_{ik} + \chi_{ik}\chi_i\chi_j - \chi_{ij}\chi_i\chi_k - \chi_i^2\chi_j\chi_k) + \\
& + \sum_{k \neq i,j} f_{jk}(\chi_{ik} + \chi_i\chi_k - \chi_{ij}\chi_{jk} + \chi_{jk}\chi_i\chi_j - \chi_{ij}\chi_j\chi_k - \chi_i\chi_j^2\chi_k) + \\
& + (\chi_i^2\chi_j - \chi_j - \chi_i\chi_{ij}) \sum_l f_{il}\chi_{il} + (\chi_i\chi_j^2 - \chi_i - \chi_j\chi_{ij}) \sum_l f_{jl}\chi_{il} + \\
& + \sum_{\substack{k < l \\ k,l \neq i,j}} f_{kl}(\chi_{ik}\chi_j\chi_l + \chi_{jk}\chi_i\chi_l + \chi_{il}\chi_j\chi_k + \chi_{jl}\chi_i\chi_k + \chi_{ik}\chi_{jl} + \chi_{il}\chi_{jk}) + \\
& - \sum_{k \neq i,j} \chi_i\chi_{jk} \sum_l \chi_{il}f_{kl} - \sum_{k \neq i,j} \chi_j\chi_{ik} \sum_l \chi_{il}f_{kl}
\end{aligned} \tag{80}$$

The latter is already the final stage of our calculation and it will be the starting point of our future calculations; nevertheless, for the sake of elegance, it is possible to rewind the sums (*i.e.* reversing the “decomposition” where we treat separately cases in which some indices are equal). The outcome is our second important result for this section: for $i \neq j$,

$$\begin{aligned}
\dot{\chi}_{ij} = & - (4\mu + rc_{ij})\chi_{ij} - 2\chi_{ij}(f_i\chi_i + f_j\chi_j) + 2f_{ij}\chi_{ij}(\chi_{ij} + 2\chi_i\chi_j) + \\
& - 2\chi_{ij} \sum_k \left[f_{ik}(\chi_{ik} + \chi_i\chi_k) + f_{jk}(\chi_{jk} + \chi_j\chi_k) \right] + \sum_{k,l} f_{kl}\chi_{ik}\chi_{jl}.
\end{aligned} \tag{81}$$

3.1.3. New Inference Formula for Epistasis

A primary interest with eq.(78, 80) is to understand their stationary solutions, which entails solving simultaneously $\mathcal{O}(L^2)$ equations. However, since here we are modestly interested in the regime with high mutation and/or recombination rate, we limit ourselves to the case $(4\mu + rc_{ij}) \rightarrow \infty$ [56].

As a first step, we will investigate the further subcase where there is a purely epistatic fitness landscape and $\chi_i = 0 \forall i$, therefore the results of this subsection will not hold when $f_i \neq 0$ or when something else causes the first order cumulants to substantially deviate from zero.

Since the first cumulants all vanish, we are only interested in eq.(80) so let us rewrite it in the simpler form of current interest:

$$\begin{aligned}
\dot{\chi}_{ij} = & - (4\mu + rc_{ij})\chi_{ij} + f_{ij}(1 - \chi_{ij}^2) + \sum_{k \neq i,j} \left[f_{ik}(\chi_{jk} - \chi_{ij}\chi_{jk}) + f_{jk}(\chi_{ik} - \chi_{ij}\chi_{jk}) \right] + \\
& + \sum_{\substack{k < l \\ k,l \neq i,j}} f_{kl}(\chi_{ik}\chi_{jl} + \chi_{jk}\chi_{il}).
\end{aligned} \tag{82}$$

Let us define $\epsilon = 1/(4\mu + rc_{ij}) \rightarrow 0^+$, to be used as small parameter for the expansion.⁹ The trick is now to assume:

$$\chi_{ij} = \chi_{ij}^{(0)} + \epsilon \chi_{ij}^{(1)} + \epsilon^2 \chi_{ij}^{(2)} + \epsilon^3 \chi_{ij}^{(3)} + \mathcal{O}(\epsilon^4) \quad (83)$$

and impose the stationary condition $\dot{\chi}_{ij} = 0$ from eq.(82), order by order in ϵ . The first terms are easy to work out:

$$\begin{aligned} \mathcal{O}(\epsilon^{-1}) : \chi_{ij}^{(0)} &= 0 \\ \mathcal{O}(1) : \chi_{ij}^{(1)} &= f_{ij} \\ \mathcal{O}(\epsilon) : \chi_{ij}^{(2)} &= 2 \sum_{k \neq i,j} f_{ik} f_{jk} \\ \mathcal{O}(\epsilon^2) : \chi_{ij}^{(3)} &= \sum_{\substack{k < l \\ k,l \neq i,j}} f_{kl} (f_{ik} f_{jl} + f_{jk} f_{il}) + \sum_{k \neq i,j} f_{ik} \left(2 \sum_l f_{jl} f_{kl} - f_{ij} f_{ik} \right) + \\ &+ \sum_{k \neq i,j} f_{jk} \left(2 \sum_l f_{il} f_{kl} - f_{ij} f_{jk} \right) - f_{ij}^3 \end{aligned}$$

Therefore, up to the first order in ϵ , we can write:

$$\chi_{ij} = \frac{f_{ij}}{4\mu + rc_{ij}} \quad (84)$$

to be compared with eq.(28). We note that the n -th order term is of relative size $L\sigma(f)$ compared to the $(n-1)$ -th; therefore, we may expect the first order to be accurate as far as $L\sigma(f) < 1$.

If we additionally drop the hypothesis of $\chi_i = 0 \forall i$ and consider the full eq.(80) with the assumption eq.(83), following the same steps as above we get

$$\mathcal{O}(\epsilon^{-1}) : \chi_{ij}^{(0)} = 0 \quad (85)$$

$$\begin{aligned} \mathcal{O}(1) : \chi_{ij}^{(1)} &= f_{ij} (1 - \chi_i^2) (1 - \chi_j^2) \\ \mathcal{O}(\epsilon) : \chi_{ij}^{(2)} &= \sum_k f_{ik} (\chi_{jk}^{(1)} + \chi_{ik}^{(1)} \chi_i \chi_j - \chi_i \chi_k \chi_{ij}^{(1)}) + \\ &- \sum_{k,l} f_{kl} \chi_i \chi_l \chi_{jk}^{(1)} - \sum_l f_{il} \chi_l \chi_i \chi_{ij}^{(1)} + \\ &+ \sum_{k < l} f_{kl} \left(\chi_{ik}^{(1)} \chi_j \chi_l + \chi_{il}^{(1)} \chi_j \chi_k - 2 f_i \chi_i \chi_{ij}^{(1)} \right. \\ &\left. + f_{ij} \chi_i \chi_j \chi_{ij}^{(1)} \right) + \{i \longleftrightarrow j\} \end{aligned} \quad (86)$$

where, for the sake of clarity, in the last equation we have left implicit the terms like $\chi_{ij}^{(1)}$ as specified in eq. (85).

⁹In principle, we should write ϵ_{ij} but since in this work we typically have a crossover rate $\sim \mathcal{O}(1)$, see Sec.(1.2.5), we can safely assume it is indeed constant and forget about this unimportant complication.

Up to the first order in ϵ we have

$$\chi_{ij} = \frac{f_{ij}}{4\mu + rc_{ij}}(1 - \chi_i^2)(1 - \chi_j^2) . \quad (87)$$

As it should be, we recover eq.(84) when setting $\chi_i = 0 \forall i$. Turning around this into an inference formula we get:

$$f_{ij}^* = \chi_{ij} \cdot \frac{4\mu + rc_{ij}}{(1 - \chi_i^2)(1 - \chi_j^2)}$$

(88)

ewhere the star in f_{ij}^* means that these are regarded as *inferred* fitness parameters. eq.(88) has a self-evident advantage with respect to eq.(28): there is *no more need for any DCA inference*, since epistasis is reconstructed directly from the population averages $\{\chi_i\}, \{\chi_{ij}\}$. This result is important for practical reasons, since the inference procedure, even in its most streamlined versions (*e.g.* MF), can be very expensive in terms of computational time.

3.2. Gaussian Closure Under Examination

Testing eq.(88) versus eq.(28) is precisely the goal of [56], which will guide us throughout this section. We will follow a similar approach as the one presented in Sec.(2.6) based on [13]; it is briefly summarized here together with the description of the setup.

- **Simulation Generalities.** Our simulation tool FFPopSim can be exploited to simulate a population of (on average) N individuals, each of which is a gene chain made of L loci $s_i = \pm 1$. We let this population evolve for T generations driven by the mechanisms discussed in Sec.(1.2): mutations at rate μ , recombination at rate r and natural selection encoded in the fitness function $F(g) = \sum_i f_i s_i + \sum_{i < j} f_{ij} s_i s_j$.
- **Simulation Settings.** Since our Gaussian Closure is expected to work also for non-zero $\{\chi_i\}$, differently from [13], we assume non-zero additive components $\{f_i\}$ of $F(g)$. Specifically, both additive and epistatic fitness parameters will be Gaussian distributed with zero means and standard deviations σ_a, σ_e , respectively: $f_i \sim \mathcal{N}(0, \sigma_a)$, $f_{ij} \sim \mathcal{N}(0, \sigma_e)$. In the range of parameters tested in [56], there is no evidence of a dependence of the fitness effects on the specific realizations of the Gaussian distributed parameters, therefore we will safely consider σ_a, σ_e as effective coarse-grained descriptors of additive and epistatic fitness. We will run simulations for different parameters μ, r, σ_e , fixing all the others. The simulation ranges/values for each parameter are shown in Tab.(2). c_{ij} as in eq.(16).
- **Probing Gaussian Closure: Algorithm.** We will use *all-time* data to smooth out fluctuations due to the finite size of the population, see Sec.(2.6). From them, it is possible to get population-averaged quantities $\{\chi_i\}, \{\chi_{ij}\}$ and enforce the two approaches under examination: either inferring epistatic fitness components directly from correlations and means exploiting eq.(88) or implementing DCA

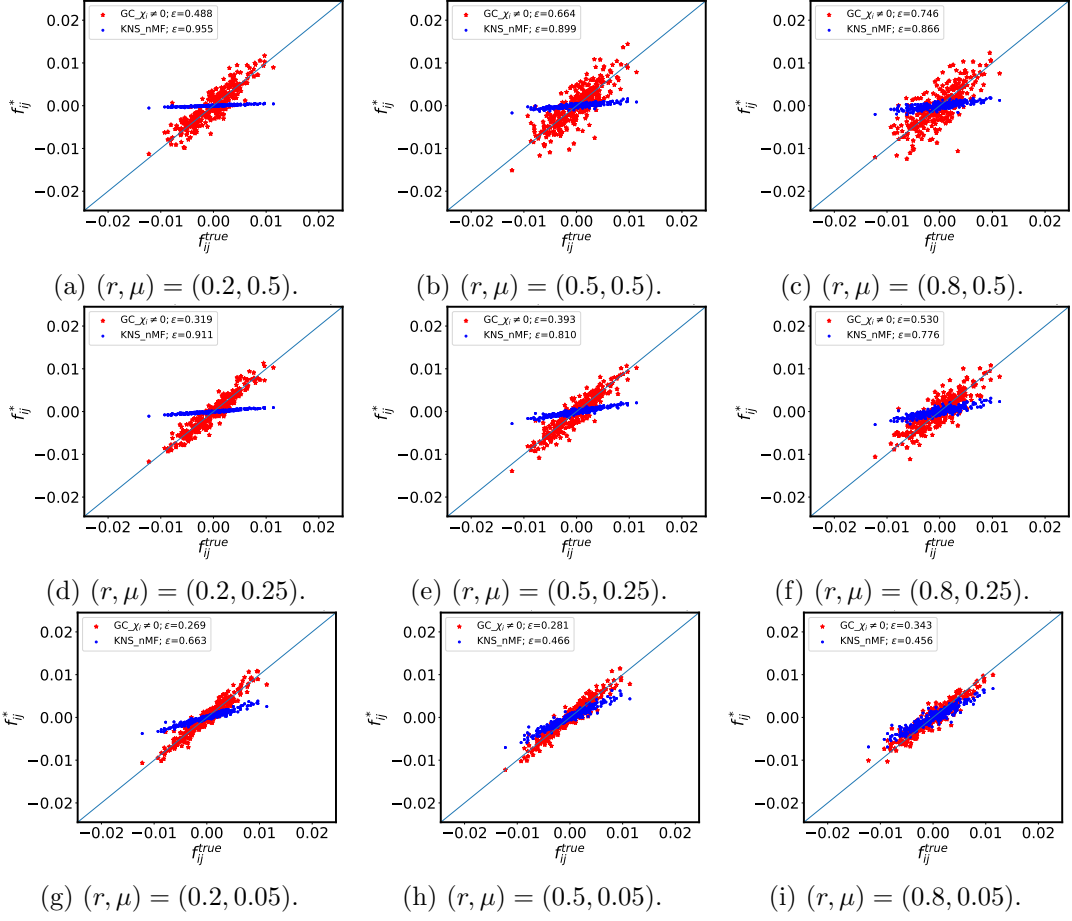


Figure 5.: Scatter Plots for MR. The red stars result from the inference based on the Gaussian Ansatz, eq.(88); blue dots for KNS reconstruction eq.(28) with MF inferred couplings. Epistatic fitness strength $\sigma_e = 0.004$, other parameters as shown in Tab.(2). From [56].

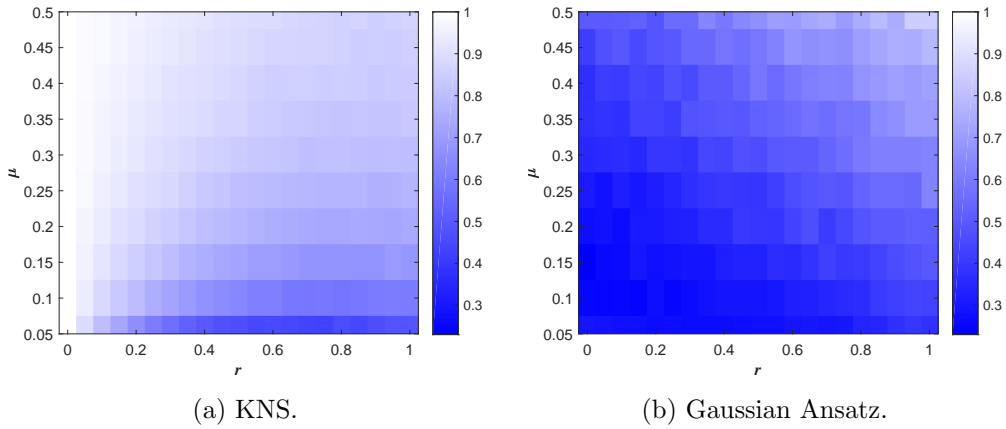


Figure 6.: Heat Maps for the MR set. The colour represents the reconstruction error ε given in eq.(70). Left: KNS reconstruction eq.(28) with MF inferred couplings. Right: inference based on the Gaussian Ansatz, eq.(88). Epistatic strength $\sigma_e = 0.004$, other parameters as in Tab.(2). From [56].

	FFPopSim	Values	Description
Structure	N	200	carrying capacity
	L	25	n. of loci
	T	10,000	n. of generations
	ρ	0.5	crossover rate
	σ_a	0.05	$f_i \sim \mathcal{N}(0, \sigma_a)$
Drivers	r	[0.0, 1.0]	outcrossing rate
	μ	[0.05, 0.5]	mutation rate
	σ_e	[0.004, 0.04]	$f_{ij} \sim \mathcal{N}(0, \sigma_e)$

Table 2.: Simulation settings for FFPopSim as employed in [56]. Light Gray for parameters that are varied in order to test the reconstructions routes GC vs KNS.

to reconstruct $\{J_{ij}\}$, then finally using eq.(28) with a Mean Field inference MF, results for PLM are found to be similar (data not shown). We use the latter as a benchmark to compare the relative improvement of the new formula with respect to the one obtained ignoring the contribution of mutations. Finally, we will compare the results of the reconstructed $\{f_{ij}^*\}$ (by GC and KNS) with the true values $\{f_{ij}\}$ in input and, in so doing, test the relative performance of the two procedures. The error in the reconstruction can be quantified by the root mean square error introduced in eq.(70):

$$\varepsilon = \sqrt{\frac{\sum_{i,j} (f_{ij}^* - f_{ij})^2}{\sum_{i,j} f_{ij}^2}},$$

which we want to be as small as possible.

- **Scanning the parameter space.** Our simulations will be divided in two sets. The first one, named **MR**, aims to explore the parameter space in the μ, r directions for a fixed epistatic strength $\sigma_e = 0.004$. In Fig.5 we show some scatter plots as resulting from the algorithm aforementioned; each column has the same r , increasing from left to right, and each row has the same mutation rate, increasing from bottom to top. For each inference technique, the core information of each scatter plot can be captured by $\varepsilon \in \mathbb{R}^+$, eq.(70). In Fig.6 there is an heat map for ε , as evaluated while scanning the parameter space in the directions $\mu \in [0.05, 0.5]$ and $r \in [0.0, 1.0]$. The second set of simulations, we shall call it **ER**, is intended to ascertain the performances of the two reconstructions as a function of σ_e, r , for a fixed $\mu = 0.2$. In Fig.7 each column has the same r , increasing from left to right, and each row has the same epistatic strength, increasing from bottom to top. In Fig.8, finally, the heat map for ε by tuning $\sigma_e \in [0.005, 0.04]$ and $r \in [0.0, 1.0]$.

3.2.1. Results & Comments

MR, Fig.5, 6. As we know from Sec.(1.3, 2.6), in the KNS theory the mutation rate cannot be zero, otherwise the QLE would be but a long-lived transient towards fixation. Nevertheless, eq.(28) assumes $\mu = 0$ therefore we do not expect it to work for suffi-

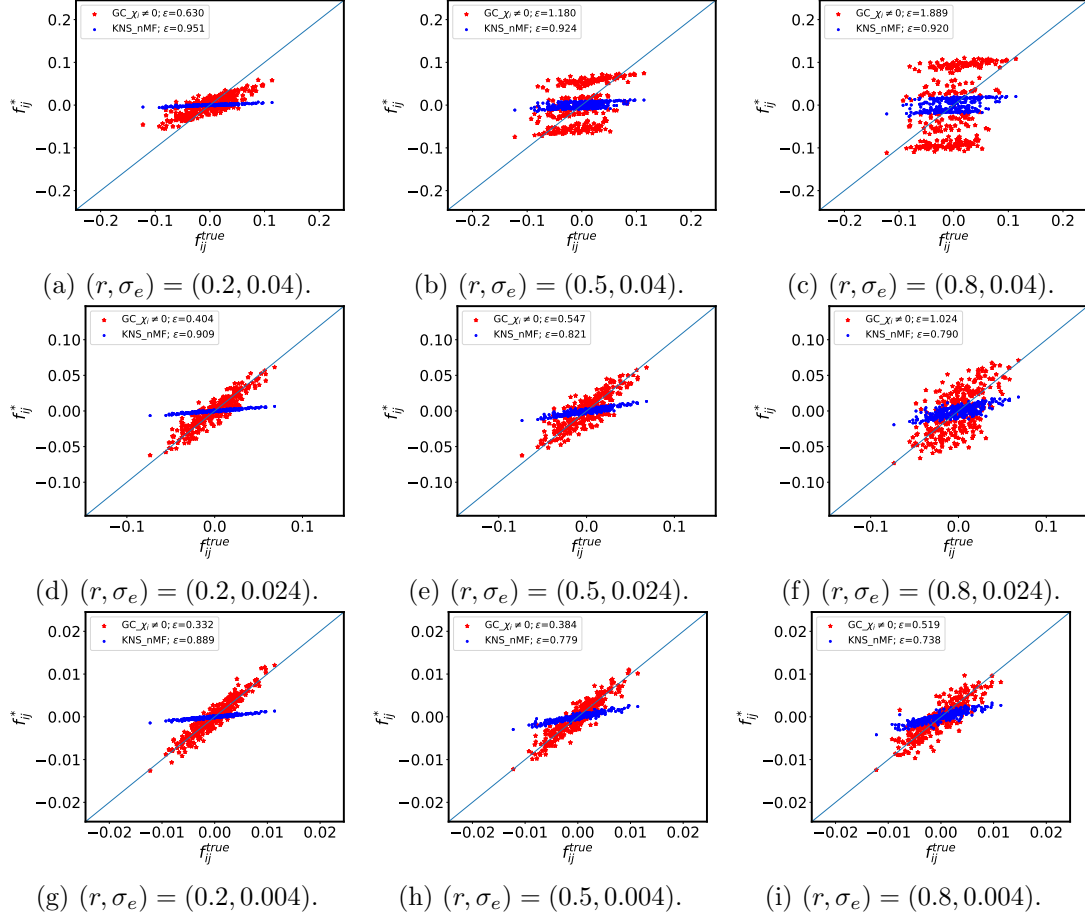


Figure 7.: Scatter Plots for set ER. The red stars result from the inference based on the Gaussian Ansatz, eq.(88); blue dots for KNS reconstruction eq.(28) with nMF inferred couplings. Mutation rate $\mu = 0.2$, other parameters as in Tab.(2). From [56].

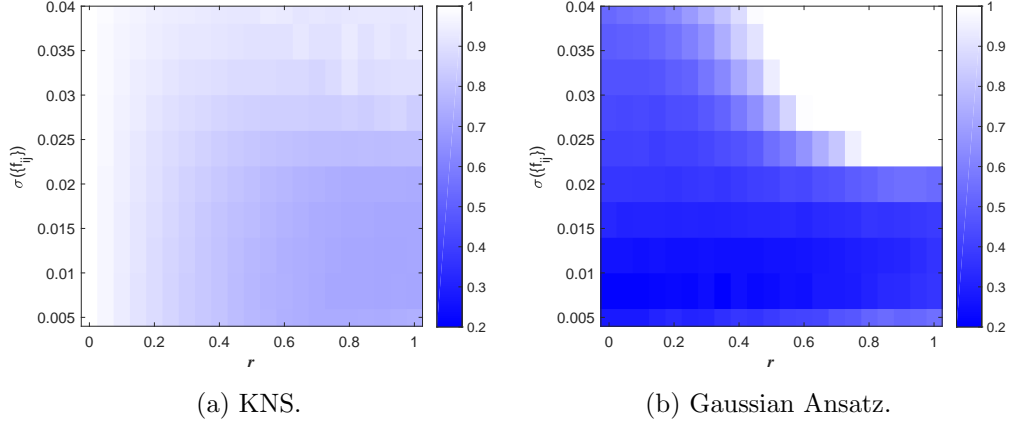


Figure 8.: Heat Maps for the ER set. The colour represents the reconstruction error ε given in eq.(70). Left: KNS reconstruction eq.(28) with nMF inferred couplings. Right: inference based on the Gaussian Ansatz, eq.(88). Mutation rate $\mu = 0.2$, other parameters as in Tab.(2). From [56].

ciently high mutation rates. Moreover, since QLE requires a high recombination rate, we do not expect it to work in a region of the phase space where $r \sim 0$ either. Both these expectations are confirmed by Fig.5, 6a. Reconstruction based on eq.(88) on the other has a better performance everywhere throughout the MR set, in particular for high mutation rates. For extremely high recombination and mutation rates (top-right) the noise due to the strength of the reshuffling of the population is likely to worsen the accuracy of the allele statistics (means and correlations) for a finite-time simulation, which ultimately results in a sparser scatter plot and a slightly higher reconstruction error ε .

ER, Fig.7, 8. Since we have fixed an high value of the mutation rate $\mu = 0.2$, we do not expect the KNS to work anywhere. Indeed, it does not. Inference based on the Gaussian Ansatz on the other hand has excellent performances except in a region of high epistasis and high recombination. We noted in Sec.(3.1.3) that the perturbative expansion is meant to be accurate whenever $L\sigma_e < 1$; accordingly in Fig.8b we see the error increasing for increasing σ_e . However, it is impossible to sweep it under the carpet: there must be a different and deeper explanation for the behaviour in the top right corner of Fig.7, which shows some clear patterns (*i.e.* the two *symmetric clouds* of reconstructed points) inexplicable in terms of a simple increased amount of noise. We will return on this below.

Finally, let us also stress that for the Gaussian Ansatz to hold, the $\{f_i\}$ have to be small, too. Increasing the magnitude of the additive fitness, the evolutionary process is more and more in danger of encouraging the emergence of clones, against the hypothesis of a monoclonal population at the very beginning of this section.

4. QLE Rupture: a New Phase

We now introduce, describe and characterize the behaviour of a population of genomes in a regime where the epistatic components of the fitness landscape are not small and dominate the dynamics. We shall call it NRC-phase, since its first clear signature is for each locus the *Non-Random Coexistence* of all the alleles in our population. We will also review some recent results from the literature hunting for further relevant insights and discuss a putative experimental observation of the NRC-phase, previously reported in literature.

Qualitatively speaking, we will explore a regime characterized by a high mutation rate μ and high epistasis σ_e (unlike QLE and Gaussian Ansatz). In the first place, we will start from describing the behaviour of genomes that are allowed to recombine $r \neq 0$ and that try to maximise a purely epistatic fitness function

$$F(g) = \sum_{i < j} f_{ij} s_i s_j ,$$

i.e. an Sherrington-Kirkpatrick (SK) fitness function, where $f = \{f_{ij}\}_{i,j}$ is an symmetric matrix of Gaussian distributed random numbers $f_{ij} \sim \mathcal{N}(0, \sigma_e)$, $f_{ii} = 0 \forall i$, $f_{ij} = f_{ji} \forall i, j$, see Sec.(2.6). We trivially observe that such a fitness function is invariant under the transformation $g \rightarrow -g$, hence we expect these two genomes to be selected with equal probability.

Let us note that out of the domain of the QLE and the Gaussian Ansatz, it would be surprising to see either eq.(28) or eq.(88) working: indeed, they both fail, as it will be clear soon, and therefore, for the time being, we leave hope to carry out inference and

will not discuss reconstruction any later.

4.1. Hallmarks of the NRC-phase

A suitable set of parameters is summarized in Tab.(3): we shall call it **RS** (Reference Simulation) and refer to it for future comparisons.

	FFPopSim	RS	Description
Drivers Structure	N	500	carrying capacity
	L	25	n. of loci
	T	10,000	n. of generations
	ρ	0.5	crossover rate
	r	0.5	outcrossing rate
	μ	0.5	mutation rate
	σ_e	0.024	$f_{ij} \sim \mathcal{N}(0, \sigma_e)$

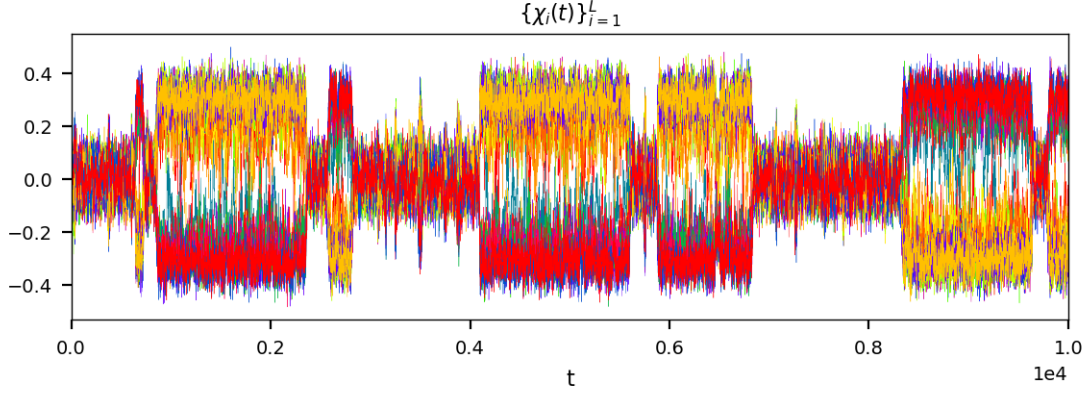
Table 3.: Parameters of the **RS**. High mutation and recombination regime, random crossovers. SK fitness function. Quenched $f_{ij} \sim \mathcal{N}(0, \sigma_e)$, $f_{ii} = 0$, $f_{ij} = f_{ji} \forall i, j$. Random initial configuration.

It is not a random choice of values, they are instead tuned so that the system dynamics lies at the edge between the well-known QLE phase and the new NRC phase, to be explored. Our line of attack will then be to describe the latter in contrast to the former, to exploit the computational and visualization tools introduced in App.(D).

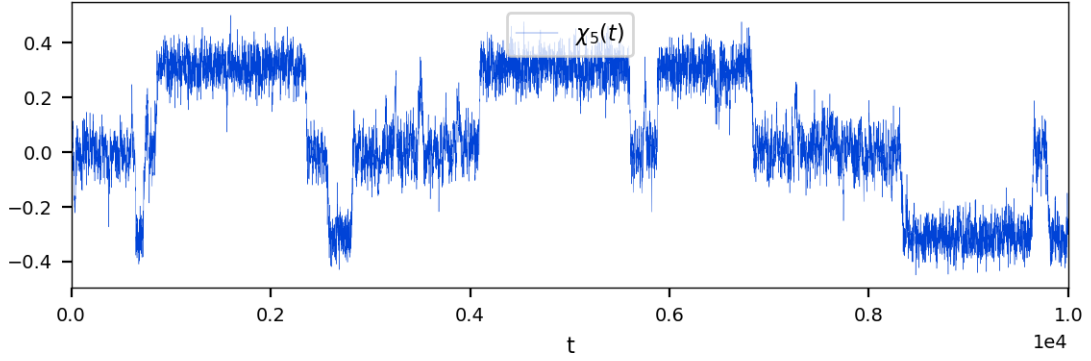
(1) **χ_i : First Order Cumulants.** In Fig.9a we show the all-time dynamics of all the magnetizations $\chi_i = \langle s_i \rangle$, cf. Fig.D1. We observe the first cumulants intermittently hovering between the expected behaviour in a QLE phase, *i.e.* $\chi_i \sim 0$, and a new phase where qualitatively $|\chi_i| \sim \alpha \neq 0$ *i.e.* where for each locus both the alleles are found in the population in a non-random fashion. The value of α is observed to primarily depend on μ, σ_e .

When increasing more and more the strength of epistasis σ_e the intermittence disappears and the dynamic of the system is always NRC-like. Obviously, being $\mu \gg 0$ we will never observe the fixation of any allele, the constant influx of mutations will always tend to destroy patters established by selection, this balance will rapidly lead to an equilibrium *i.e.* to a specific value of α . The existence of a *transition* in both directions QLE \leftrightarrow NRC is not at all trivial and one cannot assume in general that the same mechanism is responsible for both the directions. Let us also note that there is an additional element of regularity in Fig.9a: the time trajectory of all the χ_i in the latter are either of the shape shown in Fig.9b or the specular one in Fig.9c but never a mixture of these two. The already noted symmetry $g \rightarrow -g$ of the fitness function is clearly manifest in this behaviour.

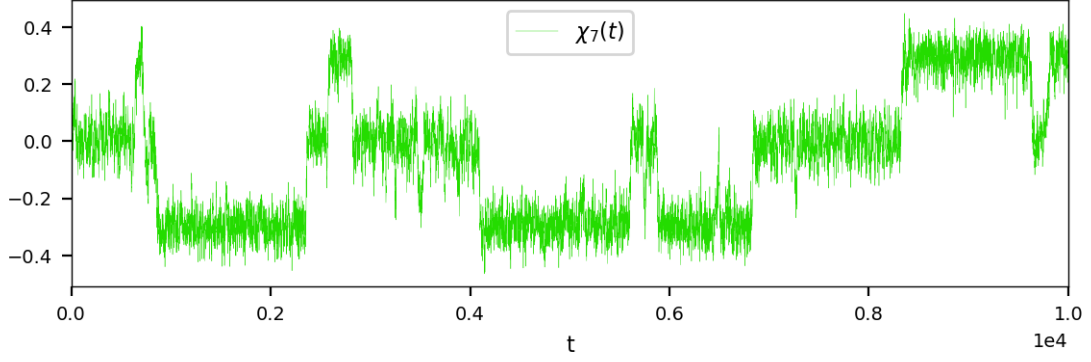
(2) **χ_{ij} : Second Order Cumulants.** In Fig.10 the all-time dynamics of a subset of the allele correlations $\{\chi_{ij}\}_{j=1}^L$ is displayed, analogous plots are observed $\forall i$, cf. Fig.D2. We notice the same pattern of intermittence as for the first order cumulants: while in QLE $\chi_{ii} = 1 - \chi_i^2 \sim 1$ and $\chi_{ij} \sim 0$, in the NRC regime one



(a) Evolution of all the L first order cumulants $\{\chi_i\}$.



(b) Evolution of χ_5 , that follows the orange-like pattern in Fig.9a.



(c) Evolution of χ_7 , that follows the red-like pattern in Fig.9a.

Figure 9.: RS, Tab.(3). Evolution for the first order cumulants $\{\chi_i\}$ at the edge of instability QLE \leftrightarrow NRC. While $\chi_i \sim 0$ in QLE, we see $|\chi_i| \sim \alpha \neq 0$ in a NRC phase. Two different groups of alleles emerge, following two symmetric trajectories.

qualitatively has $\chi_{ii} < 1$ and $|\chi_{ij}| \sim \beta \neq 0$, where β again depends primarily on μ, σ_e . In this case such behaviour is almost overshadowed by the fluctuations.

(3) **Clonal Structure.** We can assess if the observed behaviour of the first and second cumulants are due to the dynamical clonal structure of the population, in particular to a Clonal Competition (CC) regime. For instance, it is well known

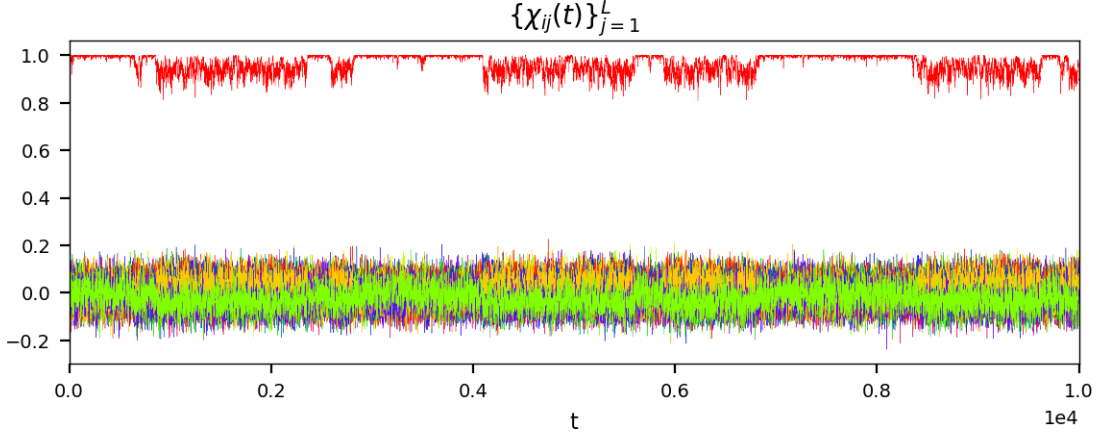


Figure 10.: RS, Tab.(3). Evolution of the second order cumulants $\{\chi_{ij}\}$ with $i = 1$ at the edge of instability QLE \leftrightarrow NRC. While $\chi_{ij} \sim 0$ for $i \neq j$ and $\chi_{ii} \sim 1$ in QLE, we see $|\chi_{ij}| \sim \beta \neq 0$ for $i \neq j$ and $\chi_{ii} < 1$ in a NRC phase. The segregation in two different families of trajectories is present also for the correlations.

that increasing epistasis with respect to recombination (in absence of mutations) enhances the probability of the onset of a CC-phase [57,58]. The mutation mechanism nevertheless is likely to affect this picture and to test these hypothesis we plot the Clonal-Structure, as shown in Fig.11, cf. Fig.D4a.

As a result, we can rule out a CC-phase, since in correspondence to a NRC region, most of the population is made by single-clone genotypes (dust-like region); however at least one non-singular clone emerges from the dust: its (fluctuating) relative size depends on μ, σ_e and this observation is true until the NRC-phase melts in the QLE randomness. Moreover, the observed fraction of individuals within the largest clone is not sufficient to explain the value $|\chi_i| \sim \alpha$: if a single large clone (in an otherwise random population) were responsible for $|\chi_i| \sim 0.3$ as in Fig.9, it would need to represent a fraction $\alpha \sim 0.3$ of the total population, which is clearly not the case of Fig.11.

- (4) **Fitness Statistics.** As last all-time plot we show the population-wide fitness statistics (mean, st.dev.), see Fig.12, cf. Fig.D3. We note that the NRC phase is characterized by a higher fitness mean with respect to the QLE expectation, therefore selection will enhance the former at the expense of the latter. Mutations, on the other hand, represent a counterforce since they destroy existing genotypes: in a regime where both of them are important, their balance is crucial. Building on this observation, we may advance the hypothesis that at the edge between the two phases, the accidental appearance of very fit clones is responsible for the transition QLE \rightarrow NRC, their accidental disappearance due to mutations is responsible for the opposite one. We will extensively explore these hypotheses in Sec.(4.1.2 - 4.1.3).
- (5) **Genotype Snapshot.** In addition to all-time plots, we can observe the population instantaneously at some point during the evolution. As a first example, we show a snapshot of the population in a NRC phase *e.g.* we fix for instance $T = 8500$, see Fig.13, cf. Fig.D5. The difference from what we had observed in the QLE phase is self-evident: strong patterns of regularity emerge, consistently

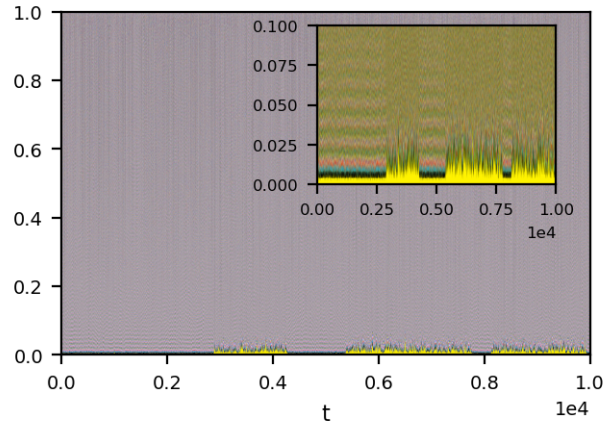


Figure 11.: RS, Tab.(3). Clonal structure throughout evolution. For each t , all the clones in the population are first ordered in descending order by size, then each one is assigned a different color (six colors repeated in the order: yellow - black - cyan - red - white - blue). Their relative size for each t is displayed as a vertical line, the largest at the bottom; a zoom is provided to the first 10% of the population. The NRC phase is marked by the emergence of non-trivial clones, yet too small for the population to be regarded as in a CC-phase, this results in a mostly dust-like plot, cf. Fig.D4.

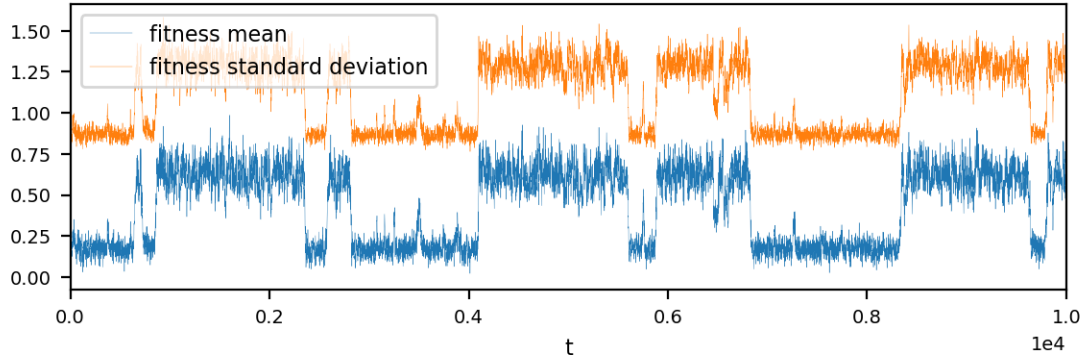


Figure 12.: RS, Tab.(3). Evolution of fitness mean and st.dev. . The QLE \leftrightarrow NRC pattern is clearly visible and entails a jump in both mean and st.dev. to higher values, suggesting the emergence of very fit genotypes.

with the allele means fluctuating around non-zero values.

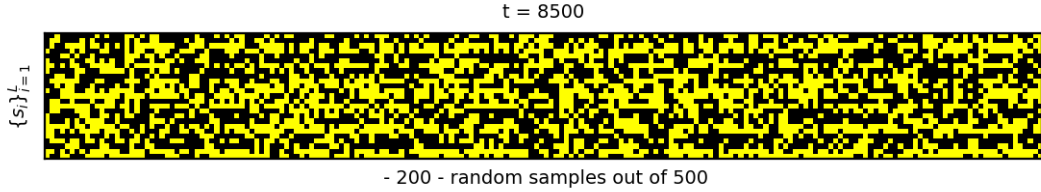


Figure 13.: RS, Tab.(3). Population snapshot for 200 samples at $t = 8500$. Y/B for $\chi_i = \pm 1$. Strong patterns emerge in a NRC phase, as suggested by the dynamics of the first order cumulants.

(6) **Fitness Distribution.** In Fig.D6 we have found that in QLE the instantaneous fitness distribution for a population evolving in a Sherrington-Kirkpatrick fitness landscape with mutations and recombination has approximately the shape of a Gaussian $\sim \mathcal{N}(0, \sqrt{L}\sigma_e)$. The analogous plot in a NRC phase shows relevant differences, a typical result is the one in Fig.14. Two major points are to be stressed:

- ★ *Asymmetry.* Ignoring for the moment the high fitness tail, let us focus on the main body of the distribution, which is not symmetric but clearly biased towards positive values. This is mostly due to the balance between mutation and strong selection: while the first favours randomness, the second tends to encourage the emergence of individual whose fitness is higher than the average, penalizing unfit individuals. Even in absence of recombination, there is a number of phenomena that arise from the balance of these two forces, see for instance [59,60].
- ★ *Fit Spikes.* Interestingly, the NRC phase is marked by the rise of a group of very fit individuals, see *zoom* in Fig.14. Their (dis)appearance is always an hallmark of the transition out from / into the NRC phase. This in turn is consistent with the jump observed in the fitness statistics, since fluctuations in the number of individuals in the fittest region have strong (delayed) effects of the fitness mean [61]. Finally, as one might expect, simulations show that the size of the fit peaks grows by increasing the fitness strength.

(7) **Quenched disorder** As a final observation, we report the dependence of the behaviour of the simulation from the *specific realization* of the $\{f_{ij}\}$. In other words, at the edge of instability, the dynamics of the system strongly depends on the details of the fitness landscape. The designation of quenched disorder comes from the analogy with the spin-glasses [62]. This tells us that σ_e is only a hyper-parameter and it not suitable to capture all the relevant information about the epistatic fitness landscape. This last point is true at the edge of instability between QLE-NRC but not for weak epistasis (always QLE) or extreme epistasis (always NRC), as we shall see in Sec.(4.1.1).

4.1.1. What If(s)

We here report some further observations on the behaviour at the edge between the QLE and the NRC phase. We address some questions that naturally arise when looking at the results illustrated in the previous section and with this spirit we put them in the form of answers to questions like "What if ... ?":

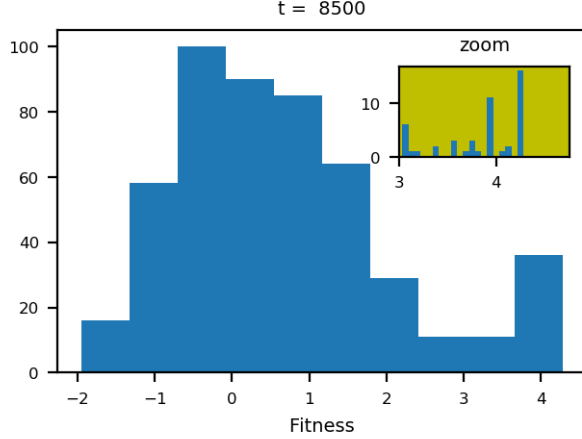


Figure 14.: RS, Tab.(3). Fitness distribution at $t = 8500$, zoom on the high fitness tail. The asymmetry of the distribution is due to the mechanism of selection, that penalizes unfit individuals. The presence of spikes in the high fitness region is peculiar of the NRC phase: its (dis)appearance follows the same pattern of instability QLE \leftrightarrow NRC as in Fig.9a.

- o $f_{ij} > 0 \forall i \neq j$ (analogously for $f_{ij} < 0 \forall i \neq j$). Let us recall $F(g) = \sum_g f_{ij} s_i s_j$, $f_{ij} \sim \mathcal{N}(0, \sigma_e)$: such system shows frustration if the epistatic components have erratic sign, while this behaviour vanishes if the f_{ij} all have the same sign. In the latter case, and for sufficiently strong epistasis with respect to other destructive forces, selection will favour either the state $\bar{g} : \{s_i = +1 \forall i\}$ or $-\bar{g}$, and it is only a matter of chance whether the dynamics will lead the system toward one or the other. In practice, in Fig.9-10 all the means/correlations will behave in the same way, following the same branch, symmetry will disappear. This trivial prediction is indeed confirmed by simulations, see Fig.15

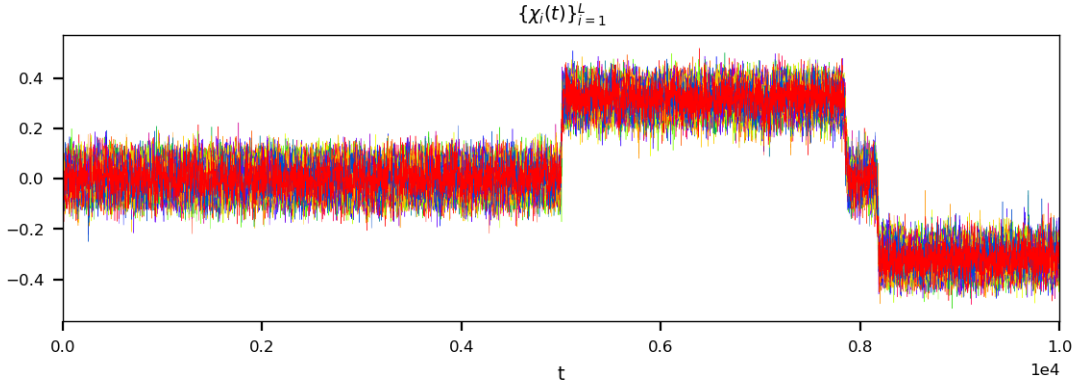


Figure 15.: Evolution of first order cumulants. Parameters of the simulation as for RS, Tab.(3), except for $\sigma_e = 0.0087$ and $f_{ij} \geq 0 \forall i, j$. The symmetry observed in Fig.9 is broken.

- o **No recombination** $r = 0$. Recombination, along with mutations, contributes to reshuffle the genetic pool, hence increasing the probability of the appearance of

new genotypes in the population. Recent theoretical efforts have investigated the role of recombination both at the genotype and phenotype level [58,63,64], despite the understanding of its interaction with other evolutionary forces remains constrained to specific framework of investigation and a general understanding is lacking.

In the context of the NRC phase, we can assess the simulations in absence of recombination, $r = 0$. Simply using RS Tab.(3) with $r = 0$ eliminates any signature of the NRC and we observe a QLE behaviour throughout the evolution. This supports the hypothesis that the probability of the appearance of fit individuals is crucial for the transition QLE \rightarrow NRC: the less the recombination, the less the such probability. One way to compensate this effect is to increase the fitness strength σ_e , in fact for a sufficiently high epistasis, we see again a behaviour of allele means similar to that observed in Fig.9, although trajectories are much more unstable, see *e.g.* Fig.16. In general, we observe much stronger fluctuations, which forces us to choose an high value of the system expected size N in order to reduce the noise. Transition probabilities appear to be sensitive to recombinations as well. Moreover, when $r = 0$, even for very high values of fitness strength, we do not observe any QLE-NRC oscillation in the plots for the clonal structure, fitness statistics and instantaneous fitness distribution, as described in the previous section. In other words, the mechanisms that sustains the birth/death of fit individuals in the high fit tail of the fitness distribution strongly depends on the presence of recombination.

In general these remarks support the hypothesis that the drivers (or consequences) of the transitions between the two phases here are fundamentally different from those in the case with recombination and one cannot regard the latter as a mere "additive" complication to the model.

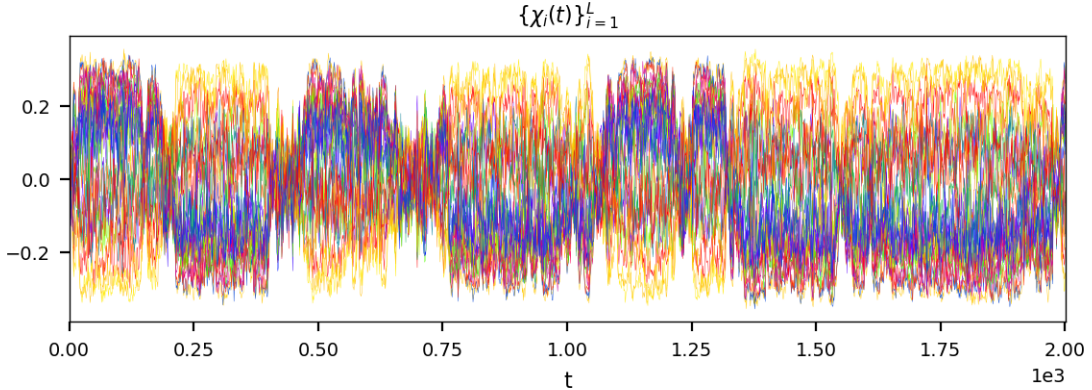


Figure 16.: Evolution of first order cumulants. Parameters of the simulation as for RS, Tab.(3) except for $N = 10.000$, $T = 2.000$, $\sigma_e = 0.09$, $r = 0$. In the case with no recombination, the behaviour of the system shows substantial differences with respect to the case $r \neq 0$.

- **Additive fitness, $f_i \neq 0$.** Additive fitness has the effect of driving each allele to fixation; more specifically $s_i \xrightarrow{\text{add.}} \text{sgn}(f_i)$. Differently from epistasis, additive fitness acts independently in each locus, and in presence of epistasis these two components of natural selection can compete and give rise to a complex equilibrium. We here focus on the narrower question: is the NRC due to the specific

role of epistasis? To test it, we can switch on additive components of fitness, for instance we can use RS with in addition $f_i \sim \mathcal{N}(0, \sigma_a)$, with $\sigma_a = 2.0 \gg \sigma_e$. As a result, we observe that even in the case high additive fitness, the observation of the QLE-NRC behaviour is present. Evidently as long as the overall fitness is sufficiently high, it does not matter whether it is additive or epistatic. In the case where both of them are present, a more suitable selection parameter is $\sigma^2 = \sigma_a^2 + \sigma_e^2$.

- **N - σ_e tuning.** As we know from Sec.(B), the size of fluctuations depends on \sqrt{N} . The higher the fluctuations in the higher the probability of finding the system in an atypical state. If the transition QLE \rightarrow NRC is triggered by the system hitting a small subset of the possible states, then we expect larger fluctuations to enhance the corresponding chances.. Accordingly, for a fixed σ_e , we will see QLE for sufficiently low N and NRC for sufficiently high N . On the other hand, for fixed N , we already know that higher epistasis will favour a NRC phase. In Fig.17 we qualitatively test these expectations for different values of $N-\sigma_e$. With regard to the intermediate region in σ_e , we see explicitly the effect of the dependence of the system fate on the specific realization of the $\{f_{ij}\}$ (some simulations may seem to be QLE or NRC for $T < \infty$ even if in a instability region); on the contrary, the extrema do not show such behaviour.

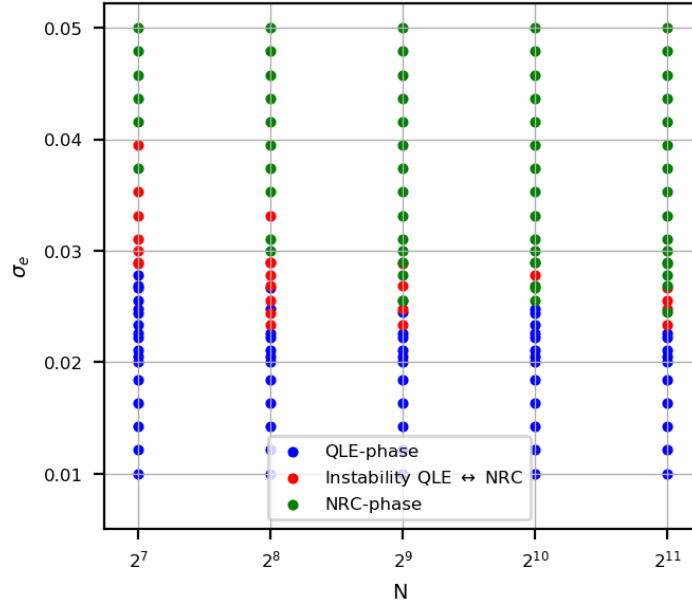


Figure 17.: Qualitative scan of the parameter space in the N, σ_e directions, all other settings as in RS, Tab.(3). Each point is obtained as follows: we fix a pair (N, σ_e) and run two simulations for $T = 10.000$ generations. If at any point we observe a transition $\text{QLE} \leftrightarrow \text{NRC}$, we mark the point as red, instability. If the system throughout the simulations appears to always be in a QLE/NRC phase, we colour the point in blue / green, respectively. In order to classify the two phases automatically, we choose the fitness mean, cf. Fig.12, as an observable and set a threshold. Due to the finite simulation time and to the dependence on the quenched disorder, the instability region is likely to be broader than what shown here.

4.1.2. QLE to NRC : heuristics

A number of previous contributions have investigated the balance between mutations and selection, *e.g.* [59,65] A typical approach consists in estimating the typical timescales for the appearance, establishment (*i.e.* survival to random drift) and fixation of new mutations, depending on the parameters of the model. We can pursue a similar line of thought to develop a plausible mechanism that could drive the QLE \rightarrow NRC transition in the framework of our interest. Let us consider a system like the one in RS, two processes should be relevant:

1. Appearance of a genotype with high fitness in the population. Let's call $P_A(g|\mu, r, N, \{f_{ij}\})$ the probability for a sufficiently fit genotype g to appear. We have only $N \ll 2^L$ individuals, there should be some $t_A(\mu, r, N, \{f_{ij}\})$ typical waiting time. How to estimate the t_A is an open question.
2. Establishment of the clone with the genotype g *i.e.* the clone is large enough so that it manages to survive to the random drift, mutations and recombination. Let's call $P_E(g|\mu, r, N, F(g))$ the corresponding probability.

One may think to a threshold value $F^*(\mu, r, N)$ above which a clone is likely to emerge. This could suggest an explanation for the behaviour observed Fig.17: let us define $F_{\max} = \max_g F(g)$, if σ_e is low enough, $F_{\max} < F^*$ and no genotype is able to emerge (QLE phase). When σ_e is such that $F_{\max} > F^*$ then it is possible for one or more clones to emerge (QLE/NRC instability), here the quenched disorder plays a fundamental role. Finally, for very high values of σ_e , $F_{\max} \gg F^*$, several clones emerge and disruptive forces (or whatever) do not manage to sweep them all out (NRC phase).

4.1.3. NRC to QLE : Muller's Ratchet

We have observed that the NRC phase is characterized by the presence of very fit spikes in the fitness distribution of the population. We can exploit the observation of the erosion of the fittest classes to draw correspondences with previous results in literature, in particular, with the theory of the Muller's Ratchet [66].

We briefly summarize the content of [61], a recent effort relevant for this section:

- A *click* of Muller's ratchet is the loss of the most fit class of individuals. The rate of the ratchet is given by the inverse of the mean time between successive clicks of the ratchet.
- The authors investigate a model where the population of N individuals is grouped into discrete classes, each characterized by the number k of deleterious mutations; There is no recombination $r = 0$, deleterious mutations happen at rate u , each mutation causes a fixed fitness loss $s \ll 1$. A master equation

$$\frac{d}{dt}n_k = s(\bar{k} - k)n_k - un_k + un_{k-1} + \sqrt{n_k}\eta_k$$

drives the stochastic evolution of n_k = number of individuals in the k -th class, η_k is the noise term.

- When $\lambda = u/s \gg 1$ the top fit class of individuals contains only a few individuals and is susceptible to an accidental extinction. In general, the magnitude of the fluctuations in the number of individuals of the most-fit class is governed by the combination Ns .
- Taking into account the fluctuations of most-fit class, those (delayed) of the

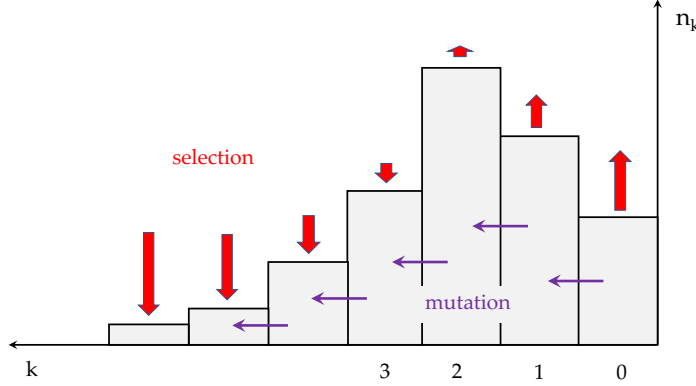


Figure 18.: Deleterious mutation-selection balance. The population is distributed among classes of individuals carrying k deleterious mutations. Classes with few mutations grow due to selection (red arrows), but lose individuals through mutations (green arrows), while classes with many mutations are selected against but replenished by mutations.

mean fitness and by exploiting a stochastic path integral approach, it is possible to estimate the mean time between clicks given by:

$$T_{\text{click}} = \frac{2.5\zeta(\lambda)}{\alpha(\lambda)s\sqrt{Nse^{-\lambda}}} e^{Nsa(\lambda)e^{-\lambda}},$$

where $\alpha(\lambda) \sim \mathcal{O}(1)$ and $\zeta(\lambda) \sim \log \lambda$.

In other words, since T_{click} is the escape time from the NRC phase, as the argument goes, we expect in a rough approximation $T_{\text{click}} \sim \exp(N)$.

4.1.4. Escape Times

As we have already pointed out, there is no *a priori* reason to believe that the two transitions QLE \leftrightarrow NRC are governed by the same mechanism: indeed, we will show in this section that they are not. We have described in the previous two sections ideas that differ substantially in methods, but target the same observable: the escape time. Let us call $t_{\text{QLE}}, t_{\text{NRC}}$ the escape times from the QLE and NRC phases, respectively, we can question our simulations about them. The algorithm is the following, see [67] for the implementation.

- (1) **Simulation.** If we tune our parameters so to set the system in a region of strong instability QLE \leftrightarrow NRC and run simulations for T as large as possible, we will observe the system undergoing multiple transitions in both directions. Let us call such a simulation ET, for instance we can set Tab.(4)

	FFPopSim	ET	Description
Drivers Structure	N	575	carrying capacity
	L	25	n. of loci
	T	150.000×10	n. of generations
	r	0.5	outcrossing rate
	ρ	0.5	crossover rate
	μ	0.5	mutation rate
	σ_e	0.029	$f_{ij} \sim \mathcal{N}(0, \sigma_e)$

Table 4.: Parameters of the ET. The total number of generations simulated is 150 times higher with respect to RS.

- (2) **Classification.** The mean fitness of the population is a suitable observable in order to set a threshold and automatically classify the two phases (above: NRC; below: QLE), hence to evaluate the number of generations spent in one phase since the last transition (escape time). As an output of this last step, we get a list of escape times from the QLE phase and analogously for the NRC phase.
- (3) **Distribution.** We can draw histograms out of those two lists and observe the distributions of the escape times $t_{\text{QLE}}, t_{\text{NRC}}$, see Fig.19. In both cases, we observe a distribution that in a first approximation can be described as exponential, so we try to fit it with

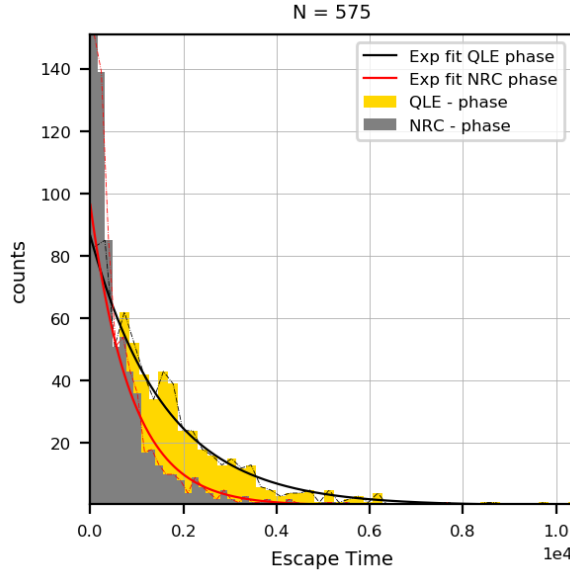
$$y(T) = \gamma_i e^{-a_i T}, \quad i = \text{QLE, NRC}. \quad (89)$$

In particular we are interested in $a_{\text{QLE}}, a_{\text{NRC}}$, that set the rates of the transitions, and use $t_{\text{QLE}} \sim 1/a_{\text{QLE}}, t_{\text{NRC}} \sim 1/a_{\text{NRC}}$ as qualitative measures of the expected escape time from the two phases.

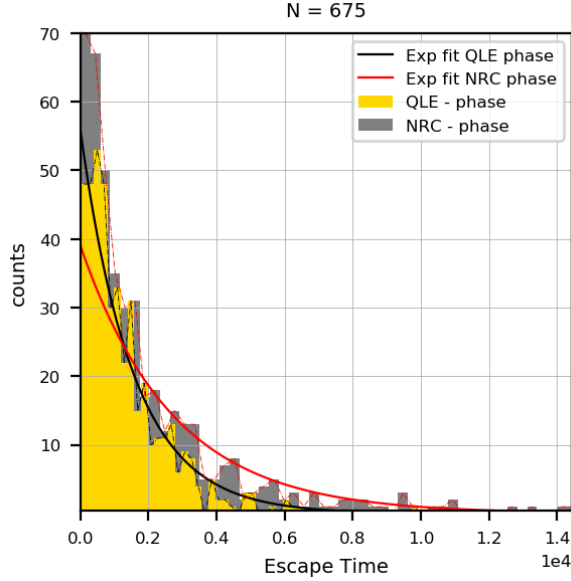
- (4) **N Dependence.** Finally, in order to check the dependence of these last quantities on the population size, as suggested in the previous section, we repeat the steps 1.-3. for different values on N and plot the behaviour of $t_{\text{QLE}}(N), t_{\text{NRC}}(N)$ in Fig.20.¹⁰

As a result, the estimate of the escape time from the QLE phase appears to be almost insensitive to the size of the system, while that from the NRC phase is compatible with an exponential behaviour $\sim \exp(N)$. This latter result is consistent with our previous discussion on the Muller's Ratchet and could be used as a starting point for a model of the phenomenon *e.g.* in terms of an escape time over a potential barrier, akin the *Arrhenius formula* $T_{\text{esc}} \sim \gamma \exp[(U(b) - U(a))/D]$, where $U(b) - U(a)$ is the height of the potential barrier and γ, D constants, see [68].

¹⁰The range of N values that can be tested is both upper and lower bounded by the computational resources: whenever the transitions are rarer, it is necessary to simulate more generations in order to collect a sufficient statistics for the histograms.



(a)



(b)

Figure 19.: Distribution of Escape Times from the QLE phase (yellow) and from the NRC phase (gray). Parameters of the simulations as in Tab.(4), two example system sizes $N = 575$ and $N = 675$. For each phase, we attempt a linear fit in the semi-log scale, in particular we get $a_{\text{QLE}}, a_{\text{NRC}}$ in eq.(89). The exponential curves in linear scale resulting from the fitting procedures are also shown.

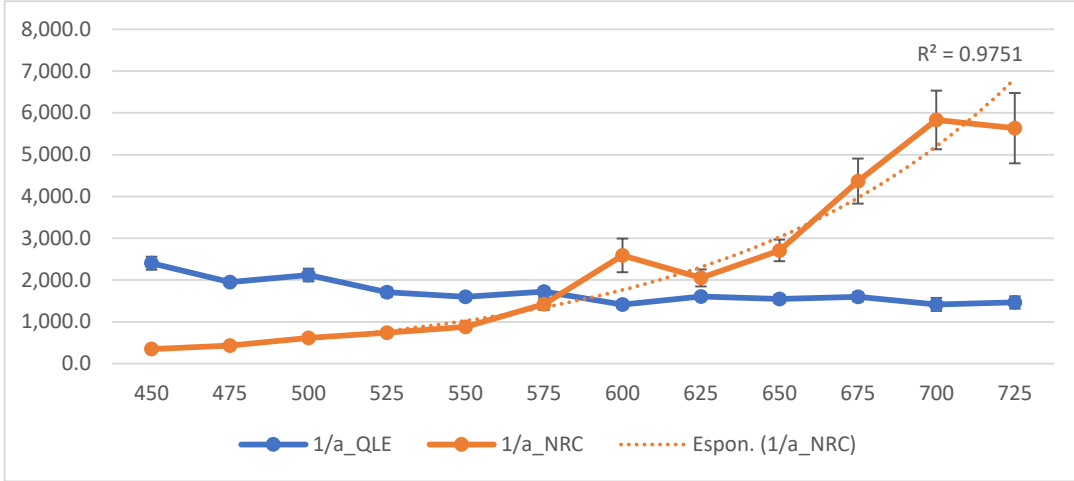


Figure 20.: Behaviour of $t_{\text{QLE}} \sim 1/a_{\text{QLE}}$, $t_{\text{NRC}} \sim 1/a_{\text{NRC}}$ as a function of the carrying capacity N . The plot is a strong evidence of the fact that the transitions QLE→NRC and NRC→QLE are due to different mechanisms. While t_{QLE} seems to be almost insensitive to N , t_{NRC} is compatible with a behaviour $\sim \exp N$, as confirmed by the coefficient of determination $R^2 \sim 1$.

4.1.5. A NRC-phase for *E.Coli*?

The celebrated R. Lenski's *E.coli* Long Term Evolution Experiment (LTEE) is an ongoing study that has been tracking genetic evolution in 12 initially identical populations of asexual *Escherichia coli*, in the same medium, since 24 February 1988 (currently more than 70,000 generations observed).

The paramount interest in this experiment lies in the fact that it is the largest dataset available that puts evolution under the spotlight of the experiment: bacteria grow, mutate, evolve (recombination is negligible for *E.coli*). The complexity of the evolutionary process emerges clearly from the ensemble of observed behaviours across populations: clades arise and diverge, small mutations leading to genetic catastrophes, intricate interactions with the environment.

In a recent contribution, the authors of [69] have worked out the latest analysis of the LTEE, enquiring the stochastic dynamical process that governs how mutations arise and spread through the populations. In particular, we focus on what the authors call *quasi-stable coexistence* therein.

The result of the experiment is showed in Fig.21. Let us focus *e.g.* on the lineage Ara-6. Current models of both "periodic selections" (where individual driver mutations fix in a sequence of discrete selective sweeps), or clonal-competition predict that, sooner or later, mutations should either fixate in the population or go extinct. But in Fig.21 we observe clearly mutations segregating into (at least) two intermediate-frequency clades that coexist for long periods, hence the name *quasi-stable coexistence*; specifically, 9/12 populations have clades that coexist for more than 10.000 generations, the relative abundance of the two clades varies from population to population.

To our best knowledge, there is so far no understanding on the mechanisms that sustain this behaviour, the authors suggest that a crucial role could be played by *negative frequency-dependent selection* (removal of deleterious alleles that depends on the current fraction of such alleles) or *coupling between ecologically divergent phenotypes*

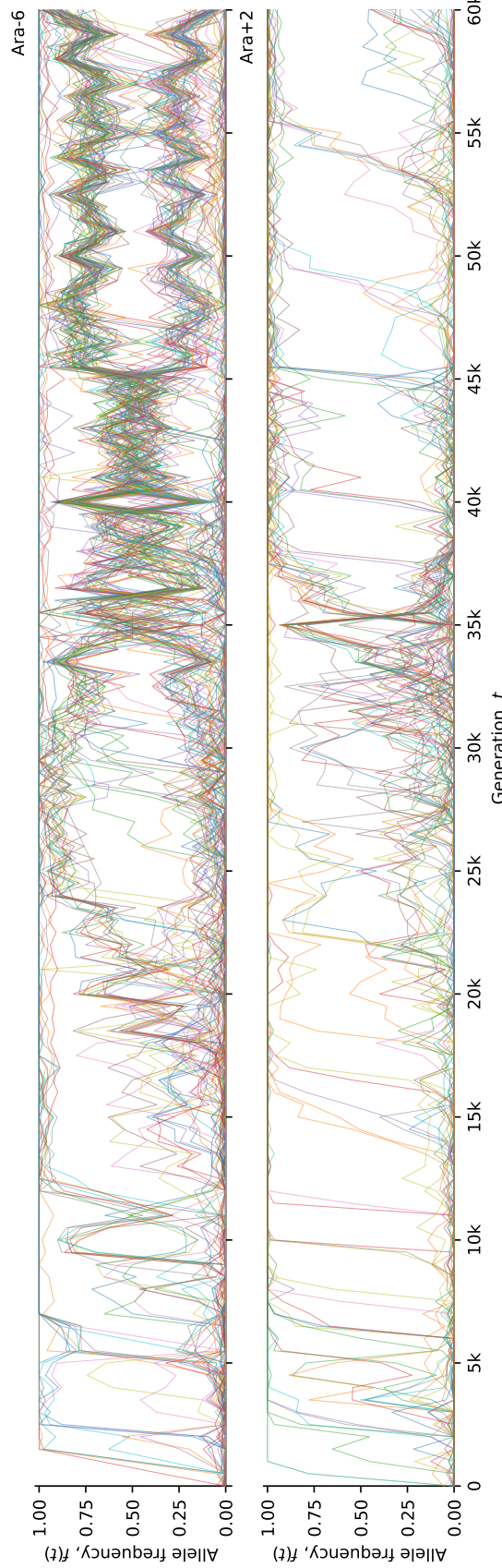


Figure 21: Allele frequency trajectories $\nu_i = (1 - \chi_i)/2 \in [0, 1]$ of all *de novo* mutations detected in the 2 of the 12 LTEE populations reported in [69], specifically the ones labeled Ara-6 and Ara+2. While Ara-6 (top row) shows an example of quasi-stable coexistence of clades, such behaviour is not present in the population Ara+2 (bottom row), where mutations fix rapidly. The analysis in [69] reveals quasi-stable coexistence in 9 out of 12 observed populations. Figure previously unpublished, private communication from B.H. Good and M.M. Desai, reproduced here with permission. Data obtained from same set of experiments as described in [69].

and fitness gain (which entails interaction at the phenotype layer between individuals and environment, projected in the genotype space through the unknown genotype-phenotype map). On the other hand, the coupling environment-selection is exactly what we encode when using a selection based on a fitness function, so we may hypothesise that such behaviour of the *E.coli* is not induced or sustained by the same fundamental mechanisms that induce or sustain the NRC phase in our simulations with $r \sim 0$ (yet, unknown).

This hypothesis offers undoubtedly an exciting line of research for the next future. On the other hand, despite the number of observations, the NRC phase remains obscure in many respects, even at the stage of the synthetic simulation. In particular, there is little understanding on which are the drivers of the transitions $\text{QLE} \leftrightarrow \text{NRC}$ and which mechanisms sustain the NRC phase and filling this gap, we believe, will be a fundamental step towards a meaningful application of NRC predictions to biological data.

5. Discussion and outlook

In this work we have provided a self-contained overview of the dynamics of a population evolving under selection (Darwinian evolution, survival of the fitness), mutation and recombination. We have shown how high rates of mutation or recombination (or both) relative to the rate of selection naturally leads to the Quasi-Linkage Equilibrium (QLE) phase first described by Kimura [11]. The QLE phase is characterized by:

- correlations between allele distributions at different loci are weak;
- multi-genome distributions approximately factorize into products of one-genome distributions;
- the distributions of individuals in the population over genotypes are well described by the Gibbs-Boltzmann distributions

All of the above makes the QLE phase qualitatively similar to equilibrium statistical mechanics, particularly to thermal equilibrium and relaxation to thermal equilibrium in the theory of gases. The one-genome distributions satisfy a nonlinear evolution equation analogous to Boltzmann equation where recombination plays the role of gas collisions. The statistical interaction terms in the Gibbs-Boltzmann distribution, analogous to energy terms, are proportional to combinations of evolution parameters describing selection and recombination. These relations take different albeit quite similar forms in the limits of respectively high recombination rate (but not mutation rate), and high mutation rate (but not recombination rate). A single formula encompasses both cases. When it holds, evolutionary parameters such as additive and epistatic fitness can be inferred from Gibbs-Boltzmann model parameters which in turn can be inferred from data. We have demonstrated that the above scheme works in silico experiments, and we have also demonstrated how to derive higher-order inference schemes than the ones alluded to above. We suggest that QLE is a fertile field for future applications of statistical physics concepts to population genetics on the whole genome level.

On a different track we have considered the dynamics at relatively higher values of selection. We have then discovered a new behaviour that breaks time translation symmetry; for sufficiently strong epistatic selection the state of the population switches randomly between a behavior qualitatively similar to QLE, and a NRC phase where the population is dominated by one fit genotype and its neighbours. We have determined how the stability boundaries of the QLE phase going towards the NRC phase

and vice versa change with model parameters including population size N .

We believe that also the NRC phase constitutes an interesting application area of statistical physics. We have further tried to relate it to behavior observed experimentally in long-time evolution experiments.

On a general level the conclusion of this work is that the statistical physics analogy is both useful and of limited use in population genetics. It is a fact that reasonable models of evolution in certain parameter ranges settle down to stationary distributions of the same form as in equilibrium statistical mechanics, which is the basis for theories such as those developed in [70–72].

A whole collection of methods, collectively known as Direct Coupling Analysis (DCA) can then be used to infer evolutionary parameters from the distribution of sequences in a population. Naturally, if and when one has access to time series data, such in Neuroscience, other inference methods can be used, and they will often be more powerful. Large-scale sequencing data on are however rarely of this type: more typically one knows the distribution of sequences (genotypes) at one or at most a few time points, and one does not have information on which sequences gave rise to which other sequences except from their similarity. In this setting the knowledge that the distribution is of the Gibbs-Boltzmann type can be leveraged to extract parameters describing the dynamics from what is essentially static information.

On the other hand, the underlying dynamics is not in thermal equilibrium *i.e.* does not obey detailed balance, and the range of possibilities is hence wider [73,74]. In the class of models considered in this work the distribution does not have to approach that of a stationary Gibbs-Boltzmann distribution with energy-like terms; dynamics can go on indefinitely, and the distribution of genotypes in a population can fluctuate without ever reaching a stationary state. Models of life, even with all the simplifying assumptions made here, hence allow for rich repertoires not easily captured by models too closely patterned after equilibrium statistical mechanics.

References

- [1] Klug W, Cummings R, CA S, et al. Concepts of genetics. 3rd ed. Pearson Education; 2012.
- [2] Yoshiura Ki, Kinoshita A, Ishida T, et al. A snp in the abcc11 gene is the determinant of human earwax type. *Nature Genetics*. 2006;38(3):324–330.
- [3] Yengo L, Sidorenko J, Kemper KE, et al. Meta-analysis of genome-wide association studies for height and body mass index in ~ 700000 individuals of European ancestry. *Human Molecular Genetics*. 2018 08;27(20):3641–3649.
- [4] Shu Y, McCauley J. GISAID: Global initiative on sharing all influenza data—from vision to reality. *Eurosurveillance*. 2017;22(13).
- [5] Hardy GH. Mendelian proportions in a mixed population. *Science*. 1908;28(706):49–50.
- [6] Weinberg W. über den nachweis der vererbung beim menschen. *Jahreshefte des Vereins für vaterländische Naturkunde in Württemberg*. 1908;64:368—382.
- [7] Fisher R. The genetical theory of natural selection. Oxford: The Clarendon Press; 1930.
- [8] Peliti L. Introduction to the statistical theory of darwinian evolution. *arXiv e-prints*. 1997 12;.
- [9] Blythe R, McKane A. Stochastic models of evolution in genetics, ecology and linguistics. *Journal of Statistical Mechanics: Theory and Experiment*. 2007 7;2007(07):P07018–P07018.
- [10] Zeng H, Aurell E. Inverse ising techniques to infer underlying mechanisms from data. *Chinese Physics B*. 2020;.

- [11] Kimura M. Attainment of quasi linkage equilibrium when gene frequencies are changing by natural selection. *Genetics*. 1965;52(5):875–90.
- [12] Neher RA, Shraiman BI. Statistical genetics and evolution of quantitative traits. *Rev Mod Phys*. 2011;83:1283–1300.
- [13] Zeng H, Aurell E. Inferring genetic fitness from genomic data. *Phys Rev E*. 2020;5; 101:052409.
- [14] Slatkin M. Linkage disequilibrium - understanding the evolutionary past and mapping the medical future. *Nature Reviews Genetics*. 2008;6:9:477–485.
- [15] Cover TM, Thomas JA. Elements of information theory. USA: Wiley-Interscience; 2006.
- [16] Wainwright MJ, Jordan MI. Graphical models, exponential families, and variational inference. *Foundations and Trends in Machine Learning*. 2008 Nov;1(1–2):1–305.
- [17] Nguyen H, Zecchina R, Berg J. Inverse statistical problems: from the inverse ising problem to data science. *Advances in Physics*. 2017;66(3):197–261.
- [18] Kappen HJ, Rodríguez FB. Efficient learning in boltzmann machines using linear response theory. *Neural Comput*. 1998;10(5):1137–1156.
- [19] Besag J. Statistical analysis of non-lattice data. *The Statistician*. 1975;24(3):179–195.
- [20] Ravikumar P, Wainwright MJ, Lafferty JD. High-dimensional ising model selection using ℓ_1 -regularized logistic regression. *Ann Stat*. 2010 Jun;38(3):1287–1319.
- [21] Vuffray M, Misra S, Lokhov A, et al. Interaction screening: Efficient and sample-optimal learning of Ising models. In: Lee DD, Sugiyama M, Luxburg UV, et al., editors. *Advances in neural information processing systems 29*. Curran Associates, Inc.; 2016. p. 2595–2603.
- [22] Berg J. Statistical mechanics of the inverse Ising problem and the optimal objective function. *J Stat Mech: Theory Exp*. 2017;2017(8):083402.
- [23] Lokhov AY, Vuffray M, Misra S, et al. Optimal structure and parameter learning of Ising models. *Sci Adv*. 2018 Mar;4(3):e1700791.
- [24] Schneidman E, Berry MJ, Segev R, et al. Weak pairwise correlations imply strongly correlated network states in a neural population. *Nature*. 2006 Apr;440(7087):1007–1012.
- [25] Weigt M, White RA, Szurmant H, et al. Identification of direct residue contacts in protein-protein interaction by message passing. *Proc Natl Acad Sci*. 2009;106(1):67–72.
- [26] Burger L, van Nimwegen E. Disentangling direct from indirect co-evolution of residues in protein alignments. *PLoS Comput Biol*. 2010 Jan;6(1):e1000633.
- [27] Morcos F, Pagnani A, Lunt B, et al. Direct-coupling analysis of residue coevolution captures native contacts across many protein families. *Proc Natl Acad Sci*. 2011;108(49):E1293–E1301.
- [28] Hopf TA, Colwell LJ, Sheridan R, et al. Three-dimensional structures of membrane proteins from genomic sequencing. *Cell*. 2012;149(7):1607–1621.
- [29] Jones DT, Buchan DWA, Cozzetto D, et al. PSICOV: precise structural contact prediction using sparse inverse covariance estimation on large multiple sequence alignments. *Bioinformatics*. 2012;28(2):184–190.
- [30] Ekeberg M, Lökvist C, Lan Y, et al. Improved contact prediction in proteins: Using pseudolikelihoods to infer potts models. *Phys Rev E*. 2013 Jan;87:012707.
- [31] Ekeberg M, Hartonen T, Aurell E. Fast pseudolikelihood maximization for direct-coupling analysis of protein structure from many homologous amino-acid sequences. *J Comput Phys*. 2014;276:341–356.
- [32] Andreatta M, Lapagne S, Li SC, et al. Prediction of residue-residue contacts from protein families using similarity kernels and least squares regularization. *arXiv*. 2014 March; 1311.1301v3.
- [33] Feinauer C, Skwark MJ, Pagnani A, et al. Improving contact prediction along three dimensions. *PLoS Comput Biol*. 2014 Oct;10(10):e1003847.
- [34] Jones DT, Singh T, Koscielok T, et al. MetaPSICOV: combining coevolution methods for accurate prediction of contacts and long range hydrogen bonding in proteins. *Bioinformatics*. 2015 Apr;31(7):999–1006.
- [35] Golkov V, Skwark MJ, Golkov A, et al. Protein contact prediction from amino acid co-evolution using convolutional networks for graph-valued images. In: Lee DD, Sugiyama M,

Luxburg UV, et al., editors. Advances in neural information processing systems 29. Curran Associates, Inc.; 2016. p. 4222–4230.

[36] Michel M, Skwark MJ, Menéndez Hurtado D, et al. Predicting accurate contacts in thousands of Pfam domain families using PconsC3. *Bioinformatics*. 2017 Sep;33(18):2859–2866.

[37] Hopf TA, Ingraham JB, Poelwijk FJ, et al. Mutation effects predicted from sequence co-variation. *Nat Biotechnol*. 2017 Jan;35(2):128–135.

[38] Ovchinnikov S, Park H, Varghese N, et al. Protein structure determination using metagenome sequence data. *Science*. 2017;355(6322):294–298.

[39] Senior AW, Evans R, Jumper J, et al. Improved protein structure prediction using potentials from deep learning. *Nature*. 2020;557(7792):706–710.

[40] Hiranuma N, Park H, Baek M, et al. Improved protein structure refinement guided by deep learning based accuracy estimation. *Nature Communications*. 2021;12:1340.

[41] Baldassi C, Zamparo M, Feinauer C, et al. Fast and accurate multivariate gaussian modeling of protein families: Predicting residue contacts and protein-interaction partners. *PLoS One*. 2014 Mar;9(3):e92721.

[42] Figliuzzi M, Jacquier H, Schug A, et al. Coevolutionary landscape inference and the context-dependence of mutations in beta-lactamase TEM-1. *Mol Biol Evol*. 2016; 33(1):268.

[43] Uguzzoni G, John Lovis S, Oteri F, et al. Large-scale identification of coevolution signals across homo-oligomeric protein interfaces by direct coupling analysis. *Proc Natl Acad Sci*. 2017;114(13):E2662–E2671.

[44] De Leonardis E, Lutz B, Ratz S, et al. RNA secondary and tertiary structure prediction by tracing nucleotide co-evolution with direct coupling analysis. *Biophys J*. 2016 Feb; 110(3, Supplement 1):364a.

[45] Skwark MJ, Croucher NJ, Puranen S, et al. Interacting networks of resistance, virulence and core machinery genes identified by genome-wide epistasis analysis. *PLoS Genet*. 2017 Feb;13(2):e1006508.

[46] Schubert B, Maddamsetti R, Nyman J, et al. Genome-wide discovery of epistatic loci affecting antibiotic resistance using evolutionary couplings. *bioRxiv*. 2018;.

[47] Zeng HL, Dichio V, Horta ER, et al. Global analysis of more than 50,000 SARS-CoV-2 genomes reveals epistasis between eight viral genes. *Proceedings of the National Academy of Sciences*. 2020;117(49):31519–31526.

[48] Roudi Y, Aurell E, Hertz JA. Statistical physics of pairwise probability models. *Front Comput Neurosci*. 2009;3(22):1–15.

[49] Stein RR, Marks DS, Sander C. Inferring pairwise interactions from biological data using maximum-entropy probability models. *PLoS Comput Biol*. 2015 Jul;11(7):e1004182.

[50] Cocco S, Feinauer C, Figliuzzi M, et al. Inverse statistical physics of protein sequences: a key issues review. *Reports on Progress in Physics*. 2018 1;81(3):032601.

[51] Sessak V, Monasson R. Small-correlation expansions for the inverse Ising problem. *J Phys A: Math Theor*. 2009;42(5):055001.

[52] Thouless DJ, Anderson PW, Palmer RG. Solution of 'solvable model of a spin glass'. *The Philosophical Magazine: A Journal of Theoretical Experimental and Applied Physics*. 1977;35(3):593–601.

[53] Georges A, Yedidia JS. How to expand around mean-field theory using high-temperature expansions. *Journal of Physics A: Mathematical and General*. 1991 may;24(9):2173–2192.

[54] Ricci-Tersenghi F. The bethe approximation for solving the inverse ising problem: a comparison with other inference methods. *Journal of Statistical Mechanics: Theory and Experiment*. 2012 aug;2012(08):P08015.

[55] Mauri E, Cocco S, Monasson R. Gaussian closure scheme in the quasi-linkage equilibrium regime of evolving genome populations. *EPL (Europhysics Letters)*. 2021;132(5):56001.

[56] Zeng HL, Mauri E, Dichio V, et al. Inferring epistasis from genomic data outside the high-recombination limit. *arXiv e-prints*. 2020 Jun;:arXiv:2006.16735.

[57] Neher RA, Shraiman BI. Competition between recombination and epistasis can cause

a transition from allele to genotype selection. *Proceedings of the National Academy of Sciences*. 2009;106(16):6866–6871.

[58] Neher R, Vucelja M, Mezard M, et al. Emergence of clones in sexual populations. *Journal of Statistical Mechanics: Theory and Experiment*. 2013;2013(01).

[59] Desai M, Fisher D. Beneficial mutation–selection balance and the effect of linkage on positive selection. *Genetics*. 2007;176(3):1759–1798.

[60] Walczak A, Nicolaisen L, Plotkin J, et al. The structure of genealogies in the presence of purifying selection: a fitness-class coalescent. *Genetics*. 2012;190(2):753–779.

[61] Neher R, Shraiman B. Fluctuations of fitness distributions and the rate of muller’s ratchet. *Genetics*. 2012;191(4):1283–1293.

[62] Castellani T, Cavagna A. Spin-glass theory for pedestrians. *Journal of Statistical Mechanics: Theory and Experiment*. 2005;2005(5):05012.

[63] Neher RA, Kessinger TA, Shraiman BI. Coalescence and genetic diversity in sexual populations under selection. *Proceedings of the National Academy of Sciences*. 2013;110(39):15836–15841.

[64] Held T, Klemmer D, Lässig M. Survival of the simplest in microbial evolution. *Nature communications*. 2019;10(1):1–11.

[65] Desai MM, Fisher DS, Murray AW. The speed of evolution and maintenance of variation in asexual populations. *Current biology*. 2007;17(5):385–394.

[66] Muller H. The relation of recombination to mutational advance. *Mutation Research/Fundamental and Molecular Mechanisms of Mutagenesis*. 1964;1(1):2 – 9.

[67] Dichio V. dichio/studiодарвин [Github]; 2021. Available from: <https://github.com/dichio/studiодарвин>.

[68] Gardiner C. *Handbook of stochastic methods for physics, chemistry and the natural sciences*. 3rd ed. (Springer Series in Synergetics; Vol. 13). Berlin: Springer-Verlag; 2004.

[69] Good B, McDonald M, Barrick J, et al. The dynamics of molecular evolution over 60.000 generations. *Nature*. 2017;551(7678):45–50.

[70] Ao P, Kwon C, Qian H. On the existence of potential landscape in the evolution of complex systems. *Complexity*. 2007;12(4):19–27.

[71] Ao P. Emerging of stochastic dynamical equalities and steady state thermodynamics from darwinian dynamics. *Communications in Theoretical Physics*. 2008 may;49(5):1073–1090.

[72] Wang J. Landscape and flux theory of non-equilibrium dynamical systems with application to biology. *Advances in Physics*. 2015;64(1):1–137.

[73] Waddington CH. *The strategy of the genes: A discussion of some aspects of theoretical biology*. Routledge; 1957:2014.

[74] Zhou JX, Aliyu MDS, Aurell E, et al. Quasi-potential landscape in complex multi-stable system. *R Soc Interface*. 2012;9:3539–3553.

[75] Gnedenko B. *Theory of probability*. 6th ed. Taylor & Francis; 1998.

[76] Zinn-Justin J. *Path integrals in quantum mechanics*. Oxford University Press; 2010.

[77] Messer P. Neutral models of genetic drift and mutation. In: Kliman RM, editor. *Encyclopedia of evolutionary biology*. Oxford: Academic Press; 2016. p. 119 – 123.

[78] Wright S. Evolution in mendelian populations. *Genetics*. 1931;16(2):97.

[79] Kimura M. Solution of a process of random genetic drift with a continuous model. *Proceedings of the National Academy of Sciences of the United States of America*. 1955;41(3):144.

[80] Neher RA, Walczak AM. Progress and open problems in evolutionary dynamics. *arXiv e-prints*. 2018 4;.

[81] Gao C, Cecconi F, Vulpiani A, et al. DCA for genome-wide epistasis analysis: the statistical genetics perspective. *Physical Biology*. 2019 1;16(2):026002.

[82] Zanini F, Neher R. Ffpopsim: an efficient forward simulation package for the evolution of large populations. *Bioinformatics*. 2012;28(24):3332–3333.

[83] Mezard M, Montanari A. *Information, physics, and computation*. Oxford University Press; 2009.

[84] Pressé S, Ghosh K, Lee J, et al. Principles of maximum entropy and maximum caliber in

statistical physics. *Rev Mod Phys.* 2013 Jul;85:1115–1141.

[85] Jaynes ET. Information theory and statistical mechanics. *Physical review.* 1957; 106(4):620.

[86] Auletta G, Rondoni L, Vulpiani A. On the relevance of the maximum entropy principle in non-equilibrium statistical mechanics. *The European Physical Journal Special Topics.* 2017;226(10):2327–2343.

[87] Aurell E. The maximum entropy fallacy redux? *PLoS computational biology.* 2016; 12(5):e1004777.

[88] Amari Si. Differential-geometrical methods in statistics. Vol. 28. Springer Science & Business Media; 2012.

[89] Amari S. Estimating functions of independent component analysis for temporally correlated signals. *Neural Computation.* 2000;12:2083–2107.

[90] Amari S. Information geometry. *Japanese Journal of Mathematics.* 2021;16:1—48.

Appendix A. Moments vs Cumulants

Here we briefly introduce moments and cumulants of a probability distribution and specify the discussion for the specific case of the Gaussian distribution. Let $\mathbf{X} = (X_1, \dots, X_n)$ be a vector of random variables with pdf $p(\mathbf{x})$, then the *characteristic function* is

$$\phi(\mathbf{q}) = \int p(\mathbf{x}) e^{i\mathbf{q}\mathbf{x}} . \quad (\text{A1})$$

with $\phi(\mathbf{0}) = 1$, $|\phi(\mathbf{q})| \leq 1$. The function $\phi(\mathbf{q})$ is a characterization of the probability distribution $p(\mathbf{q})$ *i.e.* it completely determines its behaviour and properties. If the *raw moments* $\langle \prod_i X_i^{m_i} \rangle$ exist, then

$$\langle \prod_i X_i^{m_i} \rangle = \left[\prod_i \left(-i \frac{\partial}{\partial q_i} \right)^{m_i} \phi(\mathbf{q}) \right]_{\mathbf{q}=\mathbf{0}} . \quad (\text{A2})$$

It is also possible to define the *cumulant generating function* as

$$\psi(\mathbf{q}) = \log \phi(\mathbf{q}) . \quad (\text{A3})$$

Suppose that it is possible to expand $\phi(\mathbf{q})$ and $\psi(\mathbf{q})$ in power series about the origin (*i.e.* all derivatives exist); then we can formally write:

$$\phi(\mathbf{q}) = \sum_{r=1}^{\infty} i^r \sum_{\{\mathbf{m}\}} \langle X_1^{m_1} \dots X_n^{m_n} \rangle \frac{q_1^{m_1} \dots q_n^{m_n}}{m_1! \dots m_n!} \delta\left(r, \sum_{i=1}^n m_i\right) , \quad (\text{A4})$$

$$\psi(\mathbf{q}) = \sum_{r=1}^{\infty} i^r \sum_{\{\mathbf{m}\}} \langle \langle X_1^{m_1} \dots X_n^{m_n} \rangle \rangle \frac{q_1^{m_1} \dots q_n^{m_n}}{m_1! \dots m_n!} \delta\left(r, \sum_{i=1}^n m_i\right) , \quad (\text{A5})$$

where $\langle X_1^{m_1} \dots X_n^{m_n} \rangle$ are defined in eq.(A2) and $\langle \langle X_1^{m_1} \dots X_n^{m_n} \rangle \rangle$ are the *cumulants* of the distribution $p(\mathbf{x})$. Both these two set of quantities stem from the same characteristic function $\phi(\mathbf{q})$ and are alternative parametrizations of the probability distribution.

Expanding and comparing eq.(A4, A5) one finds:

$$\begin{aligned}\langle\langle X_i \rangle\rangle &= \langle X_i \rangle, \\ \langle\langle X_i X_j \rangle\rangle &= \langle X_i X_j \rangle - \langle X_i \rangle \langle X_j \rangle, \\ \langle\langle X_i X_j X_k \rangle\rangle &= \langle X_i X_j X_k \rangle - \langle X_i X_j \rangle \langle X_k \rangle - \langle X_i X_k \rangle \langle X_j \rangle + \\ &\quad - \langle X_j X_k \rangle \langle X_i \rangle + 2 \langle X_i \rangle \langle X_j \rangle \langle X_k \rangle;\end{aligned}$$

note that the first two cumulants are the means and covariances (second *central moments*). A diagrammatic method to compute cumulants was given in [68]; an extensive treatment from the probability-theory point of view can be found in [75].

As far as this work is concerned, an important difference is to be stressed. We have $\langle X^{2n} \rangle \geq \langle X^n \rangle^2$ and thus all moments contain information about lower moments [68]. On the other hand, higher order cumulants contain information of decreasing significance and one can therefore consider the approximation that $\langle\langle X^n \rangle\rangle = 0 \ \forall n > 2$. In the language of quantum field theory, the moments $\langle X_1 \dots X_n \rangle$ are *n-point correlation functions* while the $\langle\langle X_1 \dots X_n \rangle\rangle$ are *n-point connected correlation functions* *i.e.* the sum over all *n*-points 1PI Feynman diagrams, a key ingredients of such theories [76]. Let us specify the above discussion to the case of a *multivariate Gaussian probability distribution*:

$$p(\mathbf{x}) = \frac{1}{\mathcal{Z}} e^{-\frac{1}{2}(\mathbf{x}-\boldsymbol{\mu})^T C^{-1}(\mathbf{x}-\boldsymbol{\mu})}, \quad (\text{A6})$$

where $\boldsymbol{\mu}$ is the mean and C is the covariance matrix, $\mathcal{Z} = [(2\pi)^n \det(C)]^{-\frac{1}{2}}$ is the normalization. The characteristic function of such distribution is

$$\phi(\mathbf{q}) = e^{i\mathbf{q}^T \boldsymbol{\mu} - \frac{1}{2}\mathbf{q}^T C \mathbf{q}} \quad (\text{A7})$$

and from this we see that *all cumulants of order ≥ 2 vanish*. Therefore, all moments can be expressed in terms only of first and second order cumulants. Since they are of interest for this work, let us evaluate the first four moments of this distribution using eq.(A2) (different indices).

$$\begin{aligned}\langle X_i \rangle &= -i \frac{\partial}{\partial q_i} \phi(\mathbf{q}) \Big|_{\mathbf{q}=0} \\ &= -i \left(i\mu_i - \sum_n C_{in} q_n \right) e^{i\mathbf{q}^T \boldsymbol{\mu} - \frac{1}{2}\mathbf{q}^T C \mathbf{q}} \Big|_{\mathbf{q}=0} \\ &= \mu_i \\ \langle X_i X_j \rangle_{i \neq j} &= (-i)^2 \frac{\partial}{\partial q_j} \frac{\partial}{\partial q_i} \phi(\mathbf{q}) \Big|_{\mathbf{q}=0} \\ &= - \left[-C_{ij} + \left(i\mu_j - \sum_n C_{jn} q_n \right) \left(i\mu_i - \sum_n C_{in} q_n \right) \right] e^{i\mathbf{q}^T \boldsymbol{\mu} - \frac{1}{2}\mathbf{q}^T C \mathbf{q}} \Big|_{\mathbf{q}=0} \\ &= C_{ij} + \mu_i \mu_j\end{aligned}$$

$$\begin{aligned}
\langle X_i X_j X_k \rangle_{i \neq j \neq k} &= (-i)^3 \frac{\partial}{\partial q_k} \frac{\partial}{\partial q_j} \frac{\partial}{\partial q_i} \phi(\mathbf{q}) \Big|_{\mathbf{q}=0} \\
&= i \left[-C_{jk} \left(i\mu_i - \sum_n C_{in} q_n \right) - C_{ik} \left(i\mu_j - \sum_n C_{jn} q_n \right) \right. \\
&\quad \left. - C_{ij} \left(i\mu_k - \sum_n C_{kn} q_n \right) + \left(i\mu_k - \sum_n C_{kn} q_n \right) \times \right. \\
&\quad \left. \times \left(i\mu_j - \sum_n C_{jn} q_n \right) \left(i\mu_i - \sum_n C_{in} q_n \right) \right] e^{i\mathbf{q}^T \boldsymbol{\mu} - \frac{1}{2} \mathbf{q}^T C \mathbf{q}} \Big|_{\mathbf{q}=0} \\
&= \mu_i C_{jk} + \mu_j C_{ik} + \mu_k C_{ij} + \mu_i \mu_j \mu_k \\
\langle X_i X_j X_k X_l \rangle_{i \neq j \neq k \neq l} &= (-i)^4 \frac{\partial}{\partial q_l} \frac{\partial}{\partial q_k} \frac{\partial}{\partial q_j} \frac{\partial}{\partial q_i} \phi(\mathbf{q}) \Big|_{\mathbf{q}=0} \\
&= \left\{ C_{ij} C_{kl} + C_{ik} C_{jl} + C_{jk} C_{il} + C_{kl} \left(i\mu_j - \sum_n C_{jn} q_n \right) \left(i\mu_i - \sum_n C_{in} q_n \right) + \right. \\
&\quad + C_{jl} \left(i\mu_k - \sum_n C_{kn} q_n \right) \left(i\mu_i - \sum_n C_{in} q_n \right) + C_{il} \left(i\mu_j - \sum_n C_{jn} q_n \right) \times \\
&\quad \times \left(i\mu_k - \sum_n C_{kn} q_n \right) + \left[-C_{jk} \left(i\mu_i - \sum_n C_{in} q_n \right) - C_{ik} \left(i\mu_j - \sum_n C_{jn} q_n \right) \right. \\
&\quad \left. - C_{ij} \left(i\mu_k - \sum_n C_{kn} q_n \right) + \left(i\mu_k - \sum_n C_{kn} q_n \right) \left(i\mu_j - \sum_n C_{jn} q_n \right) \times \right. \\
&\quad \left. \times \left(i\mu_i - \sum_n C_{in} q_n \right) \right] \left(i\mu_l - \sum_n C_{ln} q_n \right) \right\} e^{i\mathbf{q}^T \boldsymbol{\mu} - \frac{1}{2} \mathbf{q}^T C \mathbf{q}} \Big|_{\mathbf{q}=0} \\
&= C_{ij} C_{kl} + C_{ik} C_{jl} + C_{jk} C_{il} + C_{ij} \mu_k \mu_l + C_{ik} \mu_j \mu_l + C_{il} \mu_j \mu_k + C_{jk} \mu_i \mu_l + \\
&\quad + C_{jl} \mu_i \mu_k + C_{kl} \mu_i \mu_j + \mu_i \mu_j \mu_k \mu_l .
\end{aligned}$$

Appendix B. Random Genetic Drift

In this work we have considered the infinite population limit $N \rightarrow \infty$ and neglected issues arising from taking into account the stochastic nature of the birth/death processes in a finite population [77]. In the case $N < \infty$, the element of chance introduced by the random sampling of the individuals that survive from one generation to another is alone capable of driving an allele to fixation or extinction.

Such an effect is well known in population genetics: it is the *genetic drift*, as discussed first by R.A. Fisher [7] and S. Wright [78] (Fisher-Wright or FW model). In their simplest model of genetic drift no recombination or mutations are included and selection is absent. Stochastic effects alone then drive the evolution: one says that these are *neutral* models. For the sake of simplicity, consider an haploid population of constant size N . Evolution is encoded in a series of discrete, non-overlapping generations. Each time step $t \rightarrow t + 1$ entails a replacement of the entire population, with a process akin to the sampling with replacement of coloured balls from an urn, this is the so called *beanbag population genetics*, see Fig.B1. The FW model employs a Markov-process formalism to predict that, sooner or later, the alleles either fixate or go extinct and the corresponding probabilities only depend on their initial frequency [9].

When trying to extend this approach to the case in which mutation, recombination and selection play a role in the evolutionary process, the calculations soon become

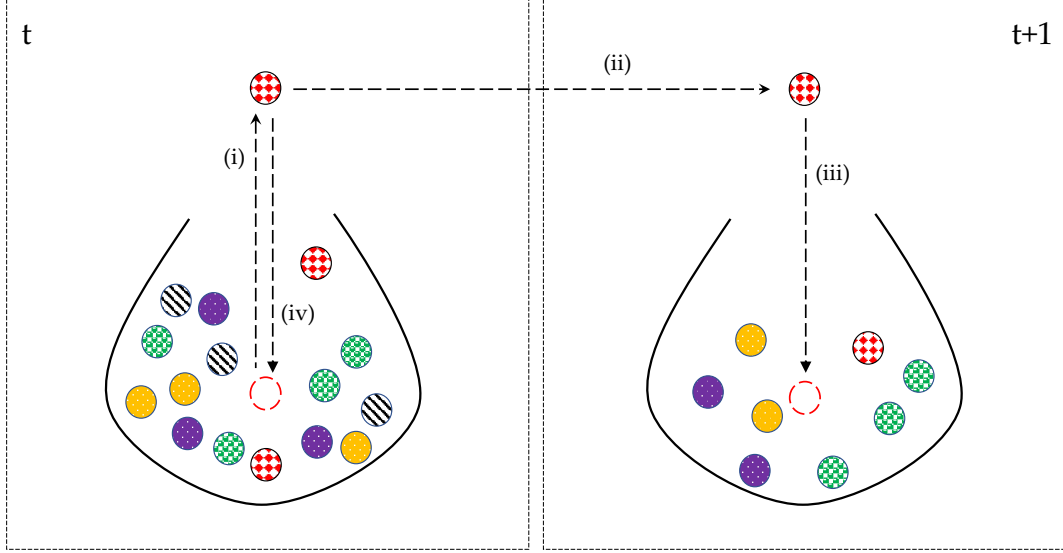


Figure B1.: Beanbag population genetics. The population at $t + 1$ is constructed from that at t (size N) by (i) selecting a gene from t at random; (ii) copying this gene; (iii) placing the copy in the next generation; (iv) returning the original to the parent population. This algorithm is repeated until until the population at generation $t + 1$ has size N .

cumbersome to work out and in order to deal with these difficulties a number approximations have been proposed. M. Kimura [79,80] showed that in large populations the discrete FW process can be approximated by a continuous time, continuous space diffusion process. Let $x = i/N$ be the frequency of the allele +1, $P(x, t)$ the probability of finding x at time t . Let us suppose that, together with genetic drift, there is also a selective advantage for the allele +1 *i.e.* the individuals with that allele have on average $1 + s$ offspring, those with -1 only on average just 1; let also σ^2 be the variance in the number of offspring. Finally, assume also that fluctuations are uncorrelated across individuals and generations (non-heritable). Then in a diffusion approximation the distribution of the variant frequency evolves according to the following Fokker-Planck Equation (Kolmogorov forward equation) [68]:

$$\frac{\partial P(x, t)}{\partial t} = \left[-s \frac{\partial}{\partial x} x(1 - x) + \frac{\sigma^2}{2N} \frac{\partial^2}{\partial x^2} x(1 - x) \right] P(x, t) . \quad (\text{B1})$$

The term with the first order derivative comes from the selection mechanism with strength s ; the second one is the drift term, which results from the variance σ^2 in offspring number. As it should be, the latter is damped when increasing the population size and vanishes when $N \rightarrow \infty$. In a population of size N , the frequency x of a variant therefore has a diffusion constant $\sigma^2/Nx(1 - x)$. Starting from eq.(B1), it is possible to evaluate several relevant statistics *e.g.* the allele-frequency distributions, fixation probabilities, expected time for fixation/extinction (...) Nevertheless, such an approximation is not feasible when, for instance, fluctuations are correlated over generations and their effect is crucial for the fate of the population.

Including genetic drift in the KNS-model described in Sec.(1.2) is in principle straightforward. We will limit ourselves to describing the framework and the main results, details will be found in [12]. The crucial step is the translation of the ordinary differential equations eq.(32, 33) into discrete Langevin equations *i.e. stochastic differential equation* [68]:

$$\chi_i(t + \Delta t) = \chi_i(t) + \Delta t \sum_j \chi_{ij} \partial_{\chi_j} \langle F \rangle + \sqrt{\Delta t} \zeta_i(t) \quad (B2)$$

$$\chi_{ij}(t + \Delta t) = \chi_{ij}(t) + \Delta t [f_{ij}(1 - \chi_i^2)(1 - \chi_j^2) - r c_{ij} \chi_{ij}] + \sqrt{\Delta t} \zeta_{ij}(t) \quad (B3)$$

where $\zeta_i(t), \zeta_{ij}(t)$ are white noise terms with zero mean and covariances determined by the multinomial sampling of the genotypes. Neglecting those of order σ/Nr and smaller, one finds the following expressions for the covariances:

$$\langle \zeta_i(t) \zeta_j(t') \rangle = \frac{\chi_{ij}}{N} \delta(t - t') , \quad \langle \zeta_{ij}(t) \zeta_{ij}(t') \rangle = \frac{(1 - \chi_i^2)(1 - \chi_j^2)}{N} \delta(t - t') . \quad (B4)$$

From these last expression we explicitly understand the role of the population size for our observables: the first and second order cumulants will be subject to fluctuations whose magnitude scales as $1/\sqrt{N}$ and vanish in the infinite population limit. As an example, let us consider the $\{\chi_{ij}\}$. In the QLE, as we have discussed, these quantities relax much faster than the $\{\chi_i\}$, hence we can assume the latter constant when studying the dynamics of the former. In particular, it is possible to decompose the solution is a deterministic part, which is our eq.(30), and a stochastic contribution:

$$\chi_{ij}(t) = \frac{f_{ij}}{r c_{ij}} (1 - \chi_i^2)(1 - \chi_j^2) + \delta \chi_{ij}, \quad (B5)$$

where the autocorrelation of the of the last term is found to be

$$\langle \delta \chi_{ij}(t) \delta \chi_{ij}(t + \Delta t) \rangle = \frac{(1 - \chi_i^2)(1 - \chi_j^2)}{2 N r c_{ij}} e^{-r c_{ij} \Delta t} : \quad (B6)$$

Apart from the dependence on the system size we also observe the dependence on the recombination rate r which dampens not only the deterministic part but also the stochastic effects. Once the autocorrelations eq.(B6) are known, the stochastic contribution to eq.(B5) is determined; however, in order to use this result, one has to distinguish the case when the stochastic component dominates from the opposite one. With this *proviso*, it is possible to study the Langevin equations for $\{\chi_i\}$ eq.(B2) using eq.(B5). This distinction between the two regimes is made by comparing the deterministic part of the $\chi_{ij}(t)$ with the stochastic term upon averaging the latter over the timescale of the dynamics of the $\{\chi_i\}$, that given by the inverse of $\partial_{\chi_i} \langle F \rangle$, see eq.(33). It is also possible to take into account the mutational contribution $\mu \neq 0$ into eq.(B2), in which case one finds the deterministic component of $\chi_{ij}(t)$ to dominate when $N\mu \gg 1$ and $f_{ij} \gg \mu$; otherwise the stochastic component dominates.

Appendix C. KNS Theory for Categorical Data

A limitation of the discussion in Sec.(1.2) is the assumption of *biallelic* loci $s_i = \pm 1$. This is rarely true in real genetic data where one can find (at least) four different alleles, namely A,C,G,T. The framework we have set up and most importantly the results we have obtained can however be generalized to the case of multi-allelic loci (categorical data). Following [81], we here briefly revisit some aspects of the KNS theory and extend it to categorical data.

We consider an infinite population, each individual is a genomic chain which consists in L loci $g = \{z_1, \dots, z_L\}$; each locus can in turn take q_i values (alleles) *i.e.* $z_i = 1, \dots, q_i$. $P(g, t)$ is the probability of finding the genotype g at time t . We generalize eq.(10) and define

$$\nu_i(\alpha) = \langle \delta_{z_i, \alpha} \rangle, \quad (C1)$$

$$M_{ij}(\alpha, \beta) = \langle \delta_{z_i, \alpha} \delta_{z_j, \beta} \rangle - \nu_i(\alpha) \nu_j(\beta) : \quad (C2)$$

here the averages are over $P(g)$, δ indicates the δ -Kronecker, $\nu_i(\alpha)$ stands for the frequency of the allele α at the i -th locus, while $M_{ij}(\alpha, \beta)$ is the element of the covariance matrix between loci i and j relative to the alleles α in i and β in j . The following normalizations hold: $\sum_{\alpha=1}^{q_i} \nu_i(\alpha) = 1$, $\sum_{\alpha=1}^{q_i} M_{ij}(\alpha, \beta) = \sum_{\beta=1}^{q_j} M_{ij}(\alpha, \beta) = 0 \forall i, j$.

We can still write formally eq.(1) but some more notational effort is required, We consider one by one the drivers of evolution.

- **Fitness.** The formal expression for the fitness term is the same as in eq.(2)

$$\frac{d}{dt} \Big|_{fit} P(g) = (F(g) - \langle F \rangle) P(g) .$$

We only need to rewrite the fitness function in a form appropriate for the multi-allelic case:

$$F(g) = \bar{F} + \sum_i f_i(z_i) + \sum_{i,j} f_{ij}(z_i, z_j) , \quad (C3)$$

where $f_i(z_i)$, $f(z_i, z_j)$ are functions of the alleles z_i, z_j and in general $f_{ij}(z_i, z_j) \neq f_{ji}(z_i, z_j)$. Unlike the biallelic case the matrix of epistatic fitness effects between loci i and j does not reduce to one real number.

- **Mutations.** Let $\mu_{\alpha, \beta}^{(i)}$ be the mutation rate at which the allele α mutates into β at locus i . In the most general framework, $\mu_{\alpha, \beta}^{(i)} \neq \mu_{\beta, \alpha}^{(i)}$. We can generalize eq.(5) to the following

$$\frac{d}{dt} \Big|_{mut} P(g) = \sum_i \sum_{\alpha, \beta} \delta_{z_i, \alpha} \left(\mu_{\beta, \alpha}^{(i)} P(\mathcal{M}_{\alpha, \beta}^{(i)} g) - \mu_{\alpha, \beta}^{(i)} P(g) \right) . \quad (C4)$$

The operator $\mathcal{M}_{\alpha, \beta}^{(i)}$ acts on the genomic sequence g as follows: if in the i -th locus of g there is the allele α then it is changed to β , otherwise nothing happens.

- **Recombination.** No change is needed for the contribution due to recombin-

tion, that is, we can copy-paste from eq.(7)

$$\frac{d}{dt} \Big|_{rec} P(g) = r \sum_{\xi, g'} C(\xi) \left[Q(g^{(1)}, g^{(2)}) P_2(g^{(1)}, g^{(2)}) - Q(g, g') P_2(g, g') \right].$$

In eq.(6), we only need to formally substitute $s_i \rightarrow z_i$.

All other explanations, observations, limitations hold true as described in Sec.(1.2.2 - 1.2.4). As for the biallelic case, we now assume that the two-genome distribution factorizes eq.(8) in a simple product of two one-genome Potts-like distributions:

$$P(g, t) = \frac{1}{\mathcal{Z}(t)} \exp \left(\sum_i h_i(z_i, t) + \sum_{i,j} J_{ij}(z_i, z_j, t) \right), \quad (C5)$$

which is the generalization of eq.(17): \mathcal{Z} is the partition function, $h_i(z_i, t)$, $J_{ij}(z_i, z_j, t)$ are functions of the alleles z_i, z_j and of time t , we will drop the latter dependence in the next formulae.

Due to the constraints eq.(C1-C2) it is clear that we do not need all of the parameters $\{h_i, J_{ij}\}$: there is an over parametrization issue in the previous Potts distribution as introduced here. One possible way to fix this *gauge invariance* is to impose the so called *Ising gauge*: $\sum_{\alpha} h_i(\alpha) = \sum_{\alpha} J_{ij}(\alpha, \beta) = \sum_{\beta} J_{ij}(\alpha, \beta) = 0 \forall i, j$.

The stage is set at this point to introduce the QLE assumption: in the case when recombination is prominent and selection is weak we can assume the couplings J_{ij} to be small. Neglecting the mutational contribution and following the same steps as in Sec.(1.3.1) we get to generalize eq.(25) to the following:

$$\begin{aligned} -\frac{\dot{\mathcal{Z}}}{\mathcal{Z}} + \sum_{i,\alpha} \dot{h}_i(\alpha) \delta_{z_i, \alpha} + \sum_{i,j,\alpha,\beta} \dot{J}_{ij}(\alpha, \beta) \delta_{z_i, \alpha} \delta_{z_j, \beta} &= \\ = r \sum_{i,j,\alpha,\beta} c_{ij} J_{ij}(\alpha, \beta) \left(\delta_{z_i, \alpha} E_Q[\delta_{z'_j, \beta}] + E_Q[\delta_{z'_i, \alpha}] \delta_{z_j, \beta} - \langle Q \rangle \delta_{z_i, \alpha} \delta_{z_j, \beta} - E_Q[\delta_{z'_i, \alpha} \delta_{z'_j, \beta}] \right) + \\ + \sum_{i,\alpha} f_i(\alpha) \delta_{z_i, \alpha} + \sum_{i,j,\alpha,\beta} f_{ij}(\alpha, \beta) \delta_{z_i, \alpha} \delta_{z_j, \beta}. \end{aligned} \quad (C6)$$

where c_{ij} has been introduced in eq.(14) and the following definitions have been employed:

$$\langle Q \rangle = \sum_{g'} Q(g, g') P(g') \quad (C7)$$

$$E_Q[\delta_{z'_i, \alpha}] = \sum_{g'} \delta_{z'_i, \alpha} Q(g, g') P(g') \quad (C8)$$

$$E_Q[\delta_{z'_i, \alpha} \delta_{z'_j, \beta}] = \sum_{g'} \delta_{z'_i, \alpha} \delta_{z'_j, \beta} Q(g, g') P(g') \quad (C9)$$

We can compare terms in LHS and RHS of eq.(C6) and extract a dynamical equation for the couplings of the Potts distribution:

$$\dot{J}_{ij}(\alpha, \beta) = f_{ij}(\alpha, \beta) - r \langle Q \rangle c_{ij} J_{ij}(\alpha, \beta). \quad (C10)$$

Finally, we impose the stationary condition and read off the steady state

$$J_{ij}(\alpha, \beta) = \frac{f_{ij}(\alpha, \beta)}{r\langle Q \rangle c_{ij}} , \quad (\text{C11})$$

In the case where the relative rate of recombination $Q(g, g')$ is constant for all pairs g, g' or approximately so, it can be absorbed in r . We see that the analogy between the last formula and the one for the biallelic case is complete: eq.(28) generalizes to the multi-allelic case in the simplest possible way. Here too, we underline that even if recombination cannot influence the frequencies $\{\nu_i(\alpha)\}$, it couples the dynamics of each $h_i(\alpha)$ to single locus statistics in every other site by means of the couplings $J_{ij}(\alpha, \beta)$, as it can easily read off from eq.(25). This framework has been used in [81] to reconstruct epistasis from a database of 3.000 genotypes (100.000 loci each) of the human pathogen *S. pneumoniae*.

Appendix D. Simulating Evolution with FFPopSim

For the purpose of simulating the evolutionary process, we make use of **FFPopSim**, a software developed by F. Zanini and R.A. Neher. We here briefly describe its main features and refer to the documentation for an in-dept description of the algorithms [82].

FFPopSim is implemented in C++ with a Python2.7 wrapper. It allows population genetics simulations for a population of haploid individuals, identified by their genomes $g = (s_1, \dots, s_L)$ with biallelic loci $s_i = \pm 1$. Considering the number of loci in our model is not small ($L > 20$), for the sake of computational efficiency, we choose to run individual-based simulations, which in **FFPopSim** are implemented in the class `haploid_highd`. In such a case, a discrete generation scheme is employed, in which every individual at every generation undergoes each of the processes that drive evolution with tunable probabilities. **FFPopSim** keeps track of the distribution $P(g)$ that changes under the effect of mutation, recombination, natural selection. Random drift is simulated by resampling each individual at each generation from a Poisson distribution with mean $NP(g)$, which results in a population of fluctuating size $N \pm \mathcal{O}(\sqrt{N})$. The algorithms for storing and handling genomic sequences are based on a *Fast Fourier Transform* (FFT) of the genotype space.

The class `haploid_highd` is instantiated by specifying the structure of the evolving population, the rates of the evolutionary mechanisms and initial conditions. In Tab.(D1) there is an example, we call this specific set QLE Simulation (**QLES**). In an individual-based model, the fundamental object undergoing evolution is not the genotype, but the *clone* $c_i = (g_i, n_i)$ *i.e.* the pair of a genotype g_i and the number $n_i(t)$ of individuals in the population that have that genotype at time t . In other words, the population \mathcal{P} is a set of clones. The initial conditions are specified by setting $\{c_i\}$ *i.e.* $N \times L$ Boolean values for the $\{g_i\}$ and N integers for the $\{n_i(0)\}$. We will typically set random initial condition for the genotypes and $n_i(0) = 1 \forall i$.

At each generation, the size of each clone is updated and new clones that emerge because of mutations or recombinations are added. A discrete time step (generation) $\Delta t = 1$ is implemented by enforcing mutations, recombination, selection, as follows:

- **Mutations.** Mutations are bit-flip operations in a genotype. Each individual

	FFPopSim	QLES	Description
Drivers	N	1.000	carrying capacity
	L	25	n. of loci
	T	5.000	n. of generations
	r^*	0.5	outcrossing rate
	ω	0.5	crossover rate
	μ	0.05	mutation rate
	$\{f_i\}$	0.0	additive fitness
	$\{f_{ij}\}$	$\mathcal{N}(0, \sigma_e)$	epistatic fitness

Table D1.: Parameters of the QLE Simulation (QLES). The structure of the population is specified: N is the *carrying capacity* N *i.e.* the initial size of the population; L is the *number of loci*; T is the *number of generations*; r^* is the *outcrossing rate*; ω is the *crossover rate* per site per generation; μ is the *mutation rate* per site per generation; $\{f_i, f_{ij}\}$ are the coefficients of the fitness function eq.(3). Random initial configuration. No additive fitness. Epistatic fitness coefficients are Gaussian distributed with zero mean and width $\sigma_e = 0.004$, $f_{ij} = f_{ji}$ and $f_{ii} = 0 \forall i, j$.

mutates with probability $1 - e^{L\mu}$. Every individual that has been selected for mutations, suffers at least one of them, the number K being drawn from a Poisson distribution $\mathcal{P}_{L\mu}(K)$ with mean $L\mu$.¹¹ Target loci are chosen randomly.

- **Selection.** Let $n_i(t)$ be the size of the clone i at time t . We enforce selection by updating $n_i(t) \rightarrow n_i(t+1) \sim \mathcal{P}_\lambda$ where

$$\lambda = \frac{1}{\langle e^F \rangle} e^{F(g_i) + 1 - \frac{1}{N} \sum_j n_j(t)} . \quad (\text{D1})$$

In words, we draw the size $n_i(t+1)$ of the i -th clone at time $t+1$ from a Poisson distribution with mean λ as in eq.(D1), where $F(g)$ is the fitness function eq.(3) and the average $\langle e^F \rangle$ is over the entire population. We note that for $F(g) \ll 1$, $e^{F(g)}/\langle e^F \rangle - 1 \sim F(g) - \langle F \rangle$, so that we retrieve eq.(2). The growth rate adjustment $\exp(1 - \sum_j n_j(t)/N)$ is implemented to constrain the population close to the carrying capacity N .

- **Recombination.** A fraction r^* of the offspring at the previous fitness-step are designated for sexual reproduction.¹² They are shuffled and randomly paired. For each pair a crossover pattern $\{\xi_i\}$ as in Sec.(1.2.4) is created and the re-

¹¹These probabilities are consequences of the discreteness of the computer simulation. The rate μ as introduced in Sec.(1.2.3) is referred to a continuous-time formulation of the evolution. Let \mathcal{E} be the event that a mutation appears in an individual; suppose such events are independent and that the probability of two of them happening at the same time is negligible. If their average rate is μ then the number k of events \mathcal{E} in the time interval Δt is $\sim \mathcal{P}_{\mu\Delta t}$ where $\mathcal{P}_\lambda(k) = \lambda^k e^{-\lambda}/k!$ is the Poisson distribution. The number of such mutations in a genome of length L in the interval Δt is the random variable $K = \sum_{i=1}^L k_i$ that, being the sum of L i.i.d. Poisson random variables, is again Poisson distributed, with mean $L\mu\Delta t$ *i.e.* $K \sim \mathcal{P}_{L\mu\Delta t}$. Finally, the probability that there is *at least* one mutation is $1 - \mathcal{P}_{L\mu\Delta t}(0) = 1 - e^{L\mu\Delta t}$.

¹²Note that $r^* \neq r$, the latter described in Sec.(1.2.4). The reason is that in general the outcrossing rate r^* is not the recombination rate r . In fact, r^* is treated as a probability while r is a rate that can take any positive value. Considering the discreteness of the computer simulation as done for mutations, we should have $r^* = 1 - e^{-r}$. However, as long as $r \ll 1$ they approximately coincide $r^* \sim 1 - (1 - r) = r$.

combination is implemented by discarding parents and replacing them with two new individuals accordingly. Crossovers are assumed to happen independently between any two loci with rate ω .

For the details of the technical implementation we refer to the documentation that accompanies the code in the GitHub repository [67]. As a demonstration, in Fig.D1-D6 we show the results for a simulation run with the parameters as in Tab.(D1), tuned so to set the system in a QLE regime *i.e.* weak selection effects, high recombination.

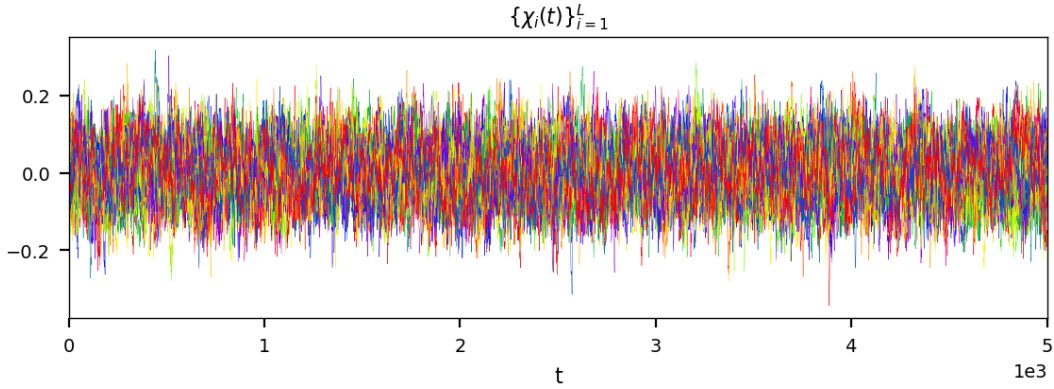


Figure D1.: Simulation QLES, Tab.(D1). All-time evolution of the L first order cumulants $\{\chi_i\}$. In a QLE phase they fluctuate around the random-state values $\chi_i \sim 0$, since strong recombination rate to prevent any fixation of an allele in the population.

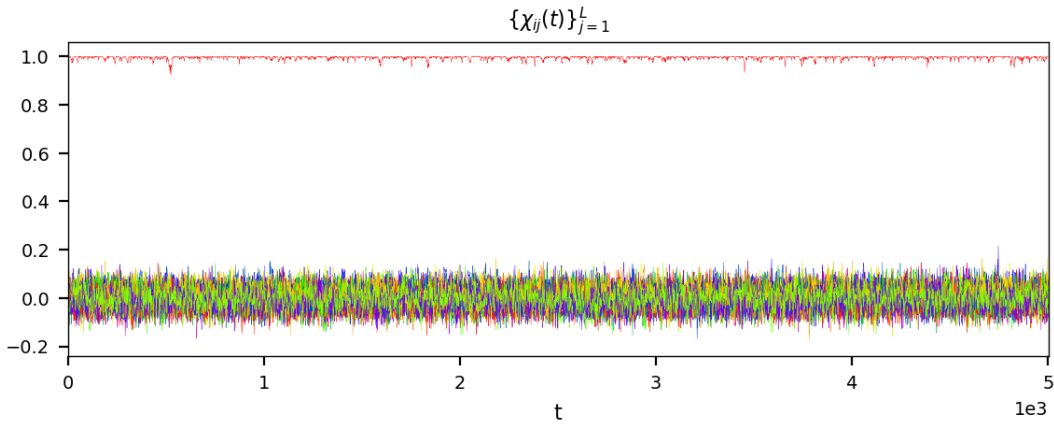


Figure D2.: Simulation QLES, Tab.(D1). All-time evolution of the L second order cumulants $\{\chi_{ij}\}_{i=1}^L$. In a QLE phase they fluctuate around the random-state values $\chi_{ij} \sim 0 \forall i \neq j$ and $\chi_{ii} = 1 - \chi_i^2 \sim 1$.

Finally, for the details of our implementation, we refer to documentation attached to [67].

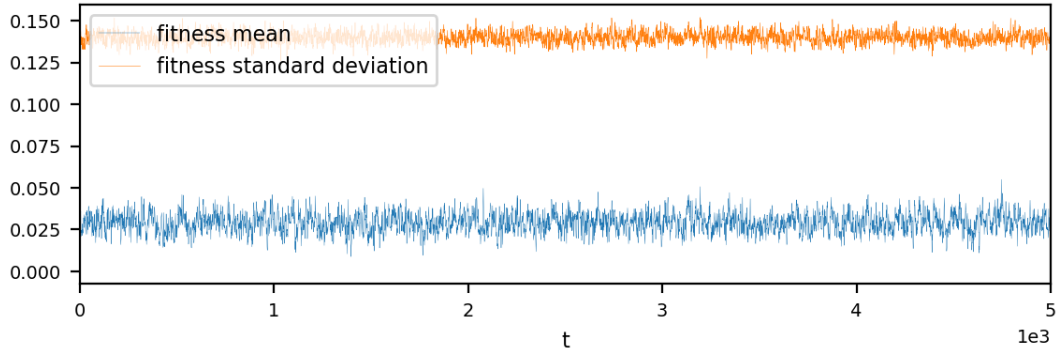


Figure D3.: Simulation QLES, Tab.(D1). All-time evolution of the fitness mean and standard deviation in the population. In a QLE phase, fluctuations aside, they rapidly settle to their asymptotic values.

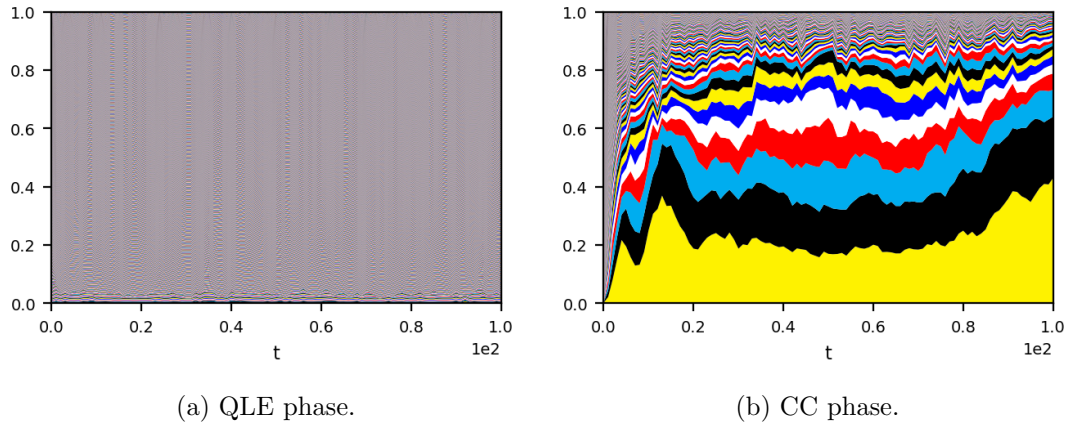


Figure D4.: All-time evolution of the clonal structure of the population for the first 100 generations. On the x-axis, time. For each t , all the clones in the population are first ordered in descending order by size, then each one is assigned a different color (six colors repeated in the order: yellow - black - cyan - red - white - blue). Their relative size for each t is displayed as a vertical line, the largest at the bottom. *Left:* Simulation QLES, Tab.(D1). In a QLE phase, no significant clones emerge, most of the genotypes are present as single copies (dust-like plot). *Right:* In order to appreciate the difference with a population in a clonal competition, where few very fit genotypes compete against each other, we use the parameters : $N = 1000, L = 25, T = 2000, \mu = 0.05, r = 0.05, \omega = 0.5, f_{ij} \sim \mathcal{N}(0, \sigma_e = 0.04)$.

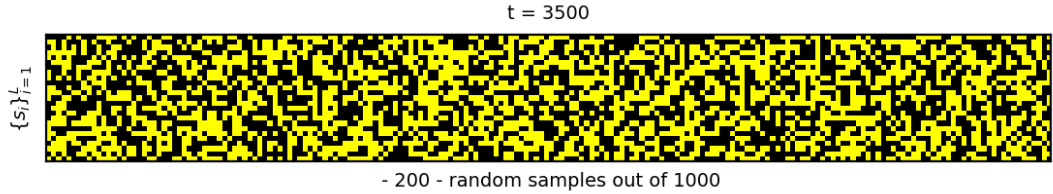


Figure D5.: Simulation QLES, Tab.(D1). Instantaneous snapshot of a random sample (200 individuals) from the population at $T = 3500$. Each vertical strip is genotype, from a random sample of 200 individuals out of N ; each horizontal strip corresponds by consequence to one of the L loci. Y/B stand for ± 1 . In QLE phase, no patterns is obvious to the naked eye.

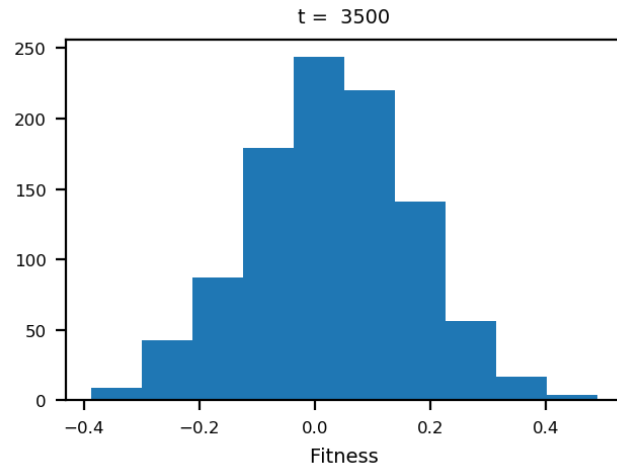


Figure D6.: Simulation QLES, Tab.(D1). Instantaneous distribution of the fitness in the population at $T = 3500$. In QLE phase with gaussian epistatic fitness components $f_{ij} \sim \mathcal{N}(0, \sigma_e)$ and weak epistasis, the resulting fitness function is approximately $F(g) \sim \mathcal{N}(0, \sqrt{L(L-1)/2} \sigma_e)$. Selection breaks the symmetry by promoting genotypes with fitness higher than the average.

Appendix E. Maximum Entropy and Information

In this last appendix we outline the link between the Boltzmann distribution, the principle of maximum entropy and information theory; in [15,83,84] extensive general treatments of this topic can be found. We limit ourselves to summarize the key ideas and apply the results to the context of the Inverse Ising Problem [17].

We first address the question of the origin of the Boltzmann distribution. When dealing with probability theory and combinatorics, a useful analogy often is that of balls in a box/urn. So let us consider M indistinguishable balls and suppose we want to place them in the R compartments of a box. We then fix the occupancy n_r , $r \in 1 \dots R$ (*i.e.* the number of balls) of each compartment, clearly $\sum_{r=1}^R n_r = M$. In the language of statistical physics we would say that we are fixing a *macrostate*. Assuming a large M we can write $n_r = Mq_r$ and the number of configurations compatible with the previous constraints is

$$W = \frac{M!}{\prod_{r=1}^R n_r!} \stackrel{(a)}{\sim} \frac{e^M M^M}{\prod_{r=1}^R e^{n_r} n_r^{n_r}} = \frac{1}{\prod_{r=1}^R q_r^{n_r}}, \quad (\text{E1})$$

where in (a) we have used the Stirling's approximation $n_r! \sim e^{n_r} n_r^{n_r}$. The logarithm of the number of microstates consistent with a given macrostate is proportional to the *Gibbs entropy*:

$$\frac{1}{M} \log W \sim - \sum_{r=1}^R q_r \log q_r. \quad (\text{E2})$$

It is observed that the argument has been based on the assumption of equal probability of microstates. If, in fact, different microstates are found with very different probabilities then the probability of the macrostate is not given by the Gibbs entropy. Let us now consider $\log W$ in eq.(E2) as a function of q_r . In the statistical physics interpretation, the argument goes as follows: each of the R compartments of the box is a *microstate* of the system, with energy E_r . The M balls in the compartments can be viewed as a set of copies of the system, named *ensemble of replicas*; each of the replicas can exchange energy with the others but the ensemble is isolated and has a fixed total energy ME . Assuming that each state of the such ensemble of replicas (*i.e.* each set of $\{q_r\}$ for which $\sum_r n_r E_r = ME$) has the same probability, the statistics of q_r will be dominated by a sharp maximum of W , hence $\log W$, as a function of q_r , subject to the constraint that $\sum_r q_r = 1$ and $\sum_r q_r E_r = E$. Following [85], we implement these constraints using the Lagrange multipliers. This is done by setting to zero the derivative of

$$-\sum_{r=1}^R q_r \log q_r + \eta \left[\sum_{r=1}^R q_r - 1 \right] + \lambda \left[\sum_{r=1}^R q_r E_r - E \right] \quad (\text{E3})$$

with respect to q_s , yielding the *Boltzmann distribution*

$$q_s = e^{-1+\eta} e^{\lambda E_s} = \frac{1}{\mathcal{Z}} e^{\lambda E_s}; \quad (\text{E4})$$

in the last expression we have defined $\eta = 1 - \log \mathcal{Z}$ and λ is determined by the

condition $E = \frac{\partial}{\partial \lambda} \log \mathcal{Z}$.

The RHS of eq.(E2) has a form of *Shannon entropy* in information theory: let X be a discrete random variable with alphabet \mathcal{X} and probability distribution $p(x) = \Pr\{X = x\}, x \in \mathcal{X}$, then

$$\mathcal{S}(X) = - \sum_{x \in \mathcal{X}} p(x) \log p(x) \quad (\text{E5})$$

is the Shannon entropy of p . This quantity is a measure of the *uncertainty* of the random variable X and has a number of properties discussed in *e.g.* [15].

In deriving eq.(E4) we have operated a constrained maximization of the entropy eq.(E2), where the constraint was a fixed total "energy". A similar argument can be used for the *maximum entropy estimation* of the shape of an unknown probability distribution, subject to one or more generic constraints. Suppose we want to determine the probability distribution p_r compatible with the constraints $\sum_r p_r = 1$ and $\sum_r p_r E_r = E$. Consider M independent casts of a fair die with R faces and let $n_r \in \{1, \dots, M\}$ be the number of time that the outcome $r \in \{1, \dots, R\}$ is observed. The probability of a specific set of outcomes $\{n_r\}$ is

$$\frac{M!}{\prod_{r=1}^R n_r!} \prod_{r=1}^R \left(\frac{1}{R}\right)^{n_r}, \quad (\text{E6})$$

and using the Stirling approximation $s! \sim s^s e^{-s}$, its logarithm is $-M \sum_r q_r \log q_r - M \log R$, where $q_r = n_r/M$, *i.e.* the Shannon entropy minus a constant. The idea now is that the best estimate for the probabilities p_r corresponds to the set of $\{n_r\}$ that are most likely and at the same time verify the desired constraint. Therefore maximizing the Shannon entropy subject to the constraints $\sum_r p_r = 1$ and $\sum_r p_r E_r = E$ is the max-entropy estimate of p_r that takes into account the information of the constraints (and nothing more). If the total "energy" $\sum_r n_r E_r$ is fixed, we have already seen that such distribution is eq.(E4). If the die is unfair, so that the outcome r has probability q_r^0 one maximises instead

$$\log \left(\frac{M!}{\prod_{r=1}^R n_r!} \prod_{r=1}^R \left(q_r^0\right)^{n_r} \right) \sim -M \sum_r q_r \log \frac{q_r}{q_r^0}. \quad (\text{E7})$$

again by exploiting the Stirling approximation. This last quantity is the *Kullback-Leibler distance* between the distributions $p_1(x)$ and $p_2(x)$ as

$$D_{KL}(p_1 || p_2) = \sum_{x \in \mathcal{X}} p_1(x) \log \frac{p_1(x)}{p_2(x)}; \quad (\text{E8})$$

which up to a sign is eq.(E7). The D_{KL} is a measure of the inefficiency of the distribution p_2 when the true distribution is p_1 , it is non-negative and it equals zero if and only if $p_1 = p_2$.

As an application of this discussion most relevant for the context of this work, let us consider the following problem. Suppose we have a system with N binary variables s_i , the distribution $p(\mathbf{s})$ of which is not known. Suppose also we have a set of observation

from which we extract the first and second moments $\chi_i = \langle s_i \rangle$, $\phi_{ij} = \langle s_i s_j \rangle$. According to the max-entropy receipt, the best guess for $p(\mathbf{s})$ given $\boldsymbol{\chi}, \boldsymbol{\phi}$ is computed by setting to zero the derivatives with respect to p of

$$-\sum_{\mathbf{s}} p(\mathbf{s}) \log p(\mathbf{s}) + \eta \left(\sum_{\mathbf{s}} p(\mathbf{s}) - 1 \right) + \sum_i h_i \left(\sum_{\mathbf{s}} p(\mathbf{s}) s_i - \chi_i \right) + \sum_{i < j} J_{ij} \left(\sum_{\mathbf{s}} p(\mathbf{s}) s_i s_j - \phi_{ij} \right), \quad (\text{E9})$$

where we have used the Lagrange multipliers $\eta, \mathbf{h}, \mathbf{J}$. We get the distribution

$$p(\mathbf{s}) = e^{-1+\eta} e^{\sum_i h_i s_i + \sum_{i < j} J_{ij} s_i s_j} = \frac{1}{\mathcal{Z}} e^{\sum_i h_i s_i + \sum_{i < j} J_{ij} s_i s_j}. \quad (\text{E10})$$

where \mathcal{Z} is fixed by the normalization and \mathbf{h}, \mathbf{J} are chosen so to reproduce the observed moments $\boldsymbol{\chi}, \boldsymbol{\phi}$. We immediately recognize in the previous equation the Boltzmann distribution eq.(35) with the Ising Hamiltonian eq.(34). The Shannon entropy of this distribution is readily computed to be

$$\mathcal{S} = - \sum_i h_i \chi_i - \sum_{i < j} J_{ij} \phi_{ij} + \log \mathcal{Z}. \quad (\text{E11})$$

Elegant as it is, the argument used above is different from that in the main body of this paper. Instead of emerging as a stationary state of a definite dynamic process, the Gibbs-Boltzmann distribution appears to be given a priori. The issue of the validity of a max-entropy approach to inference has been debated for a long time [86], for a critical appraisal by one of us, see [87]. We summarize some of the arguments that can be made in favor of a max-entropy distribution with pair-wise interactions with critical counter-points in italics:

- (1) it is justified when there is lack of data, in which case higher order statistics are poorly determined. *The choice of which statistics to consider is however up to the modeller. Suppose some investigator can determine the average speed ($\langle |v| \rangle$) of molecules in a gas in a box; the max-entropy distribution based on that observation is $\propto e^{-\beta|v|}$. But the actual distribution is Maxwell-Boltzmann $\propto e^{-\beta v^2}$, even though mean square velocity ($\langle v^2 \rangle$) is a higher order statistic which is more sensitive to outliers and noise.*
- (2) it is justified data are generated by an equilibrium model with at most pair-wise interactions. *This is indeed correct, but the underlying reason is that the Gibbs-Boltzmann distribution is a stable equilibrium for a system evolving under dynamics that satisfy detailed balance.*
- (3) it is justified when models with higher order interactions $J_{ijk\dots}$ can be reasonably approximated by simple Ising models; *This is also correct, but is a statement of relative weakness of higher order effects, which may or may not hold.*
- (4) it is justified when the true distribution is so complicated that there is no other choice than trying to employ an "effective" Ising model which can be useful in deriving bounds *e.g.* for energy and entropy. *A probability distribution can be visualized as a point in a space, which is $2^N - 1$ -dimensional for a probability distribution on N Ising spins. It is indeed often the case that it is not meaningful to look for full representation, *e.g.* due to lack of data, and that one may instead look for representations in lower-dimensional model families. The Ising model has $\frac{N(N+1)}{2}$ parameters which is much less. This $\frac{N(N+1)}{2}$ -dimensional model family has many attractive properties, but for some data other families of equal dimen-*

sionality may be a better fit. This counter-argument, orthodox from the point of view of statistics, has been developed to great length in Information Geometry, see e.g. [88–90].

Internal to this work, the results reported in Section 4 in the main body of the paper are also arguments against max-entropy; a distribution which fluctuates indefinitely in time falls outside such a framework.

Acknowledgements

We thank Profs Simona Cocco and Rémi Monasson and Dott. Eugenio Mauri for numerous discussions and for a pleasant collaboration forming the background of the material presented in Section 3.

The work of Vito Dichio was supported by Extra-Erasmus Scholarship (Department of Physics, University of Trieste) and Collegio Universitario 'Luciano Fonda' and has partially been presented in the form of a MSc thesis at University of Trieste (2020). He also warmly thanks Nordita (Stockholm, Sweden) and KTH (Stockholm, Sweden) for hospitality.

The work of HLZ was sponsored by National Natural Science Foundation of China (11705097), Natural Science Foundation of Jiangsu Province (BK20170895), Jiangsu Government Scholarship for Overseas Studies of 2018. EA acknowledges support of the Swedish Research Council through grant 2020-04980.

We also thank J. Berg for permission to re-use Fig.2, and B.H. Good and M.M. Desai for kindly allowing us to use previously unpublished Fig.21.